Regulation of Fos related antigen-1 (Fra-1) accumulation in human bladder cancer

Thesis submitted to the University of Leicester for the degree of Doctor of Philosophy

Richard F.J. Stanford
Urology Group
Department of Cancer Studies and Molecular Medicine
University of Leicester

September 2011

Abstract

Regulation of Fos related antigen-1 (Fra-1) accumulation in human bladder cancer

Richard F.J. Stanford

Bladder cancer is one of the commoner malignancies in humans and current treatments for invasive disease typically give a five year survival rate of around fifty percent. Current chemotherapeutic agents increase survival by a small amount; clearly there is the need for improved treatments and for this, novel targets need to be identified.

One putative target is the Fos family member Fos-related antigen-1 (Fra-1), which form part of the AP-1 transcription factor complex. Fra-1 is elevated in numerous human malignancies and regulates the transcription of genes involved in many aspects of the malignant process, such as migration and invasion. Regulatory control of Fra-1 has been incompletely studied to date; it is known that MAP Kinase dependent signalling can influence Fra-1 accumulation but other aspects of control are only now being elucidated.

This thesis demonstrates that Fra-1 is present in the majority of bladder cancers, that it is regulated by the structure of the C-terminus and MAP Kinase dependent phosphorylation of the amino acids Ser^{252} and Ser^{265}, and undergoes proteasomal degradation. This highlights the potential role of Fra-1 as a novel therapeutic target and provides more information on the regulation of Fra-1 which may be targeted with novel agents.

Acknowledgements

I would firstly like to thank my supervisors Professor J. Kilian Mellon and Dr Eugene Tulchinsky for giving me the opportunity to undertake this research project, and for all their support and encouragement during it.

I would also like to thank Mr Leyshon Griffiths and Dr Marina Kriajevska for their scientific support during this project, and Miss Alexandra Colquhoun for all her work in creating the database of muscle-invasive bladder tumours. I am also grateful to Miss Lynsey McHugh and Dr Richard Vickery for their assistance with some of the experimental work including in this project, and to Mrs Judy Jones for her secretarial support.

As mentioned later, in Chapter 3, much of the immunohistochemical staining of bladder tumours was performed by Mr Richard Edwards, Mrs Jenny Edwards and Mr Raj Pal, with the slides then being analysed by Dr Peter Greaves; my thanks go to them for performing this.

I am grateful to Professor Andrew Tobin and Dr Ignacio Torrecilla of the Department of Cell Physiology and Pharmacology at the University of Leicester for their help with setting up the methods used in the phosphomapping experiments (Chapter 4), and to Dr Sharad Mistry and Dr Andrew Bottrill of the Protein and Nucleic Acid Chemistry Laboratory (PNACL) at the University of Leicester for their assistance with the Edman degradation experiments.

I am also very grateful to the British Urological Foundation (now The Urology Foundation) and the University Hospitals of Leicester NHS Trust for their financial support which has made this project possible.

Finally, none of this would have been possible without the support of my family; to them I will be eternally grateful.

Contents

Chapter 1

Introduction

1.1 The Clinical Problem

Bladder cancer is one the most common malignancies, being the fourth commonest malignancy in men and the eleventh in women in England in 2007 [1] with 6215 men and 2352 women being newly diagnosed with the disease (ICD-10 code C67 "malignant neoplasm of bladder"; ranking figures exclude non-melanomatous skin cancer). During the same year in England and Wales, bladder cancer was recorded as the cause of death of 2923 men and 1437 women [2].

Greater than 90% of bladder cancers arise from the transitional epithelium, and hence are referred to as transitional cell carcinomas (TCC) [3]. Other histological subtypes of bladder cancer include adenocarcinoma (<2%) and squamous cell carcinoma. The proportion of bladder cancers which are of squamous cell type varies greatly across the globe, for example comprising 1% of all bladder cancers in England to approximately 75% in Egypt, mainly due to the higher incidence of chronic infection with *Schistosoma haematobium* in Egypt. Because of the overall prevalence of the TCC subtype, it is therefore logical that the majority of research work is aimed at this subtype, although it should always be remembered that research on TCC may still be applicable to the other histological types.

Transitional cell carcinoma of the bladder (TCCB) can be broadly divided into two subtypes, based on the pathological staging (pT stage). These types

are non-muscle invasive (comprising carcinoma *in situ* or *cis* (pT*is*), pTa and pT1) and muscle-invasive (pT2, pT3 and pT4) (Figure 1.1). At initial presentation, 85% of TCCB are non-muscle invasive and 15% are muscle-invasive. The ability to determine which group a tumour belongs to is crucial in the planning of further treatment, and also gives useful prognostic information; muscle-invasive tumours generally need more aggressive, invasive treatment and have a worse prognosis when compared with non-muscle invasive tumours.

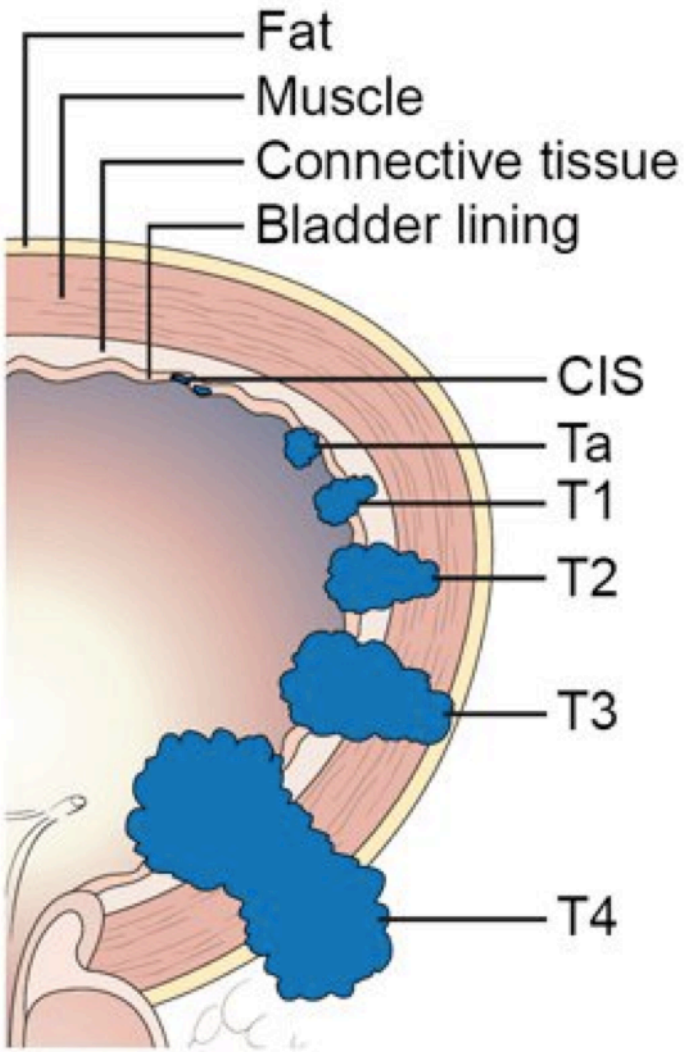

Figure 1.1. Pathological staging mechanism for transitional cell carcinoma of the bladder (2002 TNM classification). *Taken from the Cancer Research UK website, http://www.cancerhelp.org.uk*

Management of TCC bladder (TCCB) is almost always in the first instance surgical, in the form of a transurethral resection of bladder tumour (TURBT). In this procedure, the surgeon, with the patient adequately anaesthetised, uses an operating telescope (resectoscope) inserted via the urethra into the bladder to remove (resect) part or all of the suspected tumour. This provides tissue for histopathological analysis, resulting in both pathological staging information (pT stage) and grading information. This staging information may also be supplemented with data from clinical examination and radiological investigation.

1.1.1 Non-muscle invasive TCCB

Although the majority of patients non-muscle invasive TCCB patients will not develop muscle-invasive disease, i.e. potentially life-threatening disease, a small proportion will progress to muscle-invasive disease and therefore scoring systems such as the EORTC scoring system [4] has been devised (Table 1.1.) to risk-stratify patients with regard to recurrence and progression (Table 1.2.). To reduce the risk of recurrence, all patients with suspected non-muscle invasive tumours (except those with excessive bleeding or bladder perforation) are given a single intravesical dose of chemotherapy ideally within six hours post-operatively – commonly mitomycin-C, but other agents including epirubicin, thiotepa and pirarubicin have also been used. Sylvester *el al*. [5] demonstrated a relative risk reduction for recurrence of 24.2% (from 48.4% to 36.7%) by giving this single dose.

Factor	Recurrence	Progression
Number of tumours		
Single	0	0
2-7	3	3
≥ 8	6	3
Tumour diameter		
< 3 cm	0	0
≥ 3 cm	3	3
Prior recurrence rate		
Primary	0	0
≤ 1 recurrence/yr	2	2
> 1 recurrence/yr	4	2
Category		
Ta	0	0
T1	1	4
Concurrent cis		
No	0	0
Yes	1	6
Grade (WHO 1973)		
G1	0	0
G2	1	0
G3	2	5
Total Score	0-17	0-23

Table 1.1. EORTC scoring system for recurrence and progression rates for non muscle-invasive TCCB

Recurrence score	**Probability of recurrence at 1 year**		**Probability of recurrence at 5 years**		**Recurrence risk group**
	%	(95% CI)	%	(95% CI)	
0	15	(10-19)	31	(24-37)	Low risk
1-4	24	(21-26)	46	(42-49)	Intermediate risk
5-9	38	(35-41)	62	(58-65)	
10-17	61	(55-67)	78	(73-84)	High risk

Progression score	**Probability of progression at 1 year**		**Probability of progression at 5 years**		**Progression risk group**
	%	(95% CI)	%	(95% CI)	
0	0.2	(0-0.7)	0.8	(0-1.7)	Low risk
2-6	1	(0.4-1.6)	6	(5-8)	Intermediate risk
7-13	5	(4-7)	17	(14-20)	High risk
14-23	17	(10-24)	45	(35-55)	

Table 1.2. EORTC probability of recurrence and progression tables for non muscle-invasive TCCB

Although c*is* (carcinoma *in situ*) is pathologically a non-invasive tumour, the risk of progression to muscle-invasive disease is high (54%) [6]. In these patients, therefore, additional therapy is recommended, usually in the form of intravesical Bacillus Calmette-Guérin (BCG) instillations, but cystectomy (surgical excision of the bladder) may also be considered. Maintenance BCG (an induction of six initial doses of BCG given at weekly intervals, followed by periodic subsequent instillations) was shown to reduce progression in a landmark paper by Sylvester *et al*. [7].

They demonstrated a progression rate to muscle-invasive disease of 13.8% in non-BCG treated patients and 9.8% in maintenance BCG-treated patients; a relative risk reduction of 27%. Other authors have also shown benefit, although a more recent meta-analysis has demonstrated no significant difference in rates of progression, rates of survival and cause of death between patients treated with BCG and the often better tolerated mitomycin-C [8].

Most patients diagnosed with non-muscle invasive TCCB will enter a programme of surveillance cystoscopies (bladder inspections) over a period of years because it is known that these tumours do often recur. If they do recur, they tend to be of similar low stage (i.e. remain non-muscle invasive) and can be easily removed either by further TURBT or other techniques such as cystodiathermy (using electrocautery via a resectoscope to fulgurate (burn) the recurrent tumour) or laser ablation, again being delivered via a cystoscope.

1.1.2 Muscle-invasive TCCB

For patients with muscle-invasive TCCB which is confined to the bladder, either at their initial diagnosis or which has developed subsequently, it is considered that TURBT or other local procedures, and intravesical chemotherapies and immunotherapies are inadequate. These patients therefore are generally considered for more radical treatment, either in the form of cystectomy (surgical excision of the bladder) or radiotherapy, both of which may be delivered with curative intent. However, despite

undergoing these treatments, the mortality rate from muscle-invasive TCCB remains high. Shariat *et al*. [9] demonstrated a 66% bladder cancer-specific survival five years post cystectomy. Radiotherapy is perhaps less effective, with five year bladder cancer-specific survival rates varying between 20% and 50% [10], although there may well be confounding variables impeding direct comparison between outcomes following radiotherapy or cystectomy, resulting in radiotherapy appearing to have a worse outcome. However, regardless of this, mortality remains unacceptably high.

To reduce this mortality rate, it has been shown that giving neo-adjuvant combination chemotherapy including cisplatin prior to cystectomy does confer an absolute survival benefit of 5% at 5 years [11]. A more recent trial including 976 patients – the BA06 30894 trial [12] with longer follow up than [11] has examined the survival advantage of giving three cycles of CMV chemotherapy (cisplatin, methotrexate and vinblastine) prior to patients receiving either radical cystectomy (50% of patients) or external beam radiotherapy (43% of patients). Three cycles of neo-adjuvant CMV led to an increase in three year survival from 50% to 56% and in ten year survival from 30% to 36%. The increase in median survival was seven months (from 37 to 44 months). One caution with this trial however is that it includes both radiotherapy and cystectomy; patients were not randomised to the two treatment groups and the decision was either clinician or patient based. This caused heterogeneity between

the two arms - performance status, T stage and N stage were worse in the radiotherapy group, and patient age was higher in the radiotherapy group.

Two large studies have investigated the role of neo-adjuvant chemotherapy prior to external beam radiotherapy. The BC2001 study [13] included 360 patients treated with external beam radiotherapy who were randomised either to receive chemotherapy (mitomycin-C and fluouracil) or no chemotherapy prior to radiotherapy. They demonstrated a significant increase in two year disease free survival from 54% to 65%, with five year overall survival increasing from 35% to 48%. Instead of using conventional chemotherapeutic agents prior to radiotherapy, the BCON study [14] randomised patients to receiving nicotinamide and carbogen or no agent prior to radiotherapy, to investigate whether trying to overcome tumour hypoxia related radio-resistance leads to an improvement in outcome. They demonstrated a significant increase in three year loco-regional disease free survival from 43% in the radiotherapy alone cohort to 54% in the combined drug/radiotherapy group, and a significant increase in overall survival from 46% to 59% with the neo-adjuvant use of nicotinamide and carbogen.

Trials investigating the administration of chemotherapy after cystectomy (adjuvant chemotherapy) have failed to demonstrate a clear survival advantage, despite the apparent 25% decrease in risk of death; the limiting factor is the small number of patients within the study [15].

For patients with metastatic disease, curative treatments are not available; treatment is therefore considered palliative, and may include palliative chemotherapy along with radiotherapy and/or surgical intervention if the patient is troubled with such symptoms as haematuria or voiding difficulties.

Patients who die from TCCB tend to die as a result of their metastatic disease, rather than the disease within the bladder. Therefore it would seem reasonable that to reduce mortality rates, treatments should be aimed at reducing the incidence and impact of metastases. Clearly, reducing the incidence of metastasis can be achieved by removing the primary bladder tumour at an earlier stage in the disease process, however, despite advances in such areas as raising disease awareness and availability of services to investigate patients suspected of having TCCB, many patients will still enter the healthcare system when the tumour is advanced. This advanced stage may or may not be evident at the time of diagnosis. Whilst a patient with pT2 TCCB may be radiologically staged as having no local advancement or distant metastasis, it is currently impossible to detect micrometastatic disease. Any clinician involved in the management of TCCB will have met patients who have undergone cystectomy or radical radiotherapy, with curative intent, only to re-present at a later date (sometimes even just a few months post treatment) with metastatic disease, despite favourable pre-operative imaging, and in the case of cystectomy, favourable histological analysis of the excised bladder and any pelvic lymph nodes which are often excised at the same

time. In these patients, it therefore becomes clear that micrometastases were present at the time of their radical treatment.

It would seem logical therefore, that in order to reduce mortality rates from TCCB, research should be targeted at treating metastatic disease. Indeed, this is currently being carried out and already neo-adjuvant chemotherapy regimens are used to reduce mortality [11, 16], but despite this mortality rates remain unacceptably high.

1.2 Conventional chemotherapies for TCC Bladder

Current chemotherapy regimens for TCC bladder include MVAC (methotrexate, vinblastine, Adriamycin (doxorubicin) and cisplatin) or the newer regimen GC (gemcitabine and cisplatin); see Table 1.3. In general, most of these agents have quite wide ranging effects within the cell which, whilst having the desired effect of killing or inducing apoptosis within (preferentially) the cancer cell, often leads to significant side effects. Whilst, as described above, these compounds can convey some survival advantage, there is clear room for improvement.

1.3 Novel Chemotherapeutic agents

Novel chemotherapies are not just 'novel' in the sense that they are new agents; they are also 'novel' because they are often targeting novel targets, such as cell-surface signalling receptors and intra-cellular signalling pathways. Many new agents show promise whilst in the laboratory stages of development, but then when introduced into clinical trials their effect is often disappointing.

Drug	Class	Mechanism of action
Cisplatin	Alkylating agent	Covalently links alkyl groups to proteins and nucleic acids
Doxorubicin	Antitumour antibiotic	Binds DNA and intercalates between base pairs
Gemcitabine Methotrexate	Antimetabolites	Structurally similar to physiological molecules, therefore inhibits normal functions
Vinblastine	Plant alkaloid	Inhibits microtubule formation by binding to tubulin

Table 1.3. Currently used chemotherapy agents for TCC Bladder, with mechanisms of action

Numerous novel agents target growth factor receptors and their associated signal transduction pathways. With regard to growth factor receptors, Fibroblast growth factor receptor 3 (FGFR3) is known to be mutated in greater than 70% of superficial bladder tumours [17], and is also often found to be overexpressed in these tumours [18]. FGFR signalling is mediated via Ras, and H-Ras is frequently found to harbour activating mutations in TCCB [19]. Jebar *et al*. [20] have shown that these FGFR3 and H-Ras mutations are mutually exclusive, which also suggests FGFR3 signals via H-Ras. Small molecule inhibitors of FGFR3 (which also inhibit other cell surface receptor kinases including VEGFR (vascular endothelial growth factor receptor) and PDGFR (platelet derived growth factor receptor) are in development, as is an antibody to FGFR3 [21]. The Epidermal Growth Factor Receptor (EGFR, c-*erb*B1) has also been shown to be over-expressed in TCCB; EGFR positivity is associated with higher tumour stage, tumour progression and poor prognosis [22, 23]. EGFR, like the FGFR, signals via Ras, through MAP

Kinase to activate the Activator Protein-1 (AP-1) transcription factor complex [24]. EGFR therefore has also become a target for novel agents such as the tyrosine kinase inhibitors gefitinib, erlotinib, lapatinib and Erbitux. Gefitinib [25] and lapatinib [26] have failed to show any significant increase in response or survival, whilst erlotinib and Erbitux are still being investigated.

Farnesyltransferase inhibitors (FTIs) which inhibit isoprenylation of Ras have been trialled, but have shown little or no effect [27, 28], and MEK inhibitors such as AZD6244 are in pre-clinical trials [29].

As well as the Ras-MAPK signalling pathway, the phosphotidylinositol 3-kinase (PI3K) pathway is also implicated in TCCB, with reduction of PTEN expression in around half of bladder cancers [30]. Inhibitors of PI3K and mTOR (mammalian Target Of Rapamycin) are being developed and are in Phase I trials.

There is often a disappointing lack of efficacy between the *in vivo* and *in vitro* effect of novel compounds. *In vitro* effects are often measured in term of the magnitude of change in a target protein level or in cell survival, whereas the *in vivo* effect is often assessed by examining tumour size reduction or reduction in metastatic development. One mechanism for this is the intracellular phenomenon of signalling cross-talk. There are many signalling pathways within the cell; I have briefly touched on two important pathways above. It is known that these pathways are not completely separate entities; signalling via one pathway can have an effect on another pathway such that the effect of

inhibition or stimulation of the first pathway may be negated or attenuated by changes within the second pathway, either directly from the initial signalling molecule or as a result of the initial downstream effect on the first pathway. Additionally, *in vivo*, the situation is even more complex, one possible reason being due to paracrine signalling which may introduce another element of 'feedback' on the first, modulated pathway. One example of this was described by Sahai and Marshall [31] who examined different mechanisms of tumour cell motility. They demonstrated that if one mechanism – rounded cell motility – was blocked by inhibition of ROCK (Rho Kinase) and Rho, cells retained high invasive and migratory potential utilising pericellular proteolysis and integrin-dependent motility as an alternative mechanism. They then demonstrated an ability to switch mechanisms of motility in the opposite direction by using inhibitors of extracellular proteases to reduce pericellular proteolysis, and suggested that this plasticity in tumour cell function may be responsible for the failure of inhibitors of matrix metalloproteinases in clinical trials.

Therefore, whilst targeting signalling pathways seems an attractive option, it may be that targeting the pathway too close to the cell surface receptor may allow crosstalk or feedback to attenuate the amplitude of modulation of the signalling pathway. It would then seem appropriate to target molecules further along the pathways, towards the end effector, to minimise the risk of compensatory cross-talk and tumour cell plasticity.

In addition to the cell surface receptors and their associated signalling pathways, another novel target is the group of proteins that regulate the cell cycle. An important example of such an approach is represented by therapies targeting p53, an effector of multiple stress-initiated pathways. p53 is the 'gatekeeper' of the cell cycle at the G1/S checkpoint, and in response to cellular stresses such as hypoxia and DNA damage can initiate DNA repair and/or apoptosis. It is well known that inactivating mutations of p53 are found in the majority of muscle-invasive bladder cancers, and that p53 status is a prognostic indicator. Novel p53-centered therapies are based either on restoration of wild-type p53 function or by stabilising p53 by modifying the action of MDM2, an E3 ubiquitin ligase controlling p53 protein stability [32].

It can be seen from the work described above that one commonly targeted pathway is the Ras-Raf-MAP Kinase signalling pathway, either directly or via targeting of its upstream regulators – the receptor tyrosine kinases. However, as also described, the phenomenon of cross-talk may reduce the magnitude of change in signalling via pathway manipulation, and therefore targeting downstream of MAP Kinase may be a better option. Signalling via this pathway is carried on by ERK-dependent phosphorylation of downstream proteins, and one such target for ERK phosphorylation is the Activator Protein-1 (AP-1) transcription factor complex, which regulates the transcription of many genes implicated in cancer.

1.4 The Activator Protein-1 Complex

The Activator Protein-1 (AP-1) complex is formed by either heterodimerisation of a Fos protein and a Jun protein, or homodimerisation of two (not necessarily the same) Jun proteins [33]. The Fos family of proteins consists of c-Fos, FosB, FosB2, Fos related antigen-1 (Fra-1) and Fos related antigen-2 (Fra-2) (see review by Tulchinsky [34]), FosB2 being a dominant negative variant of FosB formed by alternative splicing [35, 36, 37]; the Jun family of proteins consists of c-Jun, JunB and JunD [38].

Both the Fos and Jun family of proteins belong to a large group of transcription factors characterised by the presence of a highly conserved basic (DNA binding) domain and a leucine zipper domain, involved in dimerisation – the bZIP family of transcription factors. Other members of the bZIP family, such as ATF and Maf proteins, can also form dimers with Fos and Jun proteins, and by doing so can recognise and bind to different genomic sequences (see Chinenov and Kerppola [39]), thereby increasing the range of genes controlled by these transcription factors, and potentially incorporating additional levels of regulation of transcription. Further regulation of AP-1 function, at the DNA binding level, is incorporated by the ability of non-bZIP proteins, such as Smad and Ets proteins to dimerise with Fos and Jun proteins.

An AP-1 complex can activate transcription by binding to TREs and CREs (TPA Responsive Elements – T G A C/G T C A, and cAMP Response Elements – T G A C G T C A) [39], Figure 1.2. TREs are so-called because they are strongly enhanced by 12-*O*-tetradecanoylphorbol-13-acetate (TPA)

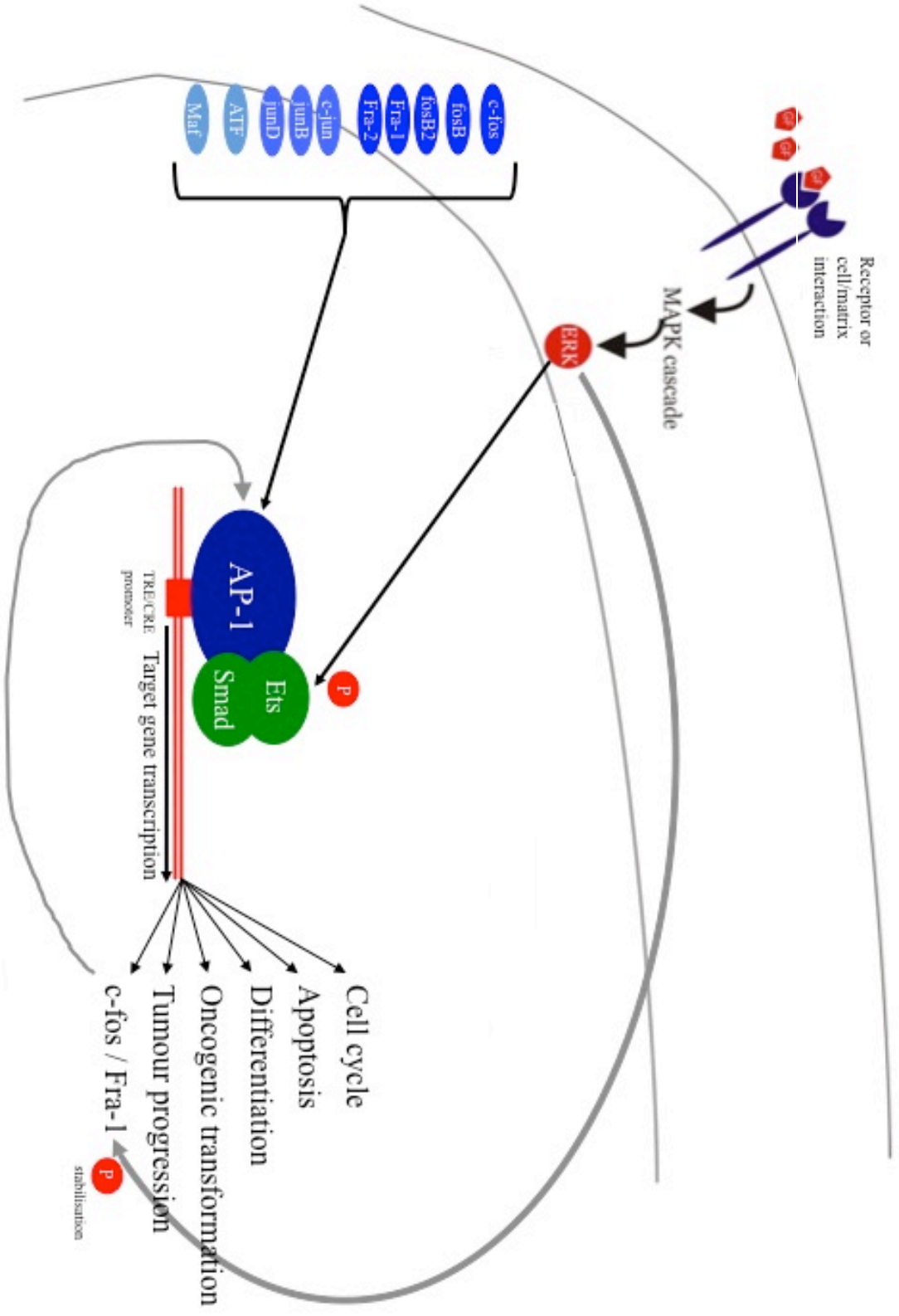

Figure 1.2. Schematic showing the composition and regulation of the AP-1 transcription factor complex

and were first identified as promoters of the metallothionein IIa (MTIIa) and simian virus 40 (SV40) genes. The TRE sequence is found within the promoter/enhancer of target genes [40, 41] and these target genes are involved in the control of the cell cycle, apoptosis, differentiation, oncogenic transformation and tumour progression (see Tulchinsky [34]).

It has been shown that Fos/Jun heterodimers bind to AP-1 sites with much higher affinity than do Jun/Jun heterodimers [42], but that there may not be much difference between the various Fos/Jun heterodimer combinations, such as Fra-1/Jun and c-Fos/Jun [43]. There are also differences in the binding affinities between the individual Fos/Jun proteins; for example Ryseck and Bravo [44] demonstrated that the FosB/Jun complex was more stable than the Fra-1/Jun and c-Fos/Jun complexes.

1.5 Function of AP-1 members

C-Fos was first identified as the cellular homologue of the viral oncoprotein v-Fos in the Finkel-Biskis-Jinkins osteosarcoma virus; c-Jun as the homologue of v-Jun in the avian sarcoma virus 17 [45] and much work subsequently has demonstrated the various roles of the AP-1 complex in regulating cellular transformation and proliferation [33]. Many authors have then identified the roles that the individual AP-1 family members perform with regard to the regulation of cellular activity and have further identified the role that this has *in vivo*; interestingly some AP-1 family members are tumorigenic, whilst others have a tumour suppressive role.

1.5.1 AP-1 tumorigenic activity

Wang *et al*. [46] and Grigoriadis [47] demonstrated that c-fos overexpression in mice led to the development of osteosarcoma; c-Jun overexpression has been shown to promote the formation of murine hepatic tumours [48].

Early work with overexpression of Fra-1 in mice demonstrated the increased formation of lung tumours [49] and that Fra-2 overexpression is related to the formation of epithelial tumours in mice [49]. Subsequent work investigating the role of Fra-1 in tumorigenesis is described in more detail later (Sections 1.11 & 1.12). Fra-2 has also been shown to have a role in human malignancies, being shown to be present in high levels in human cutaneous T-cell lymphoma [50], adult T-cell leukaemia/lymphoma [51] and has been shown to increase invasion in human breast cancer [52] and also correlates with nodal involvement and a reduction in disease-free survival [53].

1.5.2 AP-1 tumour suppressive activity

JunB and JunD lack transactivating domains and are known to have no transforming activity [54,55]; in mice it has been shown that the lack of JunB leads to the development of myeloid leukaemia [56].

This difference in function of the different AP-1 family members is interesting, and therefore means that AP-1 function can be regulated by the relative proportions of the different AP-1 dimers.

1.6 Regulation of AP-1

A variety of stimuli including growth factors, cytokines, cell/matrix interactions and physical and chemical stresses can induce AP-1 activity (see review by Shaulian and Karin [57]). These can, for example, cause activation of the MAP Kinase pathway, resulting in phosphorylation (hence activation) of Ets transcription factors. Ets transcription factors can then induce *fos* genes, leading to an increase in Fos proteins which can dimerise with Jun proteins to form an AP-1 complex (see reviews by Treisman [58] and Chang and Karin [59]). Additionally, ERK can directly phosphorylate Fos members such as Fra-1, and protect them against degradation, thereby increasing protein stability [60] and possibly enhance their DNA binding ability [61].

1.7 Fos family structure

As mentioned earlier, all Fos proteins share some structural characteristics, namely the presence of basic and leucine zipper domains (the bZIP motif). In these areas, as expected, there is significant sequence homology (74-80%) between the Fos members [62] (and see Tulchinsky [34]). There is less homology in both the C- and N-terminal regions flanking the central bZIP domain (15-30%), and it is these areas that account for the differences in function between the family members, although there is a high level of homology at the very C-terminal region. The most important difference is the presence (c-Fos and FosB) and absence (Fra-1 and Fra-2) of a conserved C-terminal transactivation domain, responsible for transactivation ability [34]. Fra-1 is a 271 amino acid protein [63] encoded by the *fosl1* gene which has been localised to the human chromosome 11q13 [64] and murine chromosome 19 [65]. Recent findings of how Fra-1 may be regulated, its presence (or

absence) in many neoplasms, and its mechanistic roles in development and tumorigenesis make it a suitable candidate for further investigation as a potential marker or therapeutic target in cancer.

1.8 Regulation of Fra-1

Regulation of Fra-1 exists at more than one level – transcriptional and post-translational.

1.8.1 Regulation at the transcriptional level

Transcriptional regulation of Fra-1 is (partly) dependent on c-Fos. Following serum stimulation, there is a rapid rise in *c-fos* expression (and c-Fos protein levels) which return to basal within three hours, c-Fos half-life being 54 minutes in COS-7 cells [66]. *Fosl1* expression is delayed; transcription is detected after 45 minutes (correlating with peak c-Fos levels), and peaks at 1.5 to 2.5 hours; *fosl1* mRNA levels still remain significantly elevated after 12 hours [65, 67]. Interestingly, Schreiber *et al*. [65] demonstrated in 3T3 fibroblasts that *fosl1* mRNA levels are much reduced, and delayed, in c-Fos deficient cells, suggesting that mitogen activation of Fra-1 is, at least in part, mediated via c-Fos. Bergers *et al*. [68] also demonstrated, using an oestrogen-inducible FosER construct in rat-1A fibroblasts, rat phaeochromocytoma (PC12) and Ep-1 cells that within one hour of oestrogen stimulation, *fosl1* expression was induced (peak 3 hours) and remained elevated (except PC12 cells, where return to basal levels occurred after 16 hours). They have further localised the site of AP-1 binding to the middle of the first intron of *fosl1*. In contrast, *c-fos* and *fosB* genes, whose transcription does not require

AP-1 activity, lack this binding site. Instead *c-fos* and *fosB* contain several other common promoter elements, reflecting similarities in their transcriptional regulation; both represent the group of immediate response genes (see also Tsuchiya *et al*. [69]).

1.8.2 Post-translational regulation

Better understanding of Fra-1 regulation arises from comparison with the prototypical Fos family member c-Fos. Tsurumi *et al*. [70] demonstrated in HeLa cells that c-Fos is degraded by the ubiquitin-proteasome pathway and that deletion of the C-terminus inhibits this degradation, i.e. the C-terminus appears to act as a degradation-promoting domain. Ferrara *et al*. [71] confirmed this observation in Balb/C 3T3 fibroblasts using rat c-Fos constructs. In addition, it has been established that the destabilising function of the C-terminus is inhibited by phosphorylation of Ser^{362} and Ser^{374} – phosphorylation sites for ERK1/2 – within the C-terminus. This confirmed earlier work reporting an identical finding in NIH 3T3 cells [72, 73].

In Fra-1, it has been shown that *fosl1* mRNA accumulation is increased by stimulation of the MEK/ERK pathway [60, 74]. It is not yet clear, however, if this increase is due to initial MEK/ERK stimulation of *c-fos*, rather than MEK/ERK stimulation of *fosl1* transcription via ternary complex factors (TCFs), or if it is due to activation of Fra-1 which has been shown to positively autoregulate its own expression via binding to its own TRE [75]. Hurd *et al*. [74] and Casalino *et al*. [75] have also

demonstrated ERK-mediated phosphorylation of Fra-1, which causes a decrease in electrophoretic mobility, reversible by treatment with λ-phosphatase. It has also recently been demonstrated in human colorectal cancer and rat thyroid cell lines that this MEK/ERK phosphorylation of Fra-1 increases the half-life of the Fra-1 protein [60, 75].

1.9 Transactivation ability of Fra-1

Whereas c-Fos and FosB contain strong transactivation domains, these domains are absent in Fra-1 and Fra-2 [62, 68], and it has been shown that expression of Fra-1 can inhibit transactivation by c-Fos/c-Jun [76]. However, more recently, Young *et al*. [77] have suggested that Fra-1 harbours a transactivation domain which is activated by ERK-mediated phosphorylation of Thr^{231} in JB6 cells, leading to AP-1 activation. Subsequent investigation by Casalino *et al*. [75] found that the activity of a GAL4/Fra-1 chimeric construct transfected into rat thyroid FRTL-5 cells is strongly inducible by Ras (which is known to activate AP-1 via the Raf/MEK/ERK cascade [78]. However, the use of a GAL4/Fra-1 construct with the leucine zipper domain deleted abrogated this inducibility. These data suggest that the transactivation potential of Fra-1 is associated with the ability to recruit Jun, rather than with the presence of an intrinsic transactivation domain. The finding that Fra-1 can substitute for c-Fos in mouse development fits nicely with this suggestion, in that Fra-1 may recruit a Jun protein, leading to an activated AP-1 complex, rather than being dependent on a Fos transactivation domain [79].

1.10 Fra-1 and mouse development

Schreiber *et al*. [80] clearly demonstrated that Fra-1 was essential for normal placental vascularisation. Mice foetuses were generated which lacked a functional *fosl1* gene. The foetuses lacking Fra-1 all died at around day 10 of gestation. Subsequent investigation showed that the foetuses had no obvious structural abnormalities and that they just appeared growth retarded. The reason for death was identified as being due to abnormal placentation – the absence of Fra-1 leads to abnormal development of the placental labyrinth layer. Importantly, this lethal defect was rescued by tetraploid blastocyst injection of Fra-$1^{-/-}$ ES cells, which led to a conceptus consisting of a Fra-1 deficient foetus, but a Fra-1 containing placenta. The rescued foetuses were morphologically normal and survived for two days after birth. The cause of the early post-natal death was a defect in lung development which resulted from the technical approach, rather than the lack of Fra-1.

In bone, Fos family members have been shown to be important for the function of osteoblasts and osteoclasts [49]. Whereas Fra-1 has no effect on osteoclast function [80], its over-expression in transgenic mice led to the development of osteosclerosis via accelerated osteoblast differentiation [49].

c-Fos has been shown to be essential for osteoclast differentiation, and the absence of c-Fos leads to the development of osteopetrosis [81, 82]. Interestingly, *in vivo* experiments involving a knock-in approach demonstrated that Fra-1 is capable of replacing c-Fos in bone development [83, 84]. However, Fra-1 and c-Fos differ in their abilities to activate

transcription [68]. Therefore it has been proposed that the function of Fos proteins in bone development is associated with transcriptional repression, or possibly with other non-canonical activities [85].

1.11 Fra-1 - A Tumour Suppressor?

Functional AP-1 sequence binding elements are located in the promoters/enhancers of many genes implicated in cancer (MMPs, uPA/uPAR, CD44, etc). Therefore, AP-1 transcription factors would be expected to have a positive, rather than a negative, role; i.e. promote transcription of these genes associated with the malignant phenotype. As described above, Fra-1 lacks a transactivation domain, and would therefore be expected to have a negative role on gene induction as suggested by Suzuki *et al*. [76], suggesting that Fra-1 may have a tumour suppressor role. However, as I will describe later, Fra-1 has been shown to be present at higher levels in some cancer cells; this is to be unexpected if Fra-1 acts as a tumour suppressor.

According to Eferl and Wagner, Fra-1 may have anti- or pro-tumorigenic functions, depending on cell type [86]. It has been suggested that the Jun component of AP-1 can influence the effect of the Fos component – c-Jun possibly being oncogenic whilst JunD and JunB may impart a suppressive function.

Sotu *et al*. [87] analysed six cervical cancer cell lines and found that Fra-1 was undetectable in three out of the six cell lines, whereas it is expressed at

much higher levels in non-malignant cells. Moreover, cancer cell lines containing Fra-1 also expressed c-Fos. The authors hypothesised that it is not merely Fra-1 expression levels, but rather the interaction with a particular Jun protein that affects the phenotype. Additionally, it has been shown that elevated Fra-1 expression can inhibit HPV gene expression, which is intimately linked with cervical cancer [88, 89]. Consistent with the proposed tumour suppressive role of Fra-1, the 11q13 locus (which contains the *fosl1* gene) is frequently rearranged or deleted in cervical cancer [90].

More recently, Mishra *et al*. [91] have shown a similar pattern of Fra-1 expression in human oral cancers, i.e. that Fra-1 expression was very high in normal oral tissue, but not expressed in malignant tissue. Ma *et al*. [92] demonstrated downregulation of Fra-1 in non-small cell lung cancer when compared with normal bronchial epithelium, and noted that low Fra-1 expression levels correlated with advanced stage and poor prognosis.

Taken together, these data suggest that in some cancer types Fra-1 has no pro-tumorigenic function, but rather has a tumour suppressor role.

1.12 Fra-1 and other malignancies – a tumour promoting role?

Contrary to the situation in cervical and non-small cell lung carcinomas, it has been clearly shown in several other solid human tumours that Fra-1 levels are elevated. These cancer types include breast [93], thyroid [94], colon [95], oesophagus [96] and endometrial carcinomas [97]. Fra-1 levels have also been found to be elevated in rat mesothelioma tissue [98] and human

mesothelioma cell lines [99], as well as being elevated in human glioblastoma multiforme cell lines [100] and human nasopharyngeal carcinoma cell lines [101].

Bamberger *et al*. [93] performed Western Blot analysis of human breast carcinoma tissue and found weak Fra-1 staining in about half of the samples; additionally, the presence of Fra-1 was associated with higher grade tumours. In agreement with these data, Fra-1 expression was in the more aggressive, rather than in the less aggressive, but still malignant, cell lines [102]. Recently, using a more mechanistic approach, Milde-Langosch *et al*. [52] have further demonstrated that transient transfection of breast cancer cell lines with Fra-1 leads to an increase in cell invasion. Likewise, in oesophageal squamous cell carcinoma samples and cell lines, Fra-1 was overexpressed in malignant compared with benign cells [96]. They then, using immunohistochemical techniques, confirmed that Fra-1 was overexpressed in 87% of their 61 tumour samples.

Thyroid tissue has also been extensively investigated with regard to the role of Fra-1. Vallone *et al*. [103] demonstrated that v-*ras*-Ki- and v-*mos*-induced neoplastic transformation led to an increase in AP-1 activity, with the most noticeable feature being a marked induction of *fosl1*. Furthermore, inhibition of Fra-1 synthesis by antisense techniques reduced formation of the malignant phenotype. These results were supported by immunohistochemical and reverse transcription PCR analysis of Fra-1 expression in the spectrum of tumour pathology (from benign, through adenoma, to malignant) [94]. Fra-1

was present in both nuclei and cytoplasm of all carcinoma samples, restricted to the nucleus alone in most of the adenomas, and not detectable in normal thyroid tissue.

The data presented above demonstrates that Fra-1 is accumulated in cancer cells indicating that this protein may have a pro-tumorigenic function. In addition, a variety of carcinogenic agents can induce Fra-1. For example, Roy *et al*. [104] demonstrated that exposure of the breast epithelial cell line MCF-10F to ionising radiation leads to an increase in Fra-1 levels. Exposing normal human mesothelial cells to asbestos also leads to an ERK-dependent increase in Fra-1 expression, and ERK inhibition reversed the effect of asbestos [105]. Fra-1 upregulation by asbestos exposure was associated with upregulation of c-*met*, a receptor tyrosine kinase activated in several forms of aggressive cancers [105, 106]. Importantly, siRNA silencing of Fra-1 prevented this upregulation of c-*met*.

These data demonstrated elevated Fra-1 levels in malignant tumours from various tissue origins. However, from the data on cervical carcinoma, it has been suggested that the relative proportions of c-Fos/Fra-1 etc., may be relevant. It has further been shown that c-Fos transcription is inhibited as a result of malignant transformation in human bronchial epithelium and human colonic carcinoma [107, 108]. To understand this phenomenon further, it has been shown that c-*fos* can downregulate its own promoter [109] and that Fra-1 can also downregulate c-*fos* transcription in *ras*-transformed fibroblasts [110].

Thus, data suggests that Fra-1 may have differing roles in tumorigenesis depending on the individual tissue. It is therefore appropriate that more work is carried out to elucidate the precise functions of Fra-1 in particular tissue types.

1.13 Mechanisms of Fra-1 accumulation in cancer

Data presented above show that the MEK/ERK pathway contributes to both transcriptional and post-translational levels of Fra-1 regulation. In particular, *fosl1* mRNA is accumulated in cells with constitutively active ERK [60, 74]. Vial and Marshall [60] and Casalino *et al*. [75] have also demonstrated that phosphorylation of Fra-1 by MEK/ERK stabilises Fra-1 protein. Therefore, ERK appears to play a fundamental role in the regulation of Fra-1, and if we consider Fra-1 as vitally important in tumorigenesis (at least in certain tumour types), and as it is a well known fact that the MEK/ERK pathway also plays a central role in tumorigenesis, could it be that MEK/ERK provides the switch to increase Fra-1 levels which then effects the malignant phenotype?

To provide further evidence that the Ras-Raf-MEK-ERK pathway has a role in malignant transformation via modulation of AP-1, it has been demonstrated in NIH 3T3 fibroblasts that transformation by Ras increases expression of c-Jun and Fra-1 [111], and that Raf [112] and MEK-1 [113] are the intermediaries involved in this pathway.

Recent evidence can be used to suggest ERK may not be the only kinase phosphorylating Fra-1. 90-kDa ribosomal S6 kinase (RSK) has been shown

to phosphorylate the c-terminus of c-Fos (Ser^{362}) [73, 114], and this area shares significant homology within the Fos family, suggesting that Fra-1 may also be a RSK target. RSK is also a downstream target of ERK1/2 and is described as a mediator of ERK signal transduction [115]. Work by Murphy *et al*. [114] has described a novel role for c-Fos in ERK signalling – c-Fos may act as a sensor for ERK1/2 signal duration, and that this role is shared by other Fos members, including Fra-1 [116]. They describe stabilisation of c-Fos by C-terminal phosphorylation by ERK1/2 and RSK in response to growth factor stimulation. This phosphorylation, as well as leading to protein stabilisation, also leads to the exposure of ERK docking DEF (docking site for ERK, F*X*FP) domain which prolongs the duration of activation of ERK. This prolongation then allows the secondary phosphorylation of a further two residues within the C-terminus of c-Fos. Their subsequent work shows that Fra-1 also contains a functionally active DEF domain and that ERK docking here can cause further phosphorylation [116].

Combining all of this data leads to a scheme of activation of Fra-1 as shown in Figure 1.3. Activation of the MEK/ERK pathway, for example by an oncogenic mutation in *ras*, or by stimulation of a growth factor receptor, such as the epidermal growth factor receptor (EGFR) initially leads to increased *c-fos* transcription and c-Fos protein production. This then has three roles. Firstly, c-Fos inhibits its own further transcription. Secondly, it can be phosphorylated by, and dock with ERK1/2 to prolong the activation of ERK1/2. Thirdly, c-Fos can induce *fosl1* transcription, which in turn can, in a positive autoregulatory loop, further induce *fosl1* transcription. The

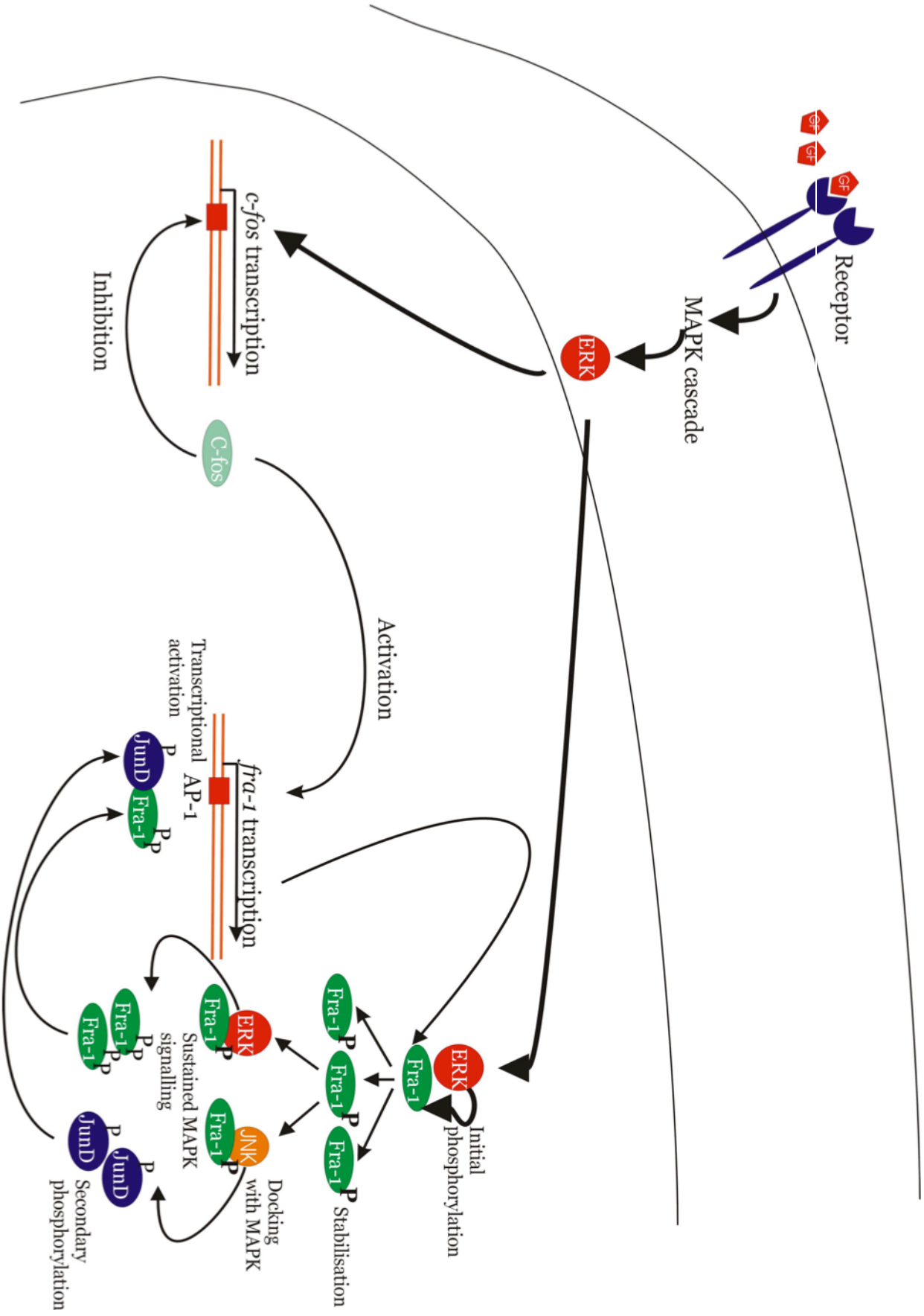

Figure 1.3 Suggested scheme of Fra-1 activation (see Section 1.13 for detailed description).

subsequent Fra-1 protein will also be stabilised by phosphorylation by ERK1/2 and will replace the function of c-Fos in maintaining the ERK1/2 signal duration. All of this then helps to increase and prolong Fra-1 levels, such that they are then further able to activate transcription of various genes involved in the development of the malignant phenotype (see below).

1.14 Fra-1 and the Wnt and Akt signalling pathways

Much work, as described above, has demonstrated the importance of the interaction between Fra-1 and the Ras-Raf-MEK/ERK pathway, but this is not the only intracellular signalling pathway with which Fra-1 is associated. This interaction with multiple intracellular signalling pathways may allow for the phenomenon of cross-talk which has been discussed earlier as a way by which the efficacy of chemotherapeutic compounds is frequently lower than expected from *in vitro* studies.

Signalling via the Wnt/ß-catenin pathway can promote *fosl1* transcription (see review by Kikuchi *et al*. (2006) [117]). In response to the binding of Wnt by its cell surface receptors, ß-catenin accumulates and promotes the activity of the T cell factor/Lymphoid enhancer factor (Tcf/Lef) transcription factor which can lead to the transcription of many genes involved in cellular proliferation and migration, including *fosl1*.

A further signalling pathway already mentioned (Section 1.3) is the PI3K-Akt pathway which has previously been implicated in bladder cancer [30]. This pathway regulates key cellular processes including proliferation and survival

(see review by Osaki *et al*. (2004) [118]) and has been shown to regulate the expression of *fosl1* [119, 120].

1.15 Fra-1 and Epithelial to Mesenchymal Transition

During Epithelial to Mesenchymal Transition (EMT), epithelial cells undergo numerous modifications such that they lose contact with the basement membrane and become more invasive and motile, i.e. take on a mesenchymal phenotype (See review by Kalluri and Weinberg, 2009 [121]). This change is a crucial event in the development of invasive malignancy [122]. Recent data has demonstrated that not only is AP-1 implicated in EMT [123], but that Fra-1 is required for MEK-mediated EMT [124, 125, 126].

1.16 The downstream effect of Fra-1

Apart from the putative role as a sensor for ERK1/2 signal duration, Fra-1 is a transcription factor. To date, many genes have been described as being Fra-1 regulated, and many of these genes encode proteins which have been implicated in tumour cell motility, invasiveness, and angiogenesis.

Many of the genes that have so far been identified as being regulated by Fra-1 are associated with the extracellular matrix. Others include the angiogenic factors VEGF-D, the DNA binding protein HMGI(Y) (high mobility group I(Y)), and the metastasis-associated protein mts1/S100A4. It can therefore been seen that all of them have the potential to play a vital role in tumorigenesis.

Kustikova *et al*. [127] used CSML0 and CSML100 mouse mammary adenocarcinoma cell lines; CSML0 cells having an epithelial morphology which form tight contacts and have low malignant potential, whereas CSML100 cells are more elongated, do not form tight contacts and have a high metastatic potential. In keeping with these differences in morphological appearance, it is shown that CSML0 cells express E-cadherin whilst it is absent in CSML100 cells. It was found in CSML100 cells that Fra-1 was expressed at high levels, whereas in CSML0 cells, Fra-1 was not detectable. They then analysed expression of a number of genes associated with tumour progression, namely E-cadherin, HMGI(Y), mts1 (s100A4), MMP-3 (matrix metalloproteinase-3, MMP-9 (matrix metalloproteinase-9), uPA (urokinase plasminogen activator), uPAR (urokinase plasminogen activator receptor), PAI-1 (plasminogen activator inhibitor type 1), tPA (tissue-type plasminogen activator), and TIMP-1 (tissue inhibitor of metalloproteinases-1). These were all found to be upregulated in CSML100 compared with CSML0 cells. DOX-regulated expression of Fra-1 in CSML0 cells induced HMGI(Y), mts1, uPA, uPAR, and PAI-1 expression, suggesting that in mammary carcinoma cells, these genes are regulated by Fra-1.

It has also been shown that Fra-1 may have a role in protecting against cell death. Vial and Marshall [60] demonstrated that inhibiting Fra-1 expression by siRNA in colorectal cancer cell lines increased levels of anoïkis – the process of apoptosis induced by loss of contact with the extracellular matrix; resistance to anoïkis is a hallmark of cancer cells.

1.17 Fra-1 and cell motility and invasiveness

One important feature of malignant cells is an increase in motility and invasiveness. Transfection of Fra-1 negative CSML0 cells with a full-length Fra-1 construct dramatically enhances the motility of the cells [128]. This increase is dependent on the intact N-terminal domain of Fra-1, and it is even greater than in cells transfected with a c-Fos-expressing construct. A change in morphology in Fra-1 transfected CSML0 cells includes alterations in the cell shape with a polar re-distribution of focal adhesions and fewer stress fibres.

Vial *et al*. [129] examined the mechanisms by which Fra-1 may increase cell motility. They demonstrated that Fra-1 inhibited RhoA via inactivation of ß1-integrin signalling, and that this led to an increase in motility by reducing the amount of stress fibres and destabilising focal adhesions. They did not identify how Fra-1 inhibited ß1-integrin function, but suggested that it could be either through regulation of expression of associated proteins, or by direct interaction with ß1-integrin – which would be an additional novel role for Fra-1. Interestingly, they also describe a second ERK-dependent event in cell motility related to the urokinase-type plasminogen activator receptor (uPAR), whose expression is known to be regulated by Fra-1 [127]. Up-regulation of uPAR resulted in the activation of RAC1 contributing to the lamellipodia extension and enhanced cell motility.

This possible role of direct interaction of Fra-1 with cytoplasmic proteins is further supported by the findings of Fra-1 in the cytoplasm in both thyroid

carcinomas [94] and non-small cell lung carcinoma [92]. Ma *et al*. [92] also reported that although Fra-1 levels were reduced in non-small cell lung cancer compared to normal bronchial epithelium, the Fra-1 that was detected in cancer cells was localised predominantly to the cytoplasm.

Fra-1-mediated enhanced tumour cell migration is often accompanied by increased invasiveness. For example, Kustikova *et al*. [127] showed that Fra-1 expression in CSML0 cells led to a four-fold increase in the number of cells passing through an artificial Matrigel membrane, i.e. cell invasion is controlled by Fra-1 in this cell model.

1.18 Fra-1 and angiogenesis

It is known that Fra-1 is essential for normal placental vascularisation [80], and that absence of Fra-1 leads to growth retardation and intra-uterine death due to defects within the placental labyrinth layer. Therefore, as it is clear that Fra-1 has a role in intra-uterine angiogenesis, it is plausible to speculate that Fra-1 may well have a role in angiogenesis in tumours as well. Indeed, vascular endothelial growth factor D (VEGF-D) is controlled by Fra-1 in a hypervascular tumour, glioblastoma multiforme [100]. In line with these data, in mouse models of melanoma, breast, colon and non-small cell lung cancer, an oral Fra-1 vaccine inhibits tumour formation by inhibiting angiogenesis; thus providing further data that Fra-1 has a role in angiogenesis (See Reisfeld *et al*. [130]).

This now suggests that not only does Fra-1 have a role in the regulation of tumour cell motility and invasion, but that it plays a role in the regulation of tumour angiogenesis. This indicates that Fra-1 is widely implicated in tumorigenesis and is particularly relevant to the metastatic process.

1.19 Fra-1 as a therapeutic target

A discussion about the clinical applications of Fra-1 brings us back to the beginning of this introductory chapter – the need to improve clinical outcomes in the management of all cancers, and not only bladder cancer. The data described above demonstrates that Fra-1 potentially has an exciting role in the management of cancer as it has been shown to be upregulated in a variety of malignancies, and work is in progress (both as the aim of this thesis, and by others) to elucidate its regulatory mechanisms. However, one must also remember that the role of Fra-1 may be dependent on cell type – in many tumours it appears upregulated, but in cervical carcinoma it is downregulated.

Fra-1 is an important downstream effector of Ras-Raf-MEK-ERK signalling. Therefore it can be up-regulated by many cancer-associated events including mutations in different components of the pathway (H-Ras, K-Ras, B-Raf, etc.) or by constitutive activation of molecular pathways upstream of Ras. Moreover, Fra-1 regulates the transcription of a variety of genes implicated in tumorigenesis, and may even prolong the aberrant signal by acting as a sensor for ERK activation. This clearly makes Fra-1 a potential therapeutic target, with strategies such as anti-sense and vaccines possibly being potentially viable.

In fact, the above-mentioned DNA vaccine containing ubiquitinated Fra-1 and IL-18, carried by attenuated *Salmonella typhimurium* has been shown to reduce tumour growth in mice inoculated with D2F2 and 4T1 breast cancer cells or D121 non-small cell lung carcinoma cells, to reduce the growth of established pulmonary metastasis in breast-cancer affected mice, and also to prevent the formation of pulmonary metastasis in mice with breast cancer by decreasing tumour angiogenesis and suppress tumour growth and metastasis [131,132] . In BALB/c mice immunised with the Ub-Fra-1/IL-18 vaccine, following sub-cutaneous injection of D2F2 breast carcinoma cells, 50% were tumour free 77 days later. In those mice immunised with a non-Fra-1/IL-18 vaccine, 100% were dead by around 50 days; those immunised with an IL-18 containing vaccine were all dead by day 60. This effect is mediated via $CD8^+$ T-cells and in addition to reducing the tumour burden when administered to mice with established metastatic disease, also generates a long-lived T-cell memory response; the authors hypothesise that this should give prolonged protection against metastatic disease [131].

1.20 Fra-1 as a biomarker

The term biomarker is often used to refer to a measurable entity that reflects an aspect of a disease or illness. Two commonly used variants of the term biomarker are Prognostic Biomarker and Predictive Biomarker [133]. A Prognostic Biomarker can be used to measure the likely outcome of a disease on an individual, regardless of treatment. A Predictive Biomarker can measure the likely (probable) effect of treatment on a patient.

An example of a prognostic biomarker with respect to bladder cancer, for instance, would be a protein whose levels could be assessed and correlates with a specific outcome, such as death; an example of a predictive biomarker would be a protein whose presence/absence/level would predict the likely response to treatment.

In addition to its potential role as a direct therapeutic target, one other potential clinical application of Fra-1 is that of a biomarker. Potential roles include both a predictive and prognostic biomarker. As Fra-1 is regulated via the Ras-Raf-MEK-ERK pathway that is most frequently hyperactivated in many forms of cancer, it may be possible to utilise Fra-1 to assess the *in vivo* and *in vitro* effects of novel compounds such as the small molecule tyrosine kinase inhibitors and farnesyl transferase inhibitors which modulate signalling along this pathway (see Section 1.3), i.e. a predictive biomarker. This concept could be extended further by suggesting that if Fra-1 was not detected in the original tumour, is there any benefit in using one of these compounds? This general concept of a predictive biomarker is already in use in clinical practice with regard to the management of breast cancer. HER2 (Human Epidermal growth factor Receptor 2, also known as ErbB2) status in breast cancer is assessed either by immunohistochemical staining for HER2 protein or by HER2 gene amplification by fluorescence *in situ* hybridisation; patients with HER2 positive tumours will then be considered for anti-HER2 treatment [134, 135]. Similarly in breast cancer, oestrogen receptor status (ER status) is always assessed immunohistochemically and is used to guide therapy with

either tamoxifen or the aromatase inhibitors exemestane, anastrozole or letrozole in those patients who are ER positive [135].

Fra-1 could also theoretically have a role as a prognostic biomarker. IHC analysis of Fra-1 in tumour tissue may assist the histopathologist in determining the presence or absence of malignancy, or assist in the analysis of histological grade; all features which I have described in Section 1.1.1. as having an established role in predicting likely recurrence or progression rates. One well described example of Fra-1 as a biomarker, in thyroid tissue, shows that the level of Fra-1 expression, and the sub-cellular localisation of Fra-1 changed as tissue underwent malignant change – from being absent in normal thyroid tissue, being expressed only the nuclei in most adenomas, to being present in both the nuclei and cytoplasm of all thyroid carcinoma samples [94].

1.21 Summary and aim of this thesis

There is strong data, described above, to support the further investigation into Fra-1 and its clinical applications. Since Fra-1 has a strong potential for diagnosis, prognosis and treatment in cancer, more work needs to be carried out on the role and regulation of Fra-1 in different cancer types. Though expression of Fra-1 in bladder cancer has not been studied in the past, there are several considerations justifying this research. Firstly, the Ras-Raf-MEK-ERK pathway is likely to be hyperactivated in a proportion of bladder cancers. The underlying mechanisms may involve H-Ras or FGFR3 mutations which are found in many bladder tumours [17, 18, 19]. In

addition, the receptor tyrosine kinases c-Met and EGFR which activate this pathway upstream of Ras are positively associated with bladder cancer aggressiveness, with EGFR status correlating with increasing stage, progression and poorer prognosis [22, 23].

Secondly, urokinase plasminogen activator (UPA), a specific transcriptional target of Fra-1 [127, 136] is associated with a poorer outcome in bladder cancer [137].

In addition, high levels of vascularisation are positively associated with bladder cancer aggressiveness. Fra-1 is essential for normal placental vascularisation [80] and induces expression of genes implicated in angiogenesis [100, 127].

The first part of this thesis examines the presence of Fra-1 in human bladder cancer, both in human tissue and in human cell lines. Within human tissue, the presence of Fra-1 will be investigated and correlated with the tumour stage (i.e. non-muscle invasive and muscle-invasive) and with additional clinical parameters. A panel of human bladder cancer cell lines will then be characterised with regard to Fra-1 status, and with differing characteristics of the cell lines themselves.

The second part of the thesis aims to investigate regulatory mechanisms of Fra-1 within the human bladder cancer cell lines with the focus on the role of the Fra-1 C-terminus. A significant amount of progress has been made in the

understanding of transcriptional and post-translational regulation of c-Fos, including the important roles played by ERK/RSK-mediated phosphorylation of the two C-terminal serines, Ser^{362} and Ser^{374} [71]. There is significant sequence homology between c-Fos and Fra-1 in this region (Figure 1.4). Therefore we suggest a similar mechanism of stabilisation may occur in Fra-1; we will attempt to elucidate the relevant amino acids.

Fra-1	…C^{244}SSAHRKSSSSSGDPSSDPLGSPTLLAL^{271}
c-Fos	…C^{354}AAAHRK-GSSSNEPSSDSLSSPTLLAL^{380}
Fra-2	…S^{299}CSKAHRRSSSSGDQSSDSLNSPTLLAL^{326}
FosB	…V^{311}SAFAGAQRTSGSDQPSDPLNSPSLLAL^{338}

Figure 1.4 Conservation of the C-terminus in members of the Fos family of transcription factors

To elucidate the amino acid(s) involved in stabilisation of Fra-1, initially the role of the C-terminus will be crudely assessed by deleting portions of it. Once crude mapping has been performed, phosphomapping will be used to pinpoint phosphorylated amino acids; PCR-based gene mutation techniques will then be used to confirm the significance of these residues in Fra-1 post-translational regulation. Along with this, the role of the MAP Kinase pathway on the regulation of Fra-1 in bladder cancer cell lines will also be assessed, and the effect of MAP Kinase on the amino acids identified by C-terminal deletion, phosphomapping and amino acid mutation will be examined.

Chapter 2

Materials and Methods

2.1 Cell Culture

2.1.1 Resuscitation of mammalian cells from liquid nitrogen

Stocks of HT1376, J82, RT4, RT112, T24 and UMUC3 bladder cancer cell lines, and CSML0 murine breast carcinoma cell lines already within our department were resuscitated from liquid nitrogen as follows:

Cells were thawed in a 37ºC water bath for 1 minute and then resuspended in 9 ml of pre-warmed medium (DMEM containing 4500 $mg \cdot l^{-1}$ glucose, GlutaMAX I and pyruvate, supplemented with 10% Heat Inactivated Foetal Bovine Serum, 1% MEM Non-Essential Amino Acids and 1% Penicillin (5000 $u \cdot ml^{-1}$) / Streptomycin (5000 $\mu g \cdot ml^{-1}$)).

Cells were then spun down at 350 x *g* for 5 minutes in an ALG PK120R centrifuge, resuspended in 10 ml of media and spun down again; the resulting cell pellet was resuspended in 10 ml of medium and transferred to a 25 cm^2 cell culture flask.

2.1.2 Cell passaging

Cell monolayers were grown to near-confluency in the same medium as 2.1.1 at 37ºC, in 5% CO_2. Cells were then passaged as follows:

Cells were washed once in 1 x PBS (NaCl 8 $g \cdot l^{-1}$, KCl 0.2 $g \cdot l^{-1}$, Na_2HPO_4 1.15 $g \cdot l^{-1}$, KH_2PO_4 0.2 $g \cdot l^{-1}$, pH 7.3 +/- 0.2) and then incubated in Trypsin-EDTA (0.25% trypsin, 1 mM EDTA) for 3 min (J82, RT4, T24, UMUC3, CSML0) or 10 min (HT1376, RT112).

Trypsinisation was suspended by the addition of the standard cell culture medium, and a cell pellet was produced by centrifugation at 350 x *g* for 5 min.

The cell pellet was then resuspended in cell culture medium and seeded at a density of 1:10 (J82, T24, UMUC3, CSML0) or 1:5 (HT1376, RT4, RT112) to achieve confluency in three days.

2.1.3 Freezing cells for liquid nitrogen storage

Cells were trypsinised and centrifuged as in 2.1.2. 2 x 10^6 cells were resuspended in 950 μl of standard cell culture medium and 50 μl DMSO and placed in a sterile cryo-vial. Cells were initially placed at –80ºC for 48 hours in an isopropanol bath, before transfer to liquid nitrogen.

2.2 Transfection of mammalian cell lines using Electroporation

Our laboratory had previously used electroporation as its preferred choice of transfection, and accordingly had gained expertise in this technique. However, we had not previously electroporated bladder cancer cell lines, therefore the protocol for this needed to be optimised.

For optimisation of the electroporation protocol, J82 and RT112 cells were selected (J82 cells having a mesenchymal phenotype, RT112 cells having a epithelial phenotype) and five different electroporation protocols were compared, using pEGFP-C1 (BD Clontech) as the transfected plasmid for visualisation using a Nikon Eclipse TE2000-S epifluorescence inverted microscope, and therefore comparison of the trial protocols.

A near confluent cell monolayer was incubated in fresh standard cell culture medium for three hours. Cells were then harvested using Trypsin-EDTA (as in 2.1.2) and washed twice in 10 ml PBS. Cells were then resuspended in PBS at a concentration of 20 x 10^6 cells·ml^{-1}.

For each condition, 2 x 10^6 cells in 100 μl PBS were mixed with 5 μg pEGFP-C1 in an electroporation cuvette (Biorad GenePulser, 4 mm electrode gap) and incubated on ice for 20 minutes. At the same time, 5 ml standard cell culture medium was placed in a 5 cm cell culture dish, pre-warmed and equilibrated with 5% CO_2 in a cell culture incubator.

The experimental electroporation protocols used for both cell types are shown in Table 2.1.

Condition no.	Voltage	Time or capacitance
1	160 V	15.0 ms
2	110 V	20.0 ms
3	160 V	500 μF
4	110 V	25.0 ms
5	250 V	250 μF

Table 2.1 Trial conditions for optimization of electroporation in bladder cancer cell lines

After electroporation using a GenePulser Xcell™ (Biorad), cells were resuspended in 800 μl pre-warmed medium and heavily triturated. This was then added to the remainder of the 5 ml of medium in a 5 cm dish and incubated overnight.

In J82 cells, the highest transfection efficiency was achieved using the settings 250 V, 250 μF (Table 2.2, Figure 2.1a). In RT112 cells, settings of 160 V, 500 μF gave the highest efficiency (Table 2.3, Figure 2.1b), although 250 V, 250 μF resulted in only marginally lower efficiency. Therefore it was decided that future transfections in all cell lines be performed using 250 V, 250 μF.

Condition no	Voltage	Time or Capacitance	Efficiency (rank)
1	160 V	15.0 ms	Reasonable (3)
2	110 V	20.0 ms	Poor (4)
3	160 V	500 μF	Reasonable (2)
4	110 V	25.0 ms	V. poor (5)
5	250 V	250 μF	V. good (1)

Table 2.2 Efficiency of EGFP transfection using trial conditions in J82 cells

Condition no	Voltage	Time or Capacitance	Efficiency (rank)
1	160 V	15.0 ms	Poor (3)
2	110 V	20.0 ms	V. poor (5)
3	160 V	500 μF	Good (1)
4	110 V	25.0 ms	V. poor (4)
5	250 V	250 μF	Good (2)

Table 2.3 Efficiency of EGFP transfection using trial conditions in RT112 cells

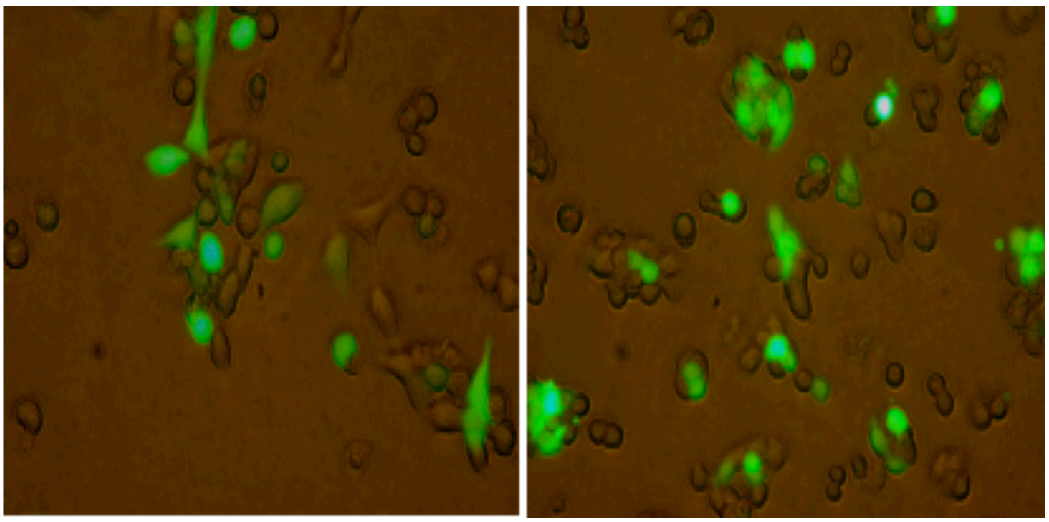

a **b**

Figure 2.1 a,b J82 cells (a) and RT112 cells (b) transfected with pEGFP-C1, using electroporation settings of 250 V, 250 μF

2.3 Amplification of plasmid DNA

2.3.1 Transformation of *E. coli* with plasmid DNA

15 μl of OneShot™ TOP10 Chemically Competent *E. coli* were thawed on ice and mixed gently with 1.5 μg of plasmid DNA. This mixture was then incubated on ice for 40 minutes before cells were then heat shocked for 45 seconds at 42ºC and further incubated on ice for 2 minutes.

200 μl of pre-warmed Luria Broth (10 g Peptone 140, 5 g Yeast Extract, 10 g NaCl per litre) was then added to the reaction and incubated for 1 hour at 37ºC in an Eppendorf Thermomixer, agitating at 300 rpm.

All of the reaction mixture was then evenly spread over LB Agar (10 g Peptone 140, 5 g Yeast Extract, 5 g NaCl, 12 g Agar per litre) plates containing an appropriate selection antibiotic (either Ampicillin 100 $\mu g \cdot ml^{-1}$ or Kanamycin 30 $\mu g \cdot ml^{-1}$) and incubated at 37ºC overnight.

For large scale amplification of plasmids, on the following day a small number of colonies were picked and transferred to 200 ml Luria Broth containing the appropriate selection antibiotic (Ampicillin 100 $\mu g \cdot ml^{-1}$ or Kanamycin 30 $\mu g \cdot ml^{-1}$) and incubated at 37ºC overnight with agitation.

For small scale amplification of plasmids, for example after ligation reactions, a single colony was transferred to 2 ml of Luria Broth containing the appropriate selection antibiotic as above and incubated overnight.

2.3.2 Large-scale purification of plasmid DNA from *E. coli*.

Purification of plasmid DNA from 200 ml overnight cultures of *E. coli* was performed using the QIAfilter Plasmid Maxi kit.

The 200 ml overnight culture was centrifuged at 4000 x *g* in a Sorvall Legend RT centrifuge for 20 minutes at 4ºC. The resultant pellet was resuspended in 10 ml Buffer P1 (50 mM TrisCl pH 8.0, 10 mM EDTA, 100 $\mu g \cdot ml^{-1}$ RNase A) and bacterial lysis was then performed by the addition of 10 ml Buffer P2 (200 mM NaOH, 1% SDS (w/v)). Lysis was performed at room temperature for 5 minutes and then terminated by the addition of 10 ml chilled Buffer P3 (3.0 M potassium acetate, pH 5.5), and incubated for a further 10 minutes at room temperature.

The resultant suspension was then filtered through the QIAfilter Cartridge and the filtrate collected in a QIAGEN-tip 500 column which had previously been equilibrated with QBT Buffer (750 mM NaCl, 50 mM MOPS pH 7.0, 15% isopropanol (v/v), 0.15% Triton™ X-100 (v/v)). The cartridge was washed twice with 30 ml Buffer QC (1.0 M NaCl, 50 mM MOPS pH 7.0, 15% isopropanol (v/v)) and then the DNA was eluted with 15 ml Buffer QF (1.25 M NaCl, 50 mM TrisCl pH 8.5, 15% isopropanol (v/v)).

Eluted DNA was mixed thoroughly with 10.5 ml propan-2-ol and centrifuged at 4000 x *g* for one hour. The resulting pellet was resuspended in 5 ml 70% ethanol (pre-chilled to –20ºC) and then further centrifuged at 4000 x *g* for 10 minutes.

The DNA pellet was redissolved in 400 μl ultra-pure H_2O and then precipitated by the addition of 20 μl 5M NaCl and 1000 μl 96% ethanol. This was centrifuged at 20,000 x *g* for 10 minutes in an Eppendorf 5417R centrifuge and the pellet redissolved in 150 μl ultra-pure H_2O at which time the concentration of DNA was calculated by measuring the absorbance at 260 nm using a Perkin-Elmer Lambda 25 spectrophotometer. The A_{260} value was converted to DNA concentration by multiplying by a factor of 50 and any dilution factor. Plasmid purity was assessed by calculating the A_{260}/A_{280} ratio.

To confirm the presence of the correct plasmid in the amplification, the plasmid was digested with appropriate restriction endonucleases (2.7.2).

DNA solutions were stored at –20ºC.

2.3.3 Small-scale purification of plasmid DNA from *E. coli.*

Purification of plasmid DNA from 2 ml overnight cultures of *E. coli* was performed using the QiaPrep Spin Miniprep kit.

The 2 ml overnight cultures were placed on ice and then thoroughly mixed using a Vortex Genie (Scientific Industries). An 800 μl aliquot was then centrifuged at 20,000 x *g* for 1 minute at 4ºC and the resulting pellet resuspended in 250 μl Buffer P1 (50 mM TrisCl pH 8.0, 10 mM EDTA, 100 $\mu g \cdot ml^{-1}$ RNase A) until no cell clumps were visible. Lysis was performed by the addition of 250 μl Buffer P2 (200 mM NaOH,

1% SDS (w/v)) and inverting the mixture 4-6 times until it became viscous and slightly clear, allowing it to proceed for a maximum of five minutes. Lysis was terminated by the addition of 350 μl Buffer N3 (Proprietary buffer, composition not published). The mixture was then centrifuged at 20,000 x *g* for 10 minutes and the supernatant transferred to a QiaPrep column which was then centrifuged at 20,000 x *g* for 1 minute. The column was washed with 750 μl Buffer PE (Proprietary buffer, composition not published) and centrifuged at 20,000 x *g* for 2 minutes (pausing at 1 minute to discard the filtrate).

DNA was eluted by the addition of 50 μl ultra-pure H_2O to the column, allowing it to stand for 1 minute at room temperature and then centrifuging for 1 minute at 20,000 x *g*. To confirm the presence of the correct plasmid in the amplification, the plasmid was digested with appropriate restriction endonucleases (2.7.2).

The DNA was then ready for downstream applications and stored at -20ºC.

2.4 Isolation of RNA using acidic phenol

A 70-80% confluent monolayer of approximately $4x10^6$ cells was washed twice with 20 ml PBS; all PBS was aspirated.

2 ml TRIzol® Reagent (phenol and guanidine isothiocyanate) was applied to the monolayer and a cell scraper was then used to facilitate cell disruption.

The resulting mixture was transferred to a fresh tube on ice and 400 μl 24:1 chloroform:isoamyl alcohol added and mixed vigorously for 20 seconds. The mixture was allowed to stand on ice for 5 minutes and then centrifuged at 4000 x *g* for 20 minutes, 4ºC. The upper phase containing RNA was transferred to a fresh tube and 2.5 ml 96% ethanol added and mixed. This was then stored at –20ºC overnight before being centrifuged at 4000 x *g* for 20 minutes, 4ºC. The pellet was resuspended in 150 μl ultra-pure H_2O and RNA precipitated by the addition of 7.5 μl 5mM NaCl and 380 μl 96% ethanol followed by centrifugation at 20,000 x *g* for 10 minutes, 4ºC. The RNA pellet was resuspended in 100 μl ultra-pure H_2O and the concentration calculated as for DNA (Section 2.3.2, but a multiplication factor of 40 used rather than 50 as for DNA).

To assess the quality and to confirm the concentrations of the isolated mRNA, gel electrophoresis was performed. 10 μg RNA was mixed with 20 μl RNA loading buffer (95% de-ionised formamide, 0.025% bromophenol blue, 5 mM EDTA pH 8.0, 0.025% sodium dodecyl sulphate and ethidium bromide (10 $\mu g \cdot ml^{-1}$)) and heated at 65ºC for 10 minutes. This was then loaded onto a 1.2% agarose, 6.4% formaldehyde in 1 x MOPS buffer (20 mM MOPS pH 7.0, 8 mM Na acetate, 1 mM EDTA pH 8.0) gel and electrophoresed at 80 V in 1 x MOPS buffer for approximately 30 minutes to allow resolution of RNA bands on exposure to UV light (365 nm).

RNA solutions were stored at –20ºC.

2.5 cDNA generation from mRNA

Three different techniques were employed to generate cDNA from mRNA. The first technique combined cDNA synthesis and PCR amplification of cDNA in one step to generate amplified cDNA fragments. The second and third techniques used Superscript III Reverse Transcriptase to generate a cDNA template for later use in PCR reactions.

2.5.1 Single step PCR amplification from mRNA

This technique employed the GeneAmp EZ *rTth* RNA PCR Kit.

A reaction mixture was created containing 25 μl H_2O, 10 μl 5xEZ buffer (Proprietary: 25 mM Bicine, 115 mM potassium acetate, 8% w/v glycerol, pH 8.2), 5 μl dNTP (2.5 mM stock), 5 μl MnOAc (25 mM stock), 2 μl 5' primer (10 μM stock), 2 μl 3' primer (10 μM stock) and 5 μg mRNA. This was then placed in a pre-heated GeneAmp 2400 PCR machine and 2 μl *rTth* DNA polymerase was added.

A typical PCR program for this reaction would be:

RT first step	T_mºC	30 min	
Pre-PCR	94ºC	1 min	x 1 cycle
	66ºC	1 min	
	72ºC	2 min	
PCR	94ºC	20 sec	x 30 cycles
	72ºC	2 min	
Final step	72ºC	7 min	

This technique was used in the early attempts to generate a Fra-1 expression vector. However, the resulting vectors contained several point mutations, therefore it was abandoned for a two stage technique (Section 2.5.2) using separate reverse transcription and PCR steps (Section 4.1).

2.5.2 Generation of cDNA from RNA using SuperScript III Reverse Transcriptase

Following early unsuccessful attempts at creation of Fra-1 expression vectors, it was decided to employ separate reverse transcription and PCR steps to increase fidelity; SuperScript III Reverse Transcriptase (RT) was therefore chosen because of its high fidelity.

3 μg RNA, 7 μl H_2O, 20 pmol oligonucleotide and 4 μl of dNTPs (1 μl each of 10 mM dATP, dCTP, dGTP and dTTP) were incubated at 65ºC for three minutes, then cooled on ice for one minute. 4 μl 5 x First Strand Buffer (supplied with SuperScript III Reverse Transcriptase), 1 μl DTT, 1 μl RNA secure (pre-diluted to 4% in H_2O) and 1 μl SuperScript III Reverse Transcriptase were then added to the reaction. The complete mixture was then subjected to the following thermal profile:

55ºC 60 min
70ºC 15 min
-20ºC thereafter

The product was then stored at -20ºC until needed for downstream applications.

2.5.3 Generation of cDNA from RNA using SuperScript III Reverse Transcriptase – refined method

Following early usage of SuperScript III Reverse Transcriptase in our laboratory, the protocol was refined, both for increased yield and ease of use.

0.75 μg RNA, 3 μl H_2O and 1 μl random hexamers (50 units of $pd(N)_6$ Na salt) were heated for 3 minutes at 90ºC in the PCR machine. This reaction was then briefly centrifuged and placed on ice.

14.3 μl of a stock mixture for reverse transcriptase containing the following was then added:

200 μl	5x First Strand Buffer (supplied with Reverse Transcriptase)
10 μl	100mM dATP
10 μl	100mM dCTP
10 μl	100mM dTTP
10 μl	100mM dGTP
10 μl	dithiothreitol (0.1M)
445 μl	H_2O
20 μl	RNase inhibitor (RNA Secure)

1 μl SuperScript III RT was then added and the complete mixture subjected to the following thermal profile:

23ºC	10 min
50ºC	50 min
95ºC	10 min

The cDNA produced was then stored at –20ºC until used for subsequent PCR reactions.

2.6 Polymerase Chain Reaction

During this project, four general PCR methods were employed. The first is described in Section 2.5.1, i.e. a combined reverse transcription/PCR reaction, but this was abandoned due to problems with poor fidelity.

The second method used to create a Fra-1 expression vector (Section 4.1) utilised *Taq* polymerase and a pre-generated cDNA template (Section 2.5.2); this resulted in a Fra-1 vector which still had some, but fewer mutations.

Because of the presence of mutations after using *Taq* polymerase, the third PCR method used utilised the high-fidelity *Pfu* polymerase.

The fourth PCR method, using Reddymix Extensor PCR Master Mix 1 was used for rtPCR-based analysis of gene expression in bladder cancer cells, and was chosen for its ease of use, and because fidelity was not as important here.

Following PCR, the reaction mixture was subjected to electrophoresis in a 1.2% agarose + ethidium bromide gel. This gel was composed of 1.2% agarose in 1x TBE buffer (0.089 M Tris Base, 0.089 M Boric Acid, 0.002 M EDTA, pH 8.3) and contained ethidium bromide 0.1 $\mu g \cdot ml^{-1}$. Prior to loading, an aliquot of the reaction was mixed with 1/5th volume of DNA gel loading

buffer (50 mM Tris-Cl, 50 mM EDTA, 0.025% bromophenol blue, 60% glycerol. This was then subjected to electrophoresis in 1x TBE buffer at 80 V for a duration determined by the size of the fragment, to ensure good resolution.

2.6.1 PCR using *Taq* polymerase

Taq polymerase was used to increase the fidelity of PCR reactions, and we also utilised a hot start using wax. A typical reaction would contain:

Upper:
- 3.75 μl 10x *Taq* buffer
- 10 ng cDNA
- 0.8 μl *Taq* polymerase
- ≈32 μl H_2O

Lower:
- 1.25 μl 10x *Taq* buffer
- 5 μl dNTPs (2.5mM stock)
- 1 μl 3' primer (10μM stock)
- 1 μl 5' primer (10μM stock)
- 4.25 μl H_2O

The two phases would be separated by a single bead of Ampliwax® PCR Gem 50, and then placed in a pre-heated PCR machine.

A typical program would be:

94ºC	2 min
T_m+2ºC	30 sec
72ºC	2 min
94ºC	20 sec } x 30 cycles
72ºC	2 min }
72ºC	7 min

where T_m is calculated using the formula

$$69.3 + \frac{(41 \times CG)}{\text{length}} - \frac{650}{\text{length}}$$

(CG = number of C or G residues in the primer)

(length = annealing length of primer)

2.6.2 PCR using *Pfu* polymerase

Taq polymerase was used in our early attempts to create a Fra-1 expression vector with separate Reverse Transcriptase/DNA polymerase steps, and resulted in mutations being present in the *fosl1* insert. To further increase the fidelity of the PCR reaction, thereby reducing the likelihood of introducing mutations, we elected to use *Pfu* polymerase.

The reaction mixture was the same as for *Taq* polymerase (Section 2.6.1), apart from 1 μl *Pfu* (2.5 units) was added and the volume of water in the upper phase adjusted accordingly.

A typical program would be:

94ºC	45 sec	
94ºC	45 sec	x 30 cycles
T_m+2ºC	45 sec	
72ºC	60 sec	
72ºC	10 min	

The DNA produced was then stored at –20ºC.

2.6.3 PCR using Reddymix

For ease of use, for applications where fidelity was less important, Reddymix Extensor PCR Master Mix 1 was used (10 μl containing 350 μM each dNTP, 2.25 mM $MgCl_2$, 1.25 units total DNA polymerases (proprietary mix).

The reaction mixture would contain:

10 μl	Reddymix Master Mix 1
4 μl	3' primer (1μM stock)
4 μl	5' primer (1μM stock)
2 μl	template (≈ 10 ng cDNA)

A typical program would be:

94ºC	3 min	
94ºC	20 sec	x 30 cycles
T_m+2ºC	45 sec	
72ºC	60 sec	
72ºC	10 min	

The DNA produced was then stored at –20ºC.

2.6.4 Primer design and sourcing

Oligonucleotide primers were designed following acquisition of cDNA, mRNA and protein sequences for the relevant genes/proteins from Pubmed Entrez Gene, Pubmed Entrez Nucleotide and Pubmed Entrez Protein (National Center for Biotechnology Information, National Library of Medicine and National Institutes of Health, http://www.ncbi.nlm.nih.gov/). Oligonucleotides were generated from this information, with length and T_m characteristics being chosen

depending on application. The oligonucleotides were then purchased from Sigma-Genosys and supplied as dry desalted powder. These were then reconstituted to a stock concentration of 100 μM with milli-Q water according to the manufacturers instructions, and stored at –20ºC.

2.7 Cloning of PCR fragments into expression vectors

2.7.1 Phenol/chloroform extraction of DNA insert

Following amplification, the DNA was purified using phenol/chloroform extraction. 35 μl of PCR product was added to 7 μl H_2O, 1 μl tRNA, 2 μl 0.5M EDTA, 25 μl phenol pH 8, 25 μl 24:1 chloroform/isoamyl alcohol. This was then mixed and centrifuged for 3 minutes at 20,000 x *g*, 4ºC. The upper phase was then transferred to 2.5 μl 5M NaCl, 130 μl 96% ethanol, mixed, incubated at –20ºC for 20 minutes and then centrifuged for 15 minutes at 20,000 x *g*, 4ºC.

The remaining pellet was resuspended in 20 μl H_2O, 1 μl 5M NaCl, 55 μl 96% ethanol, mixed and centrifuged for 15 min at 20,000 x *g*, 4ºC. The pellet was then redissolved in 12 μl H_2O for further use.

2.7.2 Endonuclease digestion of DNA

During this project, endonuclease digestion of DNA was performed for two main reasons. Firstly it was used to prepare DNA for insertion into expression vectors and secondly it was used to confirm the presence of the correct vector following amplification of DNA (Section 2.3). Both applications used the same protocol, which varied slightly according to the restriction endonucleases used.

In general, the reaction was as follows:

1.5 μl 10x reaction buffer
1 μl Reaction endonuclease 1
1 μl Reaction endonuclease 2
11.5 μl H_2O + DNA

This reaction was allowed to proceed at 37ºC for 1-2 hours depending on the application. The amount of H_2O and DNA was varied to obtain similar amounts of DNA per reaction.

2.7.3 Elution of DNA fragments from agarose gel

Following digestion, the reaction was subjected to agarose gel electrophoresis (Section 2.6). When the electrophoresis had been run for an adequate time to allow good resolution of fragments, the gel was exposed to UV light at a wavelength of 365 nm to visualise the fragments. DNA was eluted from the agarose gel using the QIAquick Gel Extraction Kit. A gel slice containing the DNA was excised and added to three volumes (by weight) of Buffer QG (proprietary buffer containing guanidium thiocyanate). This was then incubated at 50ºC for 10 minutes until completely dissolved. The dissolved DNA/gel mixture was then transferred to a DNA binding column provided in the kit and then centrifuged 13,000 x *g* for 1 minute. The column was washed with 750 μl buffer PE (proprietary buffer, composition not published) and centrifuged again at 13,000 x *g* for 2 minutes (removing the filtrate after 1 minute). DNA was eluted by the addition of 50 μl H_2O and the column centrifuged for at 13,000 x *g* for 1 minute.

To confirm successful elution, and estimate the relative amounts of DNA recovered, an aliquot of the eluted DNA was then subjected to agarose gel electrophoresis (Section 2.6).

2.7.4 Ligation of DNA fragment into expression vector

The prepared expression vector and insert were then ligated using T4 DNA ligase. A reaction mixture was made containing 1.5 μl 10x T4 DNA ligase reaction buffer, 200 units T4 DNA ligase and vector and insert to 15 μl with ratio 1:3 determined by prior gel electrophoresis. This was then incubated overnight at 16ºC.

Following this, 7.5 μl of the reaction was subjected to agarose gel electrophoresis (Section 2.6) to assess ligation efficiency.

After successful ligation, *E. coli* were transformed with 1.5 μg of the ligation reaction (Section 2.3.1) and then purified using the small-scale technique (Section 2.3.3). Isolated DNA was then digested with appropriate restriction endonucleases to confirm the presence of the desired DNA fragment; if present, the DNA was sent for DNA sequencing at the Protein and Nucleic Acid Chemistry Laboratory, University of Leicester. For sequencing, 10 μl of DNA at a concentration of 62.5 ng/μl were required per reaction. Depending on the nature of the DNA being sequenced, between one and three reactions were required to fully cover the area of interest. Sequencing data was returned in two

forms, one a text file and one containing the raw data (in .seq format). When comparing predicted with actual sequences, if any variation was noted, the raw data was viewed, using Chromas v. 1.4.5 (http://www.technelysium.com.au/chromas145-95.zip) to determine whether the variation was real or artifactual from an incorrect automated conversion from the raw data. If the sequence was then confirmed to be correct, a large-scale amplification was made to allow the DNA to be used further.

2.8 Protein Detection - Western Blotting

2.8.1 Whole cell protein lysis

Cell monolayers were washed twice with PBS and cells were then lysed in 1x SDS gel loading buffer (50 mM Tris Base pH 6.8, 2% SDS (w/v), 10% glycerol), the volume determined by the degree of confluency and the size of the monolayer. Typical volumes would be 150 μl for one well of a 6-well plate, 300 μl for a 5 cm diameter dish and 500 μl for a 25 cm^2 cell culture flask.

Cells were the scraped with a cell scraper, the lysate transferred to a screw-topped vial and boiled for 15 min before being placed on ice.

2.8.2 Whole cell protein lysis for alkaline phosphatase treatment.

Subconfluent cell monolayers in 5 cm diameter dishes were washed twice with PBS. Cells were then lysed in 300 μl of CIP lysis buffer (50 mM Tris pH 7.4, 150 mM NaCl, 3 mM $MgCl_2$, 0.5% NP-40, 1 mM PMSF,

10 μg·ml^{-1} aprotinin, 10 μg·ml^{-1} leupeptin) by incubation for 10 minutes on ice. Cells were then scraped, the lysate collected and cleared by repeated aspiration through a 25 gauge needle. Lysate protein concentrations were then calculated using the BCA assay (Section 2.8.3).

2.8.3 Protein concentration measurement

Protein concentrations of the lysates generated from Section 2.8.1 were measured using the BCA™ Protein Assay Kit (Pierce), which utilises colorimetric detection at 560 nm of the Cu^{+} cation by bicinchroninic acid, the Cu^{+} cation being produced by the reduction of the Cu^{2+} cation by protein when in alkaline conditions.

A standard control curve was created for each individual assay using Bovine Serum Albumin (supplied with the kit) in concentrations between 0 and 2000 μg·ml^{-1}.

15 μl of sample or control was placed into one well of a 96-well transparent microplate and then 200 μl of working reagent (50:1 Reagent A:Reagent B) was added. The plate was agitated for 45 seconds and then incubated at 37ºC for 30 minutes. The plate was then allowed to cool to room temperature and any bubbles were removed using a 25 gauge needle.

Absorbance at 560 nm was then measured using a Tecan GENios Microplate reader. Protein concentrations were then calculated from the standard curve using GraphPad Prism.

Following successful protein concentration measurement, 1:40 volume of 4% bromophenol blue and 1:40 volume of 14M ß-mercaptoethanol were added to the protein lysate.

2.8.4 Calf intestinal phosphatase (alkaline phosphatase) treatment of protein lysates

10 units of calf intestinal phosphatase (CIP) were added to 20 μg of protein lysate and 10% 10x reaction buffer (NEBuffer 3 – 1x contains 100 mM NaCl, 50 mM Tris-HCl, 10 mM $MgCl_2$, 1 mM Dithiothreitol, pH 7.9). Samples were incubated at 37ºC for one hour to allow protein dephosphorylation.

A control sample is processed in parallel, being kept on ice for one hour, instead of at 37ºC.

The reaction is then terminated by the addition of 2x SDS gel loading buffer (Section 2.8.1) and boiling for 15 minutes, where it can then exposed to SDS-PAGE gel electrophoresis.

2.8.5 SDS-PAGE Protein Gel Electrophoresis

SDS-PAGE gels were made in our laboratory. For resolution of Fra-1, typically 10% resolving gels were prepared (10% acrylamide (Acrylogel 30), 0.375M Tris pH 8.8, 0.1% SDS, 0.1% ammonium persulphate, 0.04% TEMED). Stacking gels were prepared containing 5% acrylamide, 130 mM Tris pH 6.8, 0.1% SDS, 0.1% ammonium persulphate, 0.1% TEMED.

20 μg of protein lysate was boiled for 1 minute prior to loading. When loaded, electrophoresis at 120V was performed in a Tris-Glycine buffer (25 mM TRIS Base, 250 mM glycine, 0.1% SDS)

2.8.6 Transfer of electrophoresed proteins to PVDF membrane

After gel electrophoresis, proteins were transferred to Immobilon-P PVDF transfer membrane (0.45 μm pore-size). A "sandwich" was constructed with three layers of 3MM Whatman Chromatography paper soaked in 1x Blotting Buffer (50 mM Tris Base, 40 mM glycine, 0.04% SDS, 20% methanol, followed by the activated PVDF membrane (membrane is activated by immersion in methanol and then is washed in 1x Blotting Buffer), the SDS-PAGE gel and finally three more layers of wet 3MM Whatman Chromatography paper (Figure 2.2). This sandwich was then placed in the blotting apparatus and the transfer was performed using a constant current of 200 mA for 90 minutes (duration varied according to the molecular weight of the protein of interest).

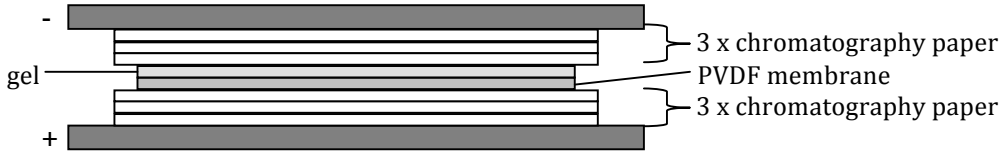

Figure 2.2 Schematic representation of 'sandwich' for blotting transfer of proteins from an SDS-PAGE gel to PVDF transfer membrane

Following transfer, the membrane was removed and stained with Ponceau S solution for 5 minutes before washing several times with H_2O to remove unbound stain. The membrane was then allowed to dry before further use.

2.8.7 Antibody detection of proteins following membrane transfer

Dried membranes were reactivated by immersion in methanol. Following this, non-specific binding was blocked by incubation at room temperature in 5% dried skimmed milk powder in TBS-T (18 mM Tris Base pH 8.0, 125 mM NaCl, 0.09% TWEEN-20) for one hour.

The primary antibody was diluted in 5% dried skimmed milk powder in TBS-T to a concentration recommended by the manufacturer; membranes were then incubated in the primary antibody for one hour at room temperature. The primary antibody was then removed and the membrane washed four times for ten minutes each in TBS-T before incubation in the secondary antibody was performed for 45 minutes (secondary antibody diluted according to the manufacturer's instructions in 5% dried skimmed milk powder in TBS-T). The membrane was then washed again four times in TBS-T for 10 minutes.

For detection of bound antibody, two different proprietary kits were used depending on the level of signal generated. For routine use, membranes were incubated for between 20 seconds and five minutes in ECL Western Blotting Detection Reagent at 0.125 ml of working solution per cm^2 of membrane, and then exposed to Kodak Biomax film for a duration long enough to generate an adequate signal. For experiments where the signal intensity was lower, SuperSignal® West Femto Maximum Sensitivity Substrate was used instead of ECL for between 20 seconds and 30 minutes at 0.125 ml of working solution per cm^2 of membrane prior to exposure to Kodak Biomax film. The film was the developed using an X-ograph CompactX2 automated developer (X-ograph imaging systems).

2.8.8 Stripping of membranes

Following detection of first protein of interest, membranes would be stripped of antibody before being re-probed for a second protein of interest.

To strip membranes, they were incubated for 30 minutes at 60ºC in Stripping Buffer (0.1M ß-mercaptoethanol, 2% SDS, 62.5mM Tris pH 6.8), before being washed four times for 10 minutes each in TBS-T.

2.9 Immunocytostaining

2.9.1 Fixation and permeabilisation of cells

Cells growing on either 18 mm coverslips or on 8 chamber tissue culture slides, were fixed when they had reached the required density. To fix cells, there were first washed twice in PBS and then incubated at room

temperature for 10 minutes in 4% paraformaldehyde. The paraformaldehyde was then removed, cells were washed twice in PBS and then the cells were permeabilised by incubating in 0.5% Triton-X 100 for 90 seconds. Finally, cells were washed three times for five minutes each in PBS.

2.9.2 Immunocytostaining

Cells that had been fixed and permeabilised as in Section 2.9.1 were then immunocytostained. This was performed by incubating the cells at room temperature for one hour in primary antibody diluted either according to manufacturer's recommendations or according to our titration, in D-MEM cell culture medium containing 10% foetal calf serum as used for cell culture work (Section 2.1.1). Following incubation with primary antibody, cells were washed three times for five minutes each in PBS, and then incubated at room temperature for one hour with secondary antibody (Alexa Fluor® 594 goat anti-rabbit IgG or Alexa Fluor® 488 donkey anti-mouse IgG) at a dilution of 1:1000 in D-MEM + 10% foetal calf serum.

Cells were then washed three times further for five minutes in PBS, but with the second wash containing DAPI 1:20,000.

After washing, the coverslip or slide was dried and covered with a coverslip, sealing with Fluoromount-G.

To view the immunocytostaining, slides were viewed either on a Nikon Eclipse TE2000-S epifluorescence inverted microscope or a Zeiss Confocal microscope. Excitation and emission wavelengths for the two antibodies are:

Alexa Fluor® 488 donkey anti-mouse
Excitation wavelength 495 nm
Emission wavelength 519 nm

Alexa Fluor® 594 goat anti-rabbit
Excitation wavelength 590 nm
Emission wavelength 617 nm

Images from the epifluorescence microscope were viewed and manipulated in Adobe Photoshop CS3 and images from the confocal microscope were viewed and manipulated using LSM Image Browser.

2.10 Immunohistochemistry

Fra-1 immunohistochemistry was performed by Mr Richard Edwards, MRC Toxicology Building, University of Leicester and Dr Raj Pal, Leicester General Hospital, University Hospitals of Leicester NHS Trust. Slides were reviewed by Dr Peter Greaves (Senior Lecturer, University of Leicester).

Briefly, sections were dewaxed and rehydrated by immersion in Xylene for five minutes each, before immersion in IMS (100% IMS for three five minute washes, then one five minute wash in 70% IMS). Sections were then gently washed under distilled water for eight minutes.

Antigen retrieval was performed by placing sections in an antigen retrieval solution (0.01M citric acid, pH 6.0) and heated for 30 minutes in a microwave at 700 watts, in a pressure cooker. Sections were then washed three times for three minutes in distilled water. Endogenous peroxidase activity was blocked by incubation for 20 minutes in hydrogen peroxide (33 ml 30% H_2O_2 (w/w) in 300 ml H_2O), before washing again twice for five minutes in distilled water.

For staining with primary antibody (Fra-1 #sc-605, Lot #C1604 Santa Cruz Biotechnology Inc.), slides were washed twice in PBS and then incubated in primary antibody diluted 1:50 for 3 hours at room temperature; slides were then washed three times with PBS. Negative controls were incubated with Normal rabbit IgG (DAKO X-0903) diluted 1:50 for 3 hours at room temperature.

The primary antibody/antigen complex was then detected using the DAKO Duet System (K-0492). This system involves incubation in a biotinylated goat anti-mouse/rabbit antibody solution diluted 1:100 in PBS for 30 minutes, with unbound antibody then being removed by washing three times with PBS. Incubation in the tertiary antibody supplied with the kit (streptavidin biotin complex/horseradish peroxidase) diluted 1:100 in PBS is then carried out for 30 minutes.

Detection was then performed by adding freshly made 3,3'-diaminobenzidine (500 $\mu g \cdot ml^{-1}$ in PBS with 1:10,000 hydrogen peroxide) for five minutes, then washing with PBS, then H_2O.

Slides were then stained with Haematoxylin (Gill's Haematoxylin, Sigma), washed with H_2O, and destained with Acid Alcohol (1% hydrochloric acid in 70% IMS), and washed again with H_2O for five minutes.

Finally, slides were immersed once in 70% IMS for 5 minutes, then three times in 100% IMS for five minutes each, followed by xylene, again three times for five minutes each before mounting with DPX.

Analysis of the IHC slides was performed by Dr Peter Greaves, Consultant Histopathologist. Fra-1 staining for the specimen was rated as negative (0), minimal (+), moderate (++) or marked (+++). Statistical analysis using SPSS with bivariate testing was then performed against the various pathological and clinical parameters available, and the appropriate statistical test applied to assess statistical significance (see Chapter 3).

2.11 Identification of Phosphorylation Sites using Phosphomapping

2.11.1 Labelling proteins with ^{32}P-orthophosphate

J82 cells were transfected with 7.5 μg HA-Fra-1 construct per 2 x 10^6 cells (Section 2.2), and seeded at a density of 4 x 10^6 cells per 75 cm^2 cell culture flask. Cell were allowed to grow for 24 hours in DMEM containing 10% foetal calf serum (Section 2.1.1) before being washed three times in PBS and incubated in serum-free DMEM (as per Section 2.1.1, but lacking serum) overnight.

On the day of labelling, cells were washed three times in pre-warmed phosphate-free Krebs Buffer (KHB) (118.4 mM NaCl, 9.99 mM HEPES, 4.69 mM KCl, 1.18 mM $MgSO_4.7H_2O$, 4.17 mM $NaHCO_3$, 1.29 mM $CaCl_2.2H_2O$, 9.99 mM Glucose). They were then incubated for one hour at 37ºC in phosphate-free KHB.

^{32}P-labelling was then performed by incubating the cells for two hours in phosphate-free KHB (3.5 ml per flask) with 1.66 mCi of ^{32}P-orthophosphate. Thirty minutes into the incubation, Epidermal Growth Factor (EGF) was added to a concentration of 100 ng·ml^{-1}.

2.11.2 Immunoprecipitation of phospholabelled proteins

After ^{32}P-labelling the labelling media was aspirated and cells washed twice in PBS. 1 ml of RIPA buffer (10 mM Tris/EDTA 2 mM, pH 7.4, 160 mM NaCl, 1% NP40, 0.5% deoxycholic acid) was added and this then left on ice for 10 minutes. The cell monolayer was then scraped with a cell scraper before the lysate was collected and transferred to a microtube. The lysate was then centrifuged at 20,000 x *g* for 3 minutes at 4ºC and then the pellet discarded.

Immunoprecipitation of HA-tagged Fra-1 was then carried out. Anti-HA antibody (12CA5, Roche) was diluted 1.2 μg in 100 μl TEG buffer (10 mM Tris/5 mM EDTA pH 7.4, 20 mM ß-glycerophosphate) and incubated at +4ºC for one hour. 180 μl Protein A Sepharose beads (from

a stock of 5 g Protein A Sepharose in 50 ml 10 mM Tris/2 mM EDTA pH 7.4) was then added and samples incubated for 45 minutes at +4ºC.

Incubated samples were the centrifuged briefly to allow the Sepharose beads to form a pellet. The supernatant was aspirated and then the beads washed three times with 1 ml TEG buffer. After the final wash, the washing buffer was thoroughly aspirated and then bound antibody-antigen complex was eluted by the addition of 1 x SDS gel loading buffer (Section 2.8.1) with 1:40 volume of 4% bromophenol blue and 1:40 volume of 14M ß-mercaptoethanol added. Samples were then thoroughly mixed, heated to 60ºC for 5 minutes and then centrifuged at 20,000 x *g* for 5 minutes.

2.11.3 Gel Electrophoresis and transfer of phospholabelled proteins to Nitrocellulose Transfer Membrane

Samples were then subjected to SDS-PAGE electrophoresis (Section 2.8.3.) on a 10% gel. At the completion of electrophoresis, the resolved proteins were transferred to Protran Nitrocellulose Transfer Membrane (0.45 μm) using BioRad apparatus for 50 minutes at 350 mA in Blotting Buffer C (10 mM $NaHCO_3$, 3 mM Na_2CO_3, 10% methanol, 0.05% SDS).

After blotting, the membrane was transferred to an X-ray exposure cassette, being kept wet with 0.5% PVP solution (0.25 g polyvinylpyrrolidone (average molecular weight 40 kDa) in 0.6% acetic

acid). Exposure to Hyperfilm MP was performed at –80ºC overnight, and the film then developed as per Section 2.8.5.

2.11.4 Trypsin Cleavage of phosphoproteins

After developing the autoradiograph, the film was superimposed on the membrane and the HA-Fra-1 bands excised from the membrane; the excised pieces of membrane then being incubated for 30 minutes at 30ºC in 0.5% PVP.

Membrane segments were then washed three times in 500 μl ultra-pure H_2O, washed in 500 μl 50 mM NH_4HCO_3 and then trypsinisation was performed by adding 2 μg sequencing grade trypsin, 0.5 mM $CaCl_2$ in 200 μl 50 mM NH_4HCO_3 and incubating overnight with agitation at 30ºC.

Following trypsinisation, the membranes were washed with ultra-pure H_2O and samples dried using an Eppendorf Concentrator 5301. They were then resuspended in 50 μl pH 1.9 Electrophoresis Buffer (Formic acid 2.2% v/v, Acetic acid 7.8% v/v in milliQ water) before drying again.

2.11.5 Two-dimensional thin layer chromatography of phosphopeptides

Dried phosphopeptide samples from Section 2.11.4 were resuspended in 8 μl pH 1.9 Electrophoresis Buffer and applied to a 20 x 20 cm cellulose-coated thin-layer chromatography (TLC) plate in 0.4 μl aliquots. When loaded, the entire plate was made wet by placing 3MM Whatman Chromatography paper soaked in pH 1.9 Electrophoresis Buffer before

placing on the Hunter Thin Layer Peptide Mapping Electrophoresis System (Model HTLE-7002). The first dimension (electrophoresis) was performed at 2,000 V in pH 1.9 Electrophoresis Buffer for 30 minutes.

Prior to the second dimension, the TLC plate was removed from the electrophoresis apparatus and allowed to dry. The second dimension (chromatography) was performed in 50 ml isobutyric acid buffer (62.5% isobutyric acid, 4.8% pyridine, 2.9% acetic acid, 1.9% n-butanol overnight. When the chromatography was completed, plates were allowed to dry before being wrapped in Saranwrap and exposed to the PhosphorImager Screen for a suitable duration to produce an acceptable signal. Following exposure, the PhosphorImager screen was then scanned using a Storm 820 scanner and the image analysed using ImageQuant TL software.

2.11.6 Edman degradation of phosphopeptides

Phosphopeptides were identified on the 2D TLC plate by overlaying either the film or the PhosphorImager image onto the plate and circumscribing the area of interest. The selected area of the TLC plate was then scraped off and transferred to a microtube.

The phosphopeptide was eluted from the cellulose by firstly adding 100 μl pH 1.9 Electrophoresis buffer (Section 2.11.4), mixing well and then centrifuging at 10,000 x *g* for 3 minutes. The supernatant was then transferred to a second microtube and the remaining pellet was washed

with a further 100 μl pH 1.9 Electrophoresis buffer, centrifuged again and the supernatant added to the second tube.

The eluted phosphopeptide was then dried and then resuspended in 20 μl of 30% Acetonitrile, 0.1% Trifluoroacetic acid (both Sigma).

The resuspended phosphopeptide was then bound to a Sequelon-AA disc by placing the entire sample, in small aliquots, onto the disc heated to 55ºC, the disc itself sitting on a Mylar sheet supplied with the Sequelon-AA kit. Binding is then performed by adding 5 μl coupling buffer (10 $mg \cdot ml^{-1}$ carbodiimide (carbodiimide supplied with the Sequelon-AA disc kit) in 0.1 M MES buffer (0.1M (N-morpholino)-ethanesulfonic acid in 15% acetonitrile, pH 5.0) and incubating at room temperature for 20 minutes. Any unbound phosphopeptide is then washed off in 1 ml 30% acetonitrile, 0.1% trifluoroacetic acid.

The phosphopeptide-coupled discs were then passed to Dr Sharad Mistry of the Protein and Nucleic Acid Chemistry Laboratory, University of Leicester, who performed the Edman degradation.

Following Edman degradation (often 30 fractions), the fractions were dried and resuspended in 5 μl pH 1.9 Electrophoresis Buffer, and were then loaded in 1 μl aliquots onto 3mm Whatman Chromatography paper. When dry, these were then exposed to the PhosphorImager Screen for up to two weeks before the image was scanned and analysed as in Section

2.11.5. The resulting image was then analysed to identify the individual fraction which contained radiolabel and this was then compared against the predicted Fra-1 trypsin digestion map to identify the phosphorylated amino acid(s).

2.11.7 Phosphoaminoacid analysis

For phosphoaminoacid analysis of Fra-1, an aliquot of the phosphopeptide eluted from the 2D TLC plate in Section 2.11.6 was first hydrolysed by drying the sample and then incubating for one hour at 110ºC in 100 μl fresh 6 M HCl. This was then transferred to a second microtube, the first tube washed with 50 μl H_2O and then added to the second microtube. This was then thoroughly mixed and dried before being resuspended in 70 μl H_2O. The resuspended amino acids were then centrifuged for five minutes at 14,000 x *g* and the supernatant transferred to a fresh tube before being dried.

Samples were then dissolved in 5 μl pH 1.9 Electrophoresis buffer (for composition see Section 2.11.4) and 1 μl of an amino acid marker mix (1 $mg \cdot ml^{-1}$ O-phospho-L-tyrosine, 1 $mg \cdot ml^{-1}$ O-phospho-L-threonine, 1 $mg \cdot ml^{-1}$ O-phospho-L-serine) was added prior to loading in 1.5 μl aliquots onto a 20 cm x 20 cm cellulose-coated Thin Layer Chromatography plate.

The TLC plate was then made wet by placing 3mm Whatman Chromatography paper soaked in pH 1.9 Electrophoresis Buffer on top.

Electrophoresis in the first dimension was then performed at 2000 V for 27 minutes in a Hunter Thin Layer Peptide Mapping Electrophoresis System. The plate was then allowed to dry before being re-wet with pH 3.5 Electrophoresis Buffer (5% acetic acid, 0.5% pyridine, 1 mM EDTA in milli-Q water). Electrophoresis in the 2nd dimension was then performed at 1800 V for 20 minutes after rotating the plate 90º anticlockwise.

When dry, the amino acid markers were visualised by spraying with Ninhydrin and allowed to develop for 15 minutes at 65ºC. The plate was then wrapped in Saranwrap before being exposed to the PhosphorImager screen for up to one week to achieve desired exposure, before being processed as in Section 2.11.5.

2.12 ^{35}S-pulse chase labelling

This method is a modification of the protocol published by Casalino *et al*. [75]

2.12.1 ^{35}S-pulse chase labelling of J82 and RT4 cells

J82 cells or RT4 cells were transfected with 5 μg HA-Fra-1 construct per 2 x 10^6 cells and seeded at either 7.5 x 10^5 (J82) or 1.5 x 10^6 cells per well of a 12 well plate, and were allowed to growth in D-MEM containing 10% foetal calf serum (Section 2.1.1).

For labelling, cells were firstly starved of L-cysteine and L-methionine by washing twice in PBS and then incubating in standard conditions for three

hours in 2 ml/well Dulbecco's Modified Eagle's Medium with 4500 $mg \cdot l^{-1}$ glucose, $NaHCO_3$, without L-methionine, L-cysteine and L-glutamine supplemented with 1% GlutaMAX I, 1% MEM Non-essential amino acids and 5% dialysed foetal calf serum.

Following starvation, cells were labelled by incubating in standard conditions with the above starvation medium supplemented with 100 $\mu Ci.ml^{-1}$ Tran^{35}S-label for one hour.

The radiolabel pulse was then terminated by the aspiration of the labelling medium and washing twice with PBS. Where appropriate, cells were then chased by the addition of non-radiolabelled D-MEM (Section 2.1.1) for the indicated duration.

Lysis was performed by the addition of 150 μl ice-cold RIPA lysis buffer (see Section 2.11.2) for ten minutes before the cell monolayer was scraped and the lysate transferred to a microtube. The lysate was then centrifuged at 20,000 x *g* for five minutes before the supernatant was snap frozen in liquid nitrogen before being transferred to –80ºC for storage prior to immunoprecipitation.

2.12.2 Immunoprecipitation

Initial attempts at this technique (using the immunoprecipitation technique used for ^{32}P-phospholabelling, Section 2.11.2) were hampered by an unacceptable level of background signal, thought to be due to excessive non-specific binding to the Protein A Sepharose. We therefore modified the technique to include a pre-clearing step, and also to change the buffer (from TEG to RIPA); this led to improved signal/noise ratios.

450 μl cold RIPA lysis buffer (Section 2.11.2) was added to 180 μl of Protein A Sepharose. The solution was then briefly centrifuged and the Protein A Sepharose pellet washed once more with 500 μl RIPA lysis buffer. The resulting pellet of Sepharose beads was then resuspended in 50 μl RIPA lysis buffer and all of the ^{35}S-labelled lysate (from Section 2.12.1) was added. This was then incubated with rotation at +4ºC for one hour before being centrifuged at 10,000 x *g* for ten minutes at +4ºC. The supernatant was transferred to a fresh tube and 1 μg of anti-HA antibody (12CA5, Roche) in 30 μl of RIPA lysis buffer (an excess of antibody) was added an incubated for one hour at +4ºC, again with rotation. 180 μl of Protein A Sepharose was then added and incubated for 45 minutes at +4ºC with rotation.

The HA-Fra-1-Antibody-Protein A Sepharose beads complex was then washed three times with 1000 μl ice-cold RIPA lysis buffer, with the supernatant being aspirated completely on the final wash. The HA-Fra-1 was then eluted from the beads by the addition of 15 μl 1 x SDS gel

loading buffer (Section 2.8.1) with 1:40 volume of 4% bromophenol blue and 1:40 volume of 14M ß-mercaptoethanol added, and boiled for five minutes before being centrifuged at 13,000 x *g* for five minutes.

2.12.3 Gel Electrophoresis of ^{35}S-labelled proteins

SDS-PAGE gel electrophoresis was performed on the immunoprecipitated ^{35}S-labelled HA-Fra-1 as described previously (Section 2.8.3) using 10% gels.

Following electrophoresis, the gel was fixed by incubating for 45 minutes in 20% acetic acid, 10% methanol before being dried on a VWR vacuum gel dryer. The dried gel was then enclosed in Saranwrap and exposed to a PhosphorImager Screen (general purpose screen) for a duration long enough to give an adequate signal, before being scanned and interpreted as described in Section 2.11.5.

2.13 Materials

2.13.1 Chemicals and reagents

123-base pair DNA ladder	D5042	Sigma
3,3'-diaminobenzidine tetrachloride hydrate	D-5637	Sigma
Acetic acid	1001BT	BDH
Acetonitrile	00712	Sigma
Acrylamide (Acrylogel 30)	443735T	BDH
Agarose	15510-019	Invitrogen
Ammonium bicarbonate	A-6141	Sigma

Ammonium persulphate	A-3678	Sigma
Ampicillin	A-9518	Sigma
Ampliwax® PCR Gem 50 beads	N808-0150	Applied Biosystems
Aprotinin	A-4529	Sigma
ß-glycerophosphate	G-6251	Sigma
ß-mercaptoethanol	M-7154	Sigma
Boric Acid	20182.297	VWR International
Bromophenol Blue	B-8026	Sigma
n-Butanol	360465	Sigma
Calcium chloride dihydrate	22,350-6	Sigma
Calf intestinal phosphatase	M0290S	New England Biolabs
Carbodiimide (supplied with kit)	#GEN920033	Applied Biosystems
Chloroform:isoamyl alcohol (24:1)	C-0549	Sigma
Chloroquine diphosphate	25745	Fluka
Citric Acid	C1909	Sigma
D-MEM + 4500mg·l^{-1} glucose +Glutamax I + pyruvate	31966	Gibco
dATP, dCTP, dGTP, dTTP pack	R0481	Fermentas
DAPI	D-1306	Molecular Probes
Deoxycholic acid	264101	Calbiochem
Dimethylsulphoxide	47,230-1	Sigma
Dithiothreitol	D-1532	Invitrogen
DPX	44581	Sigma

Dulbecco's Modified Eagle Medium with 4500 $mg \cdot l^{-1}$ glucose, $NaHCO_3$ without L-methionine, L-cysteine and L-glutamine	D-0422	Sigma
E. coli - OneShot® TOP10 Chemically Competent Cells	C4040-03	Invitrogen
Epidermal Growth Factor (Recombinant human)	100-15	PeproTech
Ethanol		University of Leicester
Ethidium Bromide	E-2515	Sigma
Ethylenediaminetetracetic acid	E-5134	Sigma
Fluoromount-G	0100-01	Cambridge Bioscience
Foetal calf serum (dialysed)	F-0392	Sigma
Foetal calf serum (heat inactivated)	CH30160.03	Perbio
Formaldehyde	F8775	Sigma
Formamide (de-ionised)	FORM D002	Qbiogene
Formic acid	F0507	Sigma
D-(+)-Glucose	G-8270	Sigma
GlutaMAX I	35050	Gibco
Glycerol	G-6279	Sigma
Glycine	G-8898	Sigma
HEPES	H-7523	Sigma
Hydrochloric acid	H-1758	Sigma
Hydrogen Peroxide	H-1009	Sigma
Hyperfilm MP	RPN6K	Amersham
Hyperladder I 200bp DNA ladder	BIO-33025	Bioline

Immobilon-P PDVF transfer membrane	IPVH00010	Millipore
Industrial Methylated Spirits		Univ. Leicester
Isobutyric acid	I1754	Sigma
Kanamycin	11815-024	Gibco
Kodak Biomax Film	2370398	Sigma
Lactacystin	PI-104	Biomol
λDNA *Bst*EII digest	N3014S	New England Biolabs
λDNA *Eco*RI/*Hind*III digest	D-9281	Sigma
LB Agar	22700-025	Invitrogen
Leupeptin	L-2884	Sigma
Luria Broth Base	12795-027	Invitrogen
Magnesium chloride hexahydrate	63068	Fluka
Magnesium sulphate heptahydrate	M-2773	Sigma
Marvel dried skimmed milk power		Premier International Foods
MEM Non-Essential Amino Acids	11140	Gibco
MEM Sodium pyruvate	11360-039	Gibco
Methanol		Univ. Leicester
MOPS buffer (10x)	0032 006.752	Eppendorf
(N-morpholino)-ethanesulfonic acid (MES)	M-8250	Sigma
Ninhydrin	N1286	Sigma
NP-40	I-8896	Sigma
O-phospho-serine	P-0878	Sigma
O-phospho-threonine	P-1053	Sigma

O-phospho-tyrosine	P-9405	Sigma
Paraformaldehyde	294474L	BDH
Penicillin (5000 u/ml)/ Streptomycin (5000 μg/ml)	15070-063	Invitrogen
Phenol:chloroform:isoamyl alcohol 25:24:1	P-2069	Sigma
Phosphate Buffered Saline tablets	BR0014G	Oxoid
Phenylmethanesulfonyl fluoride (PMSF)	P7626	Sigma
Polyvinylpyrrolidone (PVP) (ave. MW 40 kDa)	PVP40	Sigma
Ponceau-S	P-7170	Sigma
Potassium chloride	P-9541	Sigma
Potassium phosphate monobasic	P-9791	Sigma
Propan-2-ol	96946H	BDH
Protein A Sepharose Beads (CL-4B)	CL-4B17-0780-01	Amersham
Protein Marker (See-Blue)	LC5925	Invitrogen
Protran Nitrocellulose Transfer Membrane (BA-45, 0.45 μm)	732-4008	Schleicher & Schuell BioScience
Pyridine	360570	Sigma
Random Hexamers pd$(N)_6$	27-2166-01	Amersham
Sequelon-AA discs	#GEN920033	Applied Biosystems
Sodium carbonate	S-7795	Sigma
Sodium chloride	S-7653	Sigma
Sodium dodecyl sulphate	L-4390	Sigma
Sodium hydrogen carbonate	S-6297	Sigma

Trifluoroacetic acid	91709	Sigma
Tris Base	T-1503	Sigma
tRNA	R-5636	Sigma
TEMED	T-9281	Sigma
Triton X-100	T-8787	Sigma
TRIzol® Reagent	15596-026	Invitrogen
Trypsin, Modified Sequencing Grade	V5111	Promega
Trypsin-EDTA	25200-072	Gibco
TWEEN-20	P-7949	Sigma
U0126	V1121	Promega
Whatman 3MM cellulose chromatography paper	3030-931	Whatman
Xylene	534056	Sigma

2.13.2 Radiochemicals

^{32}P-orthophosphate (10 mCi·ml^{-1})	PBS 11	Amersham
Tran^{35}S-label (10.5 mCi·ml^{-1})	5100g	ICN

2.13.3 Equipment

25 cm^2, 80 cm^2, 175 cm^2 cell culture flasks	Greiner
6,12,24,96 well plates	Greiner
Coverslips (18mm)	VWR International
Cryo.S cryo-vials (sterile)	Greiner
CultureSlides (8 chamber)	BD
Microtubes (0.5 ml and 1.5 ml)	Univ. Leicester
Nunclon surface dish (5cm)	Nunclon

PhosphorImager General Purpose Screen	Amersham
Saranwrap	Univ. Leicester
Storm 820 Scanner	Amersham
Thin Layer Chromatography Plates, Cellulose, M1.05716.0001, 20 x 20 cm	Merck

2.13.4 Kits

BCA™ protein assay kit	23227	Pierce Biotechnology
Dako Duet System	K-0492	Dako
ECL Western Blotting Detection Reagent	RPN2109	Amersham
QIAfilter Plasmid Maxi Kit	12263	Qiagen
QIAprep Spin Miniprep Kit	27104	Qiagen
QIAquick Gel Extraction Kit	28704	Qiagen
SuperSignal® West Femto Maximum Sensitivity Substrate	34095	Pierce Biotechnology

2.13.5 Antibodies

Antibody	**Code**	**Species**	**Manufacturer**
α-tubulin	T5168	mouse	Sigma
c-Fos (4)	sc-52	rabbit	Santa Cruz Biotech
c-Jun (N)	sc-45	rabbit	Santa Cruz Biotech
E-cadherin (36)	610181	mouse	BD Biosciences
EGFP	8367	rabbit	BD Biosciences
Fra-1 (R20)	sc-605	rabbit	Santa Cruz Biotech
HA (Y11)	sc-805	rabbit	Santa Cruz Biotech
HA (12CA5)	11583816001	mouse	Roche

p44/42 MAPK	9102	rabbit	Cell Signaling
p-p90RSK (Thy359/Ser 363)	9344	rabbit	Cell Signaling
pERK5 (Thr218/Tyr220)	3371	rabbit	Cell Signaling
pSer	61-8100	rabbit	Zymed
pThr	9381	rabbit	Cell Signaling
pTyr	9411	mouse	Cell Signaling
RSK-1 (C-21)	sc-231	rabbit	Santa Cruz Biotech
Vimentin (RV202)	550513	mouse	BD Biosciences

Normal rabbit IgG	X-0903	Dako
Polyclonal rabbit anti-mouse immunoglobulins-HRP	Z0456	Dako
Polyclonal goat anti-rabbit immunoglobulins-HRP	P0448	Dako

Alexa Fluor® 594 goat anti-rabbit IgG	A-11012	Molecular Probes
Alexa Fluor® 488 donkey anti-mouse IgG	A-21202	Molecular Probes

2.13.6 Restriction Endonucleases / DNA/mRNA modification enzymes

*Bam*HI	E1010V	Amersham
*Bgl*II	E1021Y	Amersham
*Dpn*I	R0176S	New England Biolabs
*Eco*RI	E1040W	Amersham

*Hind*III	E1060Y	Amersham
*Kpn*I	R01425	New England Biolabs
*Nae*I	E1155Y	Amersham
*Nhe*I	E1162Y	Amersham
*Not*I	E0304Y	Amersham
*Pst*I	E1073Y	Amersham
*Sbf*I	R06425	New England Biolabs
*Xba*I	R0145S	New England Biolabs
*Xho*I	E1094Y	Amersham

Ampli*Taq* DNA polymerase	N8080160	Applied Biosystems
GeneAmp EZ *rTth* RNA PCR Kit	N8080179	Applied Biosystems
NEBuffer 3	B7003S	New England Biolabs
NEBuffer 4	B7004S	New England Biolabs
One-phor-all buffer	27-0901-02	Amersham
Pfu polymerase	600135	Stratagene
Reddymix Extensor Hi-fidelity PCR Master Mix 1	AB0794	ABgene
RNA Secure	AM7005	Ambion
SuperScript III Reverse Transcriptase	18080-044	Invitrogen
T4 DNA ligase	M0202S	New England Biolabs

2.13.7 Computer Software

Adobe Photoshop CS3
Adobe Systems Incorporated,
345 Park Avenue,
San Jose, CA 95110-2704.
USA.

Chromas v. 1.4.5
www.technelysium.com.au/chromas145-95.zip

GraphPad Prism v4.0 for Macintosh
GraphPad Software, Inc.,
2236 Avenida de la Playa,
La Jolla, CA 92037.
USA.

ImageQuant TL
GE Healthcare UK Ltd.,
Amersham Place,
Little Chalfont,
Buckinghamshire.
HP7 9NA.
United Kingdom.

LSM Imager Browser
Carl Zeiss Ltd.,
15-20 Woodfield Road,
Welwyn Garden City,
Hertfordshire.
AL7 1JQ.
United Kingdom.

Microsoft Office XP for Windows & Microsoft Office X for Mac
Microsoft Ltd.,
Microsoft Campus,
Reading.
RG6 1WG.
United Kingdom.

SPSS v14.0 for Windows
SPSS Inc.,
233 S. Wacker Drive,
11th Floor,
Chicago, IL 60606.
USA.

Zotero
www.zotero.org

2.13.8 Companies

ABgene Limited,
ABgene House,
Blenheim Road,
Epsom.
KT19 9AP.
United Kingdom.

Amersham Biosciences,
Amersham Place,
Little Chalfont,
Buckinghamshire.
HP7 9NA.
United Kingdom.

Ambion,
Lingley House,
120 Birchwood Boulevard,
Warrington.
WA3 7QH.
United Kingdom.

Applied Biosystems,
Lingley House,
120 Birchwood Boulevard,
Warrington.
WA3 7QH.
United Kingdom.

BD Biosciences,
1 Becton Drive,
Franklin Lakes,
New Jersey, 07417
USA.

Cell Signaling Technology
New England Biolabs (UK) Ltd,
75-77 Knowl Piece,
Wilbury Way,
Hitchin,
Hertfordshire.
SG4 0TY.
United Kingdom.

BDH,
VWR International Ltd,
Hunter Boulevard,
Magna Park,
Lutterworth,
Leicestershire.
LE17 4XN.
United Kingdom.

Dako UK Ltd
Cambridge House,
St Thomas Place,
Ely,
Cambridgeshire.
CB7 4EX.
United Kingdom.

Bioline Ltd.
16 The Edge Business Centre,
Humber Road,
London.
NW2 6EW.
United Kingdom.

Eppendorf UK Limited
Endurance House,
Chivers Way,
Histon,
Cambridge.
CB24 9ZR.
United Kingdom.

BIOMOL International, L.P.
Palatine House,
Matford Court,
Exeter.
EX2 8NL.
United Kingdom.

Fermentas UK
Sheriff House,
Sheriff Hutton Industrial Park,
York.
YO6 0RZ.
United Kingdom.

Calbiochem
VWR International Ltd,
Hunter Boulevard,
Magna Park,
Lutterworth,
Leicestershire.
LE17 4XN.
United Kingdom.

Cambridge BioScience Ltd.
24-25 Signet Court,
Newmarket Road,
Cambridge.
CB5 8LA.
United Kingdom.

Greiner Bio-One Ltd.
Brunel Way,
Stroudwater Business Park,
Stonehouse,
GL10 3SX.
United Kingdom.

ICN (Now MP Biomedicals)
Parc d'Innovation,
BP 50067,
67402 Illkirch.
France.

Invitrogen Ltd.
3 Fountain Drive,
Inchinnan Business Park,
Paisley.
PA4 9RF.
United Kingdom.

Millipore (UK) Ltd.
Suite 3 & 5,
Building 6,
Croxley Green Business Park,
Watford,
Hertfordshire.
WD18 8YH.
United Kingdom.

Fluka
Sigma-Aldrich Company Ltd.,
The Old Brickyard,
New Road,
Gillingham,
Dorset.
SP8 4XT.
United Kingdom.

Gibco
Invitrogen Ltd.,
3 Fountain Drive,
Inchinnan Business Park,
Paisley.
PA4 9RF.
United Kingdom.

Nunclon
VWR International Ltd.,
Hunter Boulevard,
Magna Park,
Lutterworth,
Leicestershire.
LE17 4XN.
United Kingdom.

Oxoid Ltd.
Wade Road,
Basingstoke,
Hampshire.
RG24 8PW.
United Kingdom.

PeproTech Inc.
Princeton Business Park,
5 Crescent Avenue,
PO Box 275,
Rocky Hill, NJ 08553.
USA.

Perbio Science UK Ltd.
Unit 9,
Atley Way,
North Nelson Industrial Estate,
Cramlington,
Northumberland.
NE23 1WA.
United Kingdom.

Molecular Probes
Invitrogen Ltd.,
3 Fountain Drive,
Inchinnan Business Park,
Paisley.
PA4 9RF.
United Kingdom.

New England Biolabs (UK) Ltd
75-77 Knowl Piece,
Wilbury Way,
Hitchin,
Hertfordshire.
SG4 0TY.
United Kingdom.

Promega Corporation
2800 Woods Hollow Road,
Madison, WI 53711.
USA.

Qbiogene
Wellington House,
East Road,
Cambridge.
CB1 1BH.
United Kingdom.

QIAGEN Ltd.
QIAGEN House,
Fleming Way,
Crawley,
West Sussex.
RH10 9NQ.
United Kingdom.

Roche Applied Science
Roche Diagnostics Ltd.,
Charles Avenue,
Burgess Hill.
RH15 9RY.
United Kingdom.

Pierce Biotechnology
Perbio Science UK Ltd.,
Unit 9, Atley Way,
North Nelson Industrial Estate,
Cramlington,
Northumberland.
NE23 1WA.
United Kingdom.

Premier International Foods
Bridge Road,
Long Sutton,
Spalding,
Lincolnshire.
PE12 9EQ.
United Kingdom.

Sigma-Aldrich Company Ltd.
The Old Brickyard,
New Road,
Gillingham,
Dorset.
SP8 4XT.
United Kingdom.

Stratagene
Agilent Technologies UK Ltd,
Lakeside,
Cheadle Royal Business Park
Stockport,
Cheshire.
SK8 3GR.
United Kingdom.

University of Leicester
Central Stores,
University Road,
Leicester.
LE1 9HN.
United Kingdom.

VWR International Ltd.
Hunter Boulevard,
Magna Park,
Lutterworth,
Leicestershire.
LE17 4XN.
United Kingdom.

Santa Cruz Biotechnology, Inc.
Bergheimer Str. 89-2,
69115,
Heidelberg.
Germany.

Whatman plc.
Springfield Mill,
James Whatman Way,
Maidstone,
Kent.
ME14 2LE.
United Kingdom.

Schleicher & Schuell Bioscience
VWR International Ltd.,
Hunter Boulevard,
Magna Park,
Lutterworth,
Leicestershire.
LE17 4XN.
United Kingdom.

Zymed
Invitrogen Ltd.,
3 Fountain Drive,
Inchinnan Business Park,
Paisley.
PA4 9RF.
United Kingdom.

Chapter 3 – Results 1
Fra-1 in Bladder Cancer

3.1 Immunohistochemical analysis of Human Muscle-Invasive Bladder Tumours

3.1.1 Fra-1 staining

A series of 104 muscle-invasive tumours (all transitional cell carcinomas) were previously identified and sections obtained by Miss A.J. Colquhoun (Urology Group, Department of Cancer Studies and Molecular Medicine, University of Leicester). These sections were obtained with ethical approval (Leicestershire, Northamptonshire & Rutland Research Ethics Committee Reference 6433, "A retrospective study of epidermal growth factor receptor (EGFR) status in archival bladder cancers as a potential predictor of radiosensitivity, University Hospitals of Leicester NHS Trust Research & Development Department Reference UHL7330) for a previous immunohistochemical study comparing Epidermal Growth Factor Receptor (EGFR) status and clinical outcome. An amendment was made to this Ethical Committee Approval allowing immunohistochemical staining for other molecules, including Fra-1 (Leicestershire, Northamptonshire & Rutland Research Ethics Committee 2 Reference 06/Q2502/48).

All 104 patients whose tumours were available for analysis had undergone radical external beam radiotherapy as the primary treatment for muscle-invasive bladder cancer, some having also had chemotherapy or

had subsequently gone onto have salvage cystectomy. All cases had information on pathological stage and grade along with additional clinical information (Table 3.1.1). Sections were immunohistochemically stained for Fra-1 and staining was evaluated by a Consultant Histopathologist, Dr Peter Greaves. Fra-1 staining was rated negative (0) minimal (+), moderate (++) or marked (+++). Eighty percent of muscle-invasive bladder tumours are Fra-1 positive, with 20% of tumours being negative; this and the magnitude of staining is shown in Figure 3.1.1. Examples of Fra-1 tumour staining are shown in Figure 3.1.2. It was found that the main staining pattern was a pale nuclear pattern that tended to be more marked in less well-differentiated or clearly invasive zones, and in large and often pleomorphic nuclei. Interestingly, given that Fra-1 is a transcription factor, which by its nature dictates localisation to the nucleus, four tumours also demonstrated clear cytoplasmic staining (also showing nuclei staining). This cytoplasmic staining is discussed further when Fra-1 immunocytochemical analysis of bladder transitional cell carcinoma cell lines is performed (Section 3.5.3).

Age at diagnosis
Gender
Histological type
TNM stage
Grade
Presence of ureteric obstruction
Local recurrence (& time from DXT to recurrence)
Distant recurrence (& time from DXT to recurrence)
Previous chemotherapy
Cause of death
Time from Diagnosis to death
Time from Radiotherapy to death
Time from Salvage cystectomy to death (if applicable)

Table 3.1.1 Clinical details available for all 104 muscle-invasive tumours stained for Fra-1.

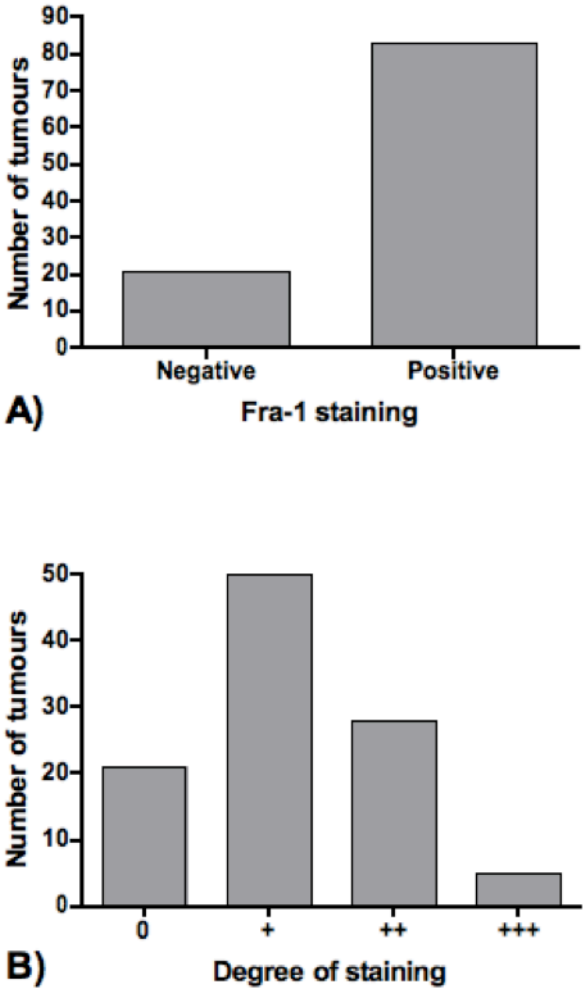

Figure 3.1.1 Fra-1 immunochemical staining of human muscle invasive bladder tumours showing a) number of negative and positive tumours, and b) breakdown of tumour staining by degree of staining.

3.1.2 Comparison of Fra-1 staining with clinical parameters

Table 3.1.1 shows the clinical information available along with the 104 muscle-invasive bladder tumours. Comparison of Fra-1 staining and these parameters was performed (see Table 3.1.2, Figures 3.1.3a-3.1.5b) using SPSS version 14 (SPSS Inc.) for Mann-Whitney U Test and Kaplan Meier plots with Mantel-Cox log rank Test, and GraphPad Prism 4 for

Macintosh Version 4.0c (GraphPad Software Inc.) for two-tailed Fisher's exact test. Of the 104 tumours, 87 were from male patients and 17 from female patients. There was no statistical correlation between gender and presence of Fra-1 (two-tailed Fisher's exact test). Comparison of Fra-1 presence with Age at diagnosis (no significant correlation) was performed using a Mann-Whitney U-Test. Comparison of Fra-1 presence with tumour grade was performed using two-tailed Fisher's exact test, and was not significant. Two-tailed Fisher's exact test was also performed to compare Fra-1 presence and the development of local recurrence, distant recurrence, and ureteric obstruction. These were all not statistically significant. Kaplan Meier plots were generated and Mantel-Cox log rank tests were performed for Time from diagnosis to death (bladder cancer-specific and all causes), Time from radiotherapy to death (bladder cancer-specific and all causes) and Time from recurrence to death (bladder cancer-specific and all causes). All of these were statistically not significant apart from Time from recurrence to death from bladder cancer ($p=0.048$), however, there were only five patients in this group whose tumours were Fra-1 negative, and this result must be interpreted with caution. No comparison was attempted with Time from cystectomy to death because only two of these patients had Fra-1 negative tumours).

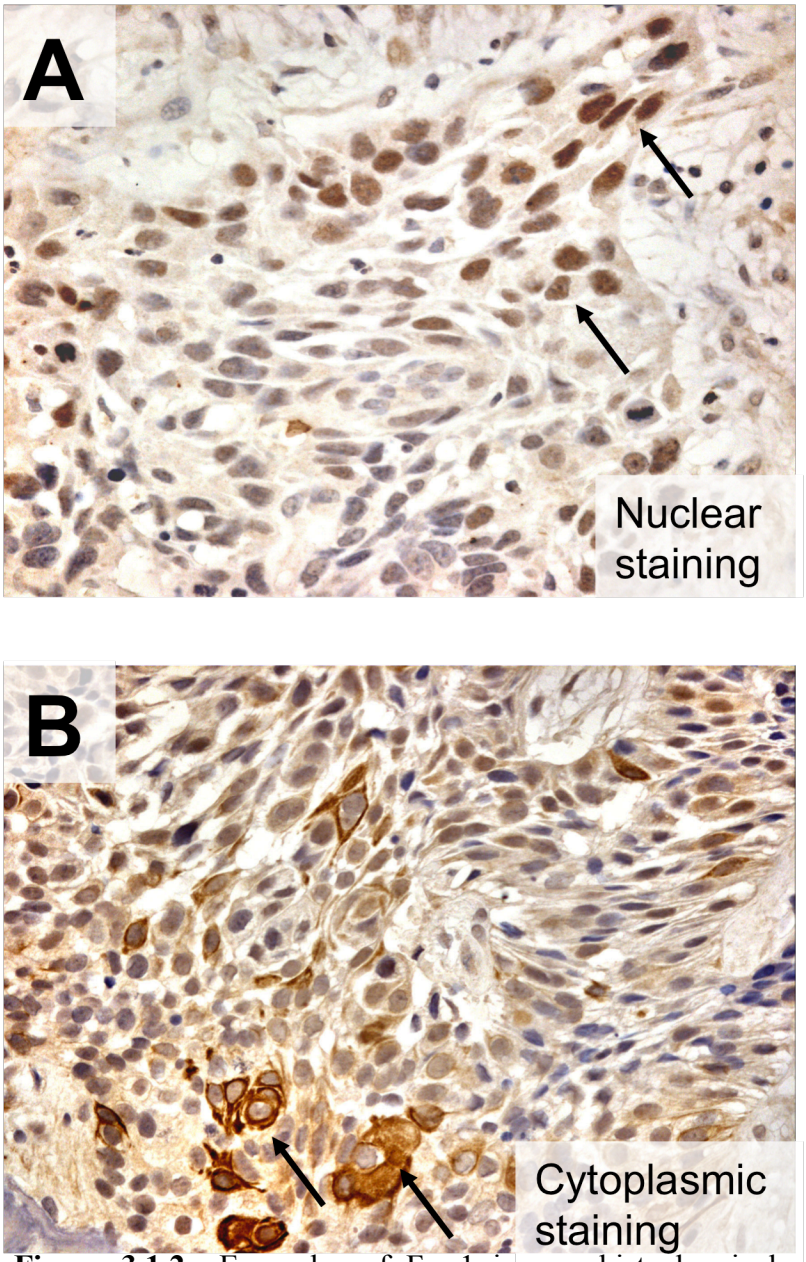

Figure 3.1.2 Examples of Fra-1 immunohistochemical staining in human muscle-invasive bladder tumours, a) demonstrating nuclear Fra-1 staining, and b) demonstrating cytoplasmic staining.

Parameter		Fra-1 negative		Fra-1 positive		Sig?	p
Age (yr) (median/range)		74	57-84	72	52-88	No	0.488
Gender	M	19		68		No	0.514
	F	2		15			
Tumour grade	2	4		12		No	0.099
	3	17		71			
Local recurrence	N	8		20		No	0.260
	Y	10		49			
Distant recurrence	N	12		39		No	0.429
	Y	6		32			
Ureteric obstruction	N	15		27		No	0.248
	Y	2		18			
Time from diagnosis to death	Bladder cancer	7 deaths		38 deaths		No	0.893
	All causes	18 deaths		66 deaths		No	0.503
Time from radiotherapy to death	Bladder cancer	7 deaths		38 deaths		No	0.178
	All causes	18 deaths		66 deaths		No	0.914
Time from recurrence to death	Bladder cancer	5 deaths		27 deaths		Yes	0.048
	All causes	8 deaths		44 deaths		No	0.074

Table 3.1.2 Comparison of Fra-1 staining in muscle-invasive bladder tumours and recorded clinical parameters. Age significance calculated with Mann Whitney U-test; Times to death calculated with Kaplan Meier, Mantel-Cox log rank test; other parameters with 2-tailed Fisher's exact test. Kaplan Meier plots are shown in Figures 3.1.3a&b, 3.1.4a&b, 3.1.5a&b

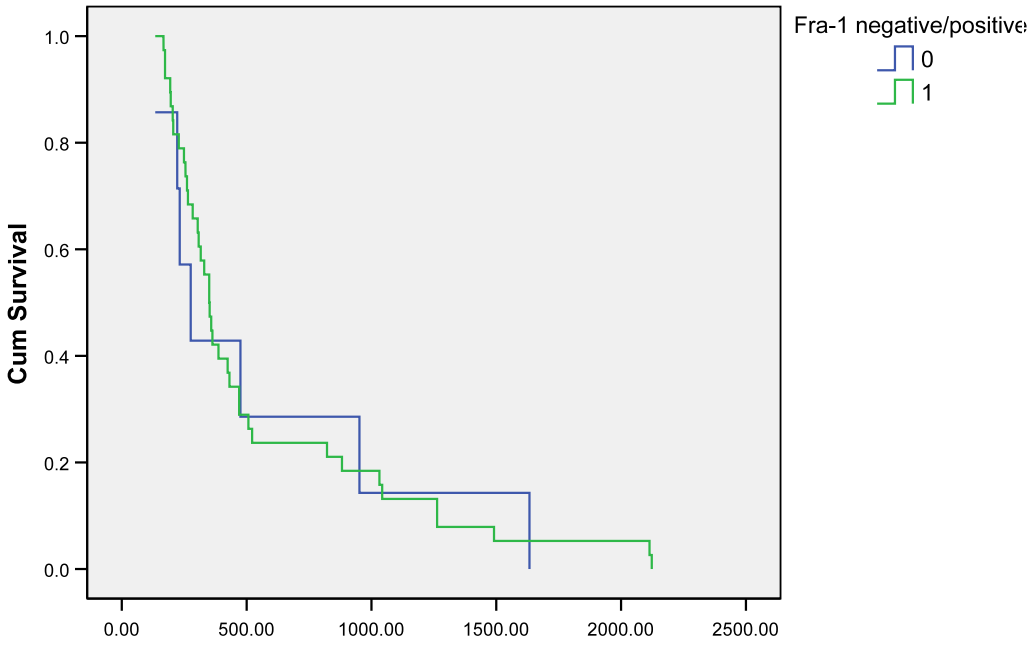

Figure 3.1.3a. Kaplan-Meier plot showing time from diagnosis to death from bladder cancer (days)

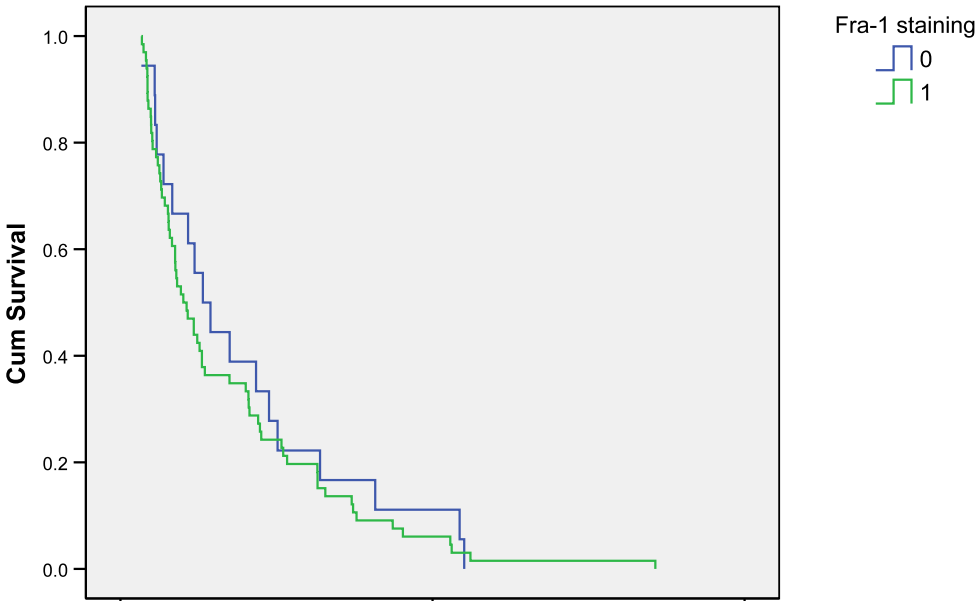

Figure 3.1.3b. Kaplan-Meier plot showing time from diagnosis to death from all causes (days)

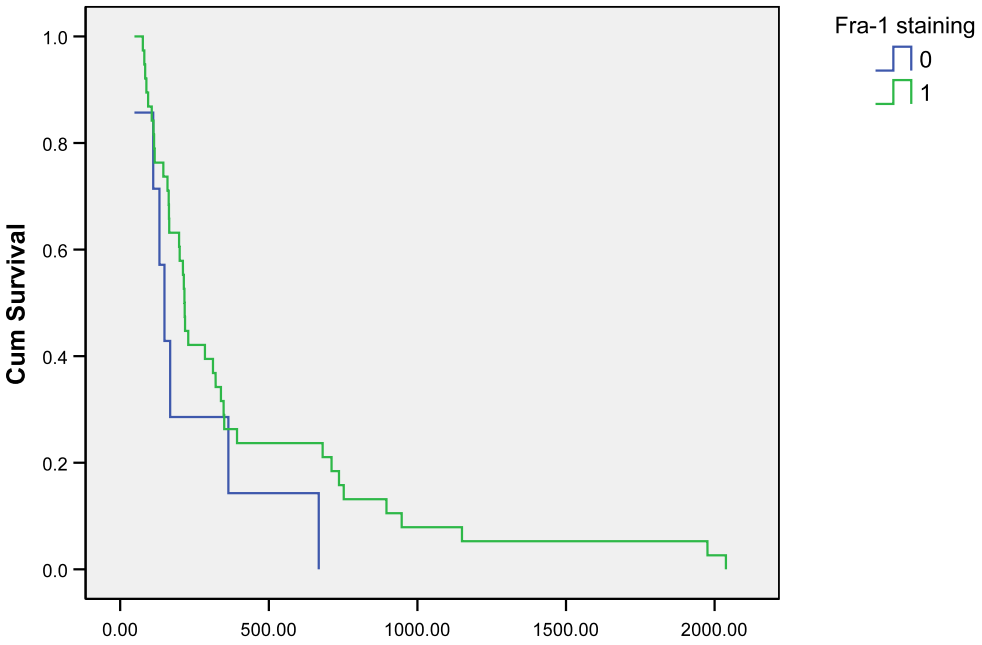

Figure 3.1.4a. Kaplan-Meier plot showing time from radiotherapy to death from bladder cancer (days)

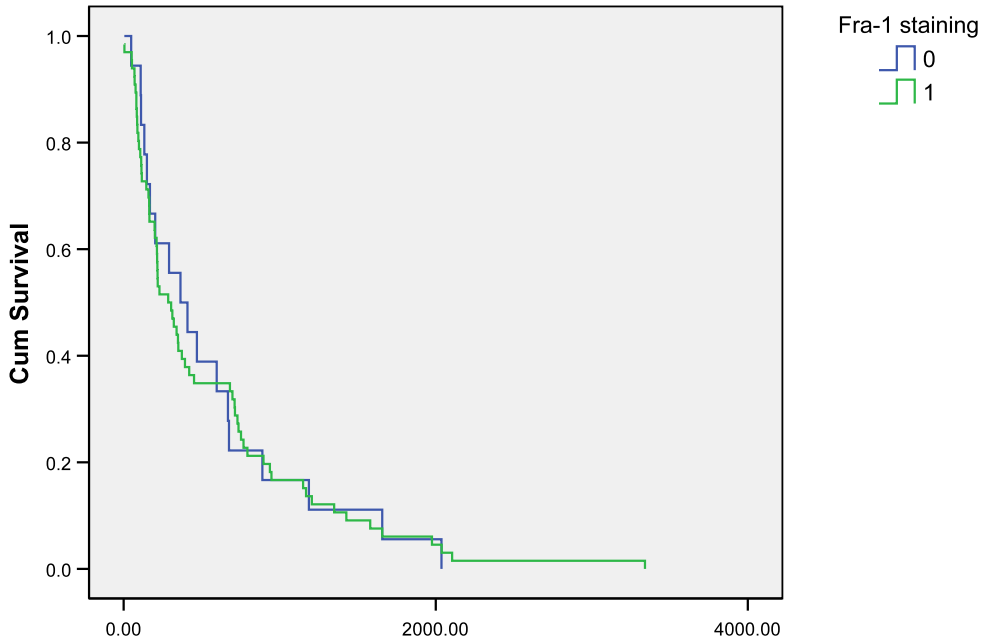

Figure 3.1.4b. Kaplan-Meier plot showing time from radiotherapy to death from all causes (days)

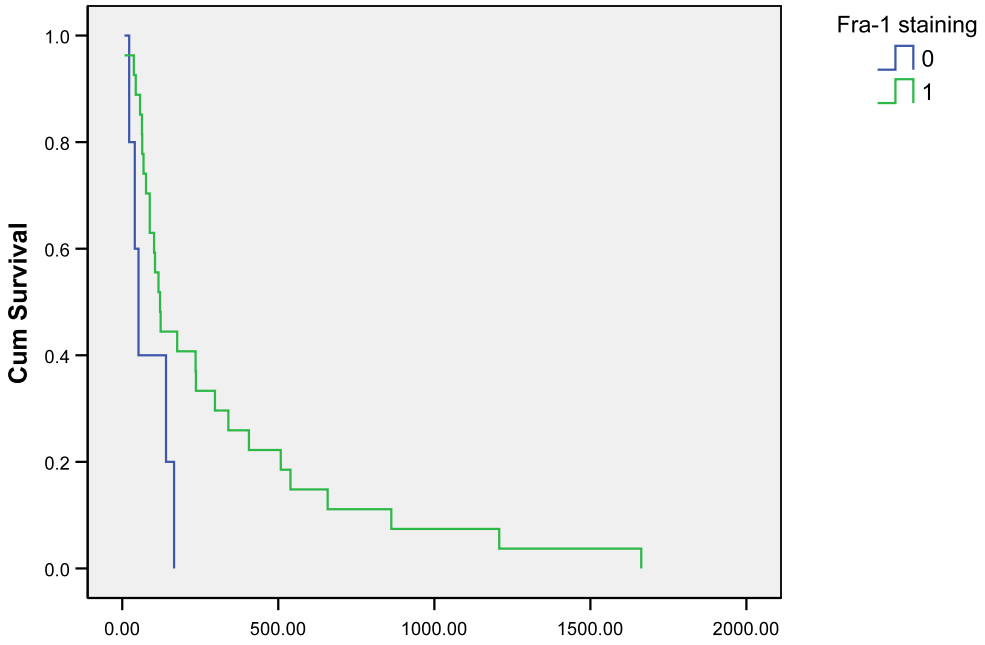

Figure 3.1.5a. Kaplan-Meier plot showing time from recurrence to death from bladder cancer (days)

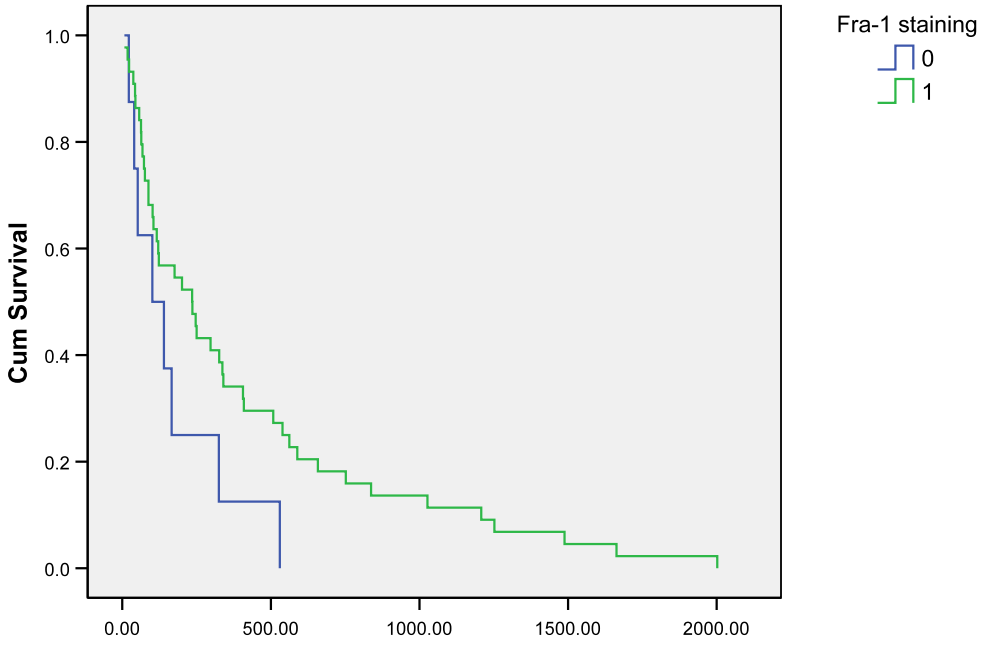

Figure 3.1.5b. Kaplan-Meier plot showing time from recurrence to death from all causes (days)

3.1.3 Comparison of Fra-1 and EGFR staining in muscle-invasive tumours

As described earlier (Section 1.8), Fra-1 levels are regulated by the MAP Kinase pathway. It is also known that EGFR activation increases MAP Kinase activity [24], therefore it is hypothesised that if tumours have an increased level in EGFR, they may also have an increase in Fra-1 levels; additionally, EGFR presence is correlated with tumour aggression, and Fra-1 has previously been shown to, or be involved with, several mechanisms which may be involved with tumour aggression (Sections 1.12 and 1.14). As can be seen in Table 3.1.3, there is no correlation between Fra-1 status and EGFR status, suggesting Fra-1 levels may depend on more than just increased levels of EGFR at the cell surface.

	EGFR negative	EGFR positive
Fra-1 negative	7	16
Fra-1 positive (+,++ & +++)	21	60

Table 3.1.3 Comparison of Fra-1 status and EGFR status in muscle invasive bladder tumours, showing no correlation, p=0.791 (Fisher's two-tailed test).

3.1.4 Summary of Fra-1 in human muscle-invasive bladder tumours

Fra-1 is present in 80% of muscle-invasive bladder tumours, confirming our earlier hypothesis (see Section 1.19) and interestingly, Fra-1 appears to be present in the cytoplasm of some tumour cells. There is no correlation between Fra-1 status and EGFR status, nor is there correlation between Fra-1 status and clinical parameters which were available to us, except possibly the time from recurrence to death from bladder cancer,

however, the small numbers in the Fra-1 negative group does cast doubt over the reliability of this analysis.

3.2 Immunohistochemical analysis of Human Non-Invasive Bladder Tumours

3.2.1 Fra-1 staining

A series of 52 non-muscle invasive bladder transitional cell carcinomas were obtained from the Leicester Bladder Tissue Bank. These samples were obtained with Ethical Approval (Leicestershire, Northamptonshire & Rutland Research Ethics Committee Reference 06/Q2502/48, "Is Fra-1 a marker of invasion in bladder cancer?", University Hospitals of Leicester NHS Trust Research & Development Department Reference UHL 10082"), and we had pathological stage and grade information for all samples.

Blocks were obtained from the Histopathology Department of the Leicester General Hospital, UHL, and these were then processed and stained for Fra-1 by Dr Raj Pal (Leicester General Hospital, UHL) and Dr Richard Edwards (MRC Toxicology Unit, University of Leicester), as per Section 2.10. Fra-1 staining was analysed, as for muscle-invasive tumours, by Dr Peter Greaves. As noted in the muscle-invasive tumour staining, the main staining pattern was a pale nuclear pattern which tended to be more marked in less well-differentiated areas and in large and often pleomorphic nuclei. Overall, 32/52 (62%) tumours were positive for Fra-1; however, in contrast to the muscle-invasive tumour

staining, a higher proportion of tumours had cytoplasmic staining (15/52, 29%), with 10 of these (19% of total tumours) having only cytoplasmic with no nuclear staining; in muscle-invasive tumours, cytoplasmic staining was only seen along with nuclear staining. 22/52 (42%) of tumours had nuclear staining for Fra-1 (Figure 3.2.1). Nuclear staining, as for muscle-invasive tumours were graded minimal (+), moderate (++) and marked (+++), and these results are shown in Figure 3.2.2.

3.2.2 Comparison of tumour stage and grade with Fra-1 staining in non-invasive tumours

Figure 3.2.3(a-c) shows the breakdown by pathological grade of the non-invasive tumours and their Fra-1 positivity, again further subdivided by intracellular location of Fra-1. There was no statistically significant correlation between Fra-1 positivity and tumour grade, regardless of the site of Fra-1 staining. However, the relatively small numbers of tumours available may affect the statistical calculations – simply eyeballing the data, there does appear to be a trend towards higher levels of Fra-1 containing tumours in the higher grade groups when compared to the lower grade groups, for example, from Figure 3.2.3(a), 1/5 Grade 1 tumours are Fra-1 positive, whereas 5/8 Grade 3 tumours are Fra-1 positive.

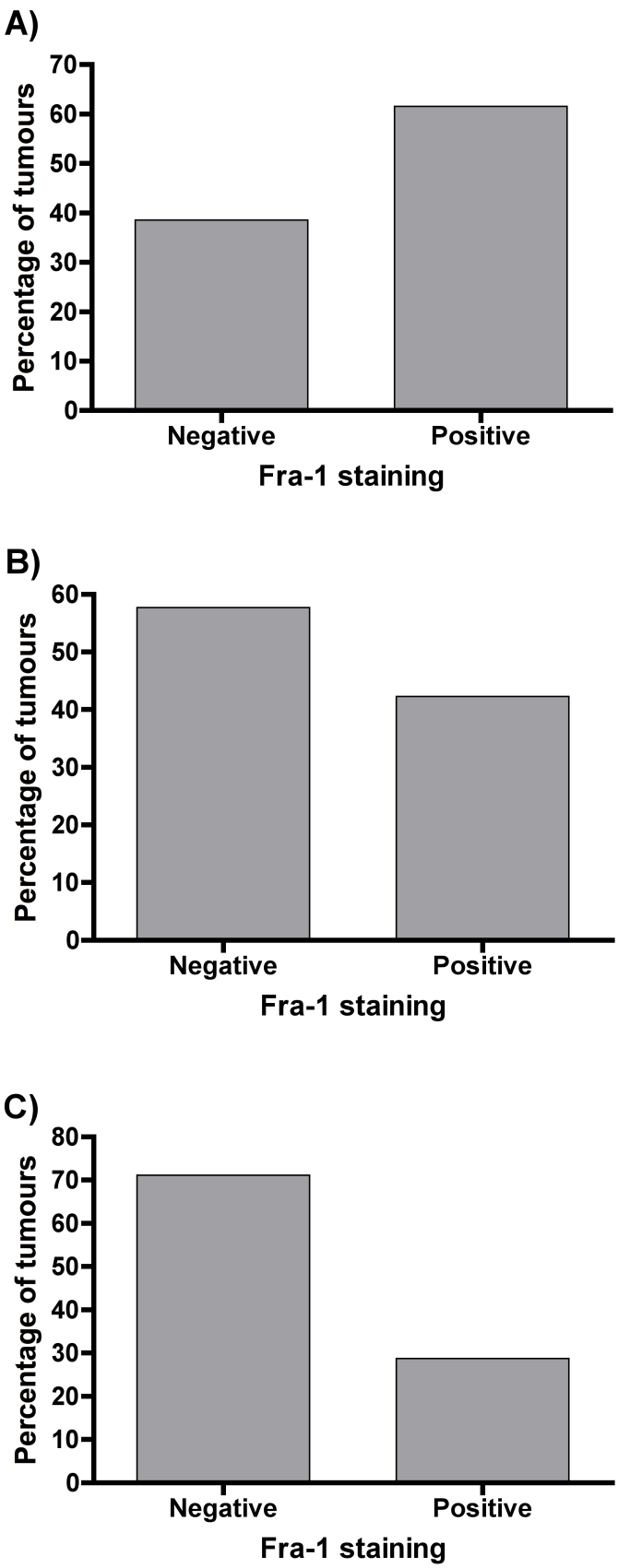

Figure 3.2.1 Fra-1 immunohistochemical staining of superficial bladder tumours showing A) total, i.e. cytoplasmic and/or nuclear positivity, B) nuclear positivity and C) cytoplasmic positivity.

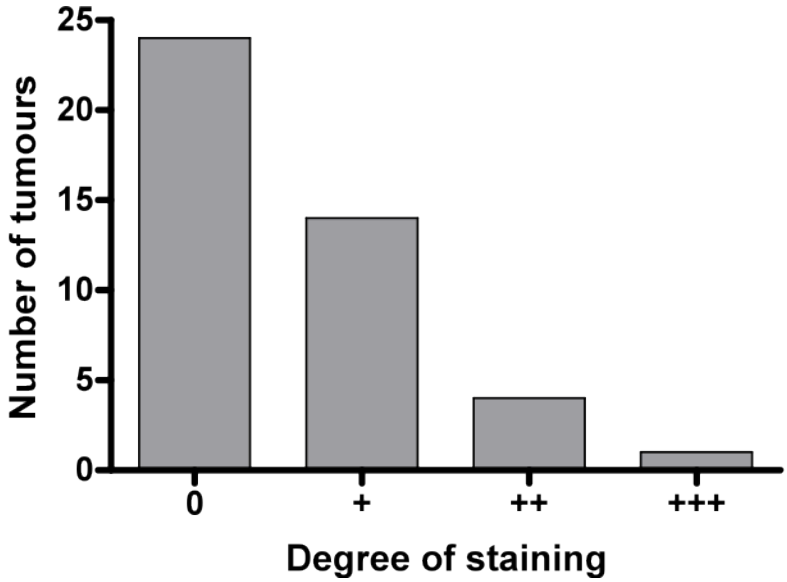

Figure 3.2.2 Fra-1 immunohistochemical staining of superficial bladder tumours showing the range of nuclear staining intensity; 0 = no staining, + = mild, ++ = moderate, +++ = marked

Table 3.2.2(a-c) shows the breakdown of pathological T stage (Ta or T1) and Fra-1 positivity, again with separate analyses for variation in intracellular Fra-1 localisation. Again, there was no statistically significant correlation between Fra-1 positivity and pathological stage of tumours.

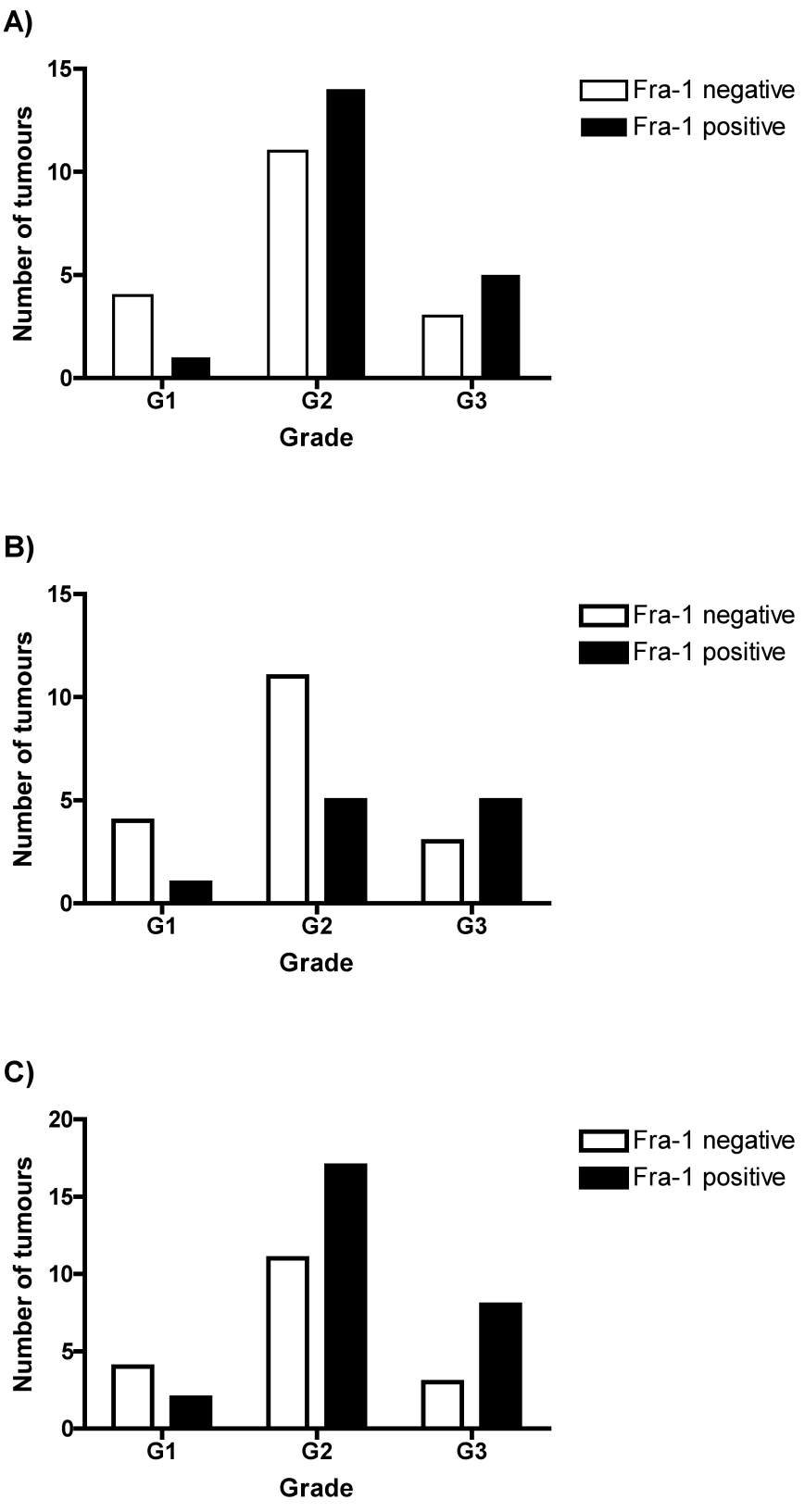

Figure 3.2.3(a-c) Breakdown by tumour grade and Fra-1 positivity in non-invasive bladder cancers, a) with nuclear Fra-1 staining (p=0.278), b) with cytoplasmic Fra-1 staining (p=0.219) and c) with nuclear and/or cytoplasmic Fra-1 staining (p=0.283). All p values calculated from chi-squared analyses

a

Stage	Fra-1 negative	Fra-1 positive
T_a	13	14
T_1	5	6

b

Stage	Fra-1 negative	Fra-1 positive
T_a	13	9
T_1	5	2

c

Stage	Fra-1 negative	Fra-1 positive
T_a	13	20
T_1	5	7

Tables 3.2.2(a-c) Breakdown by tumour stage and Fra-1 positivity in non-invasive bladder cancers, a) with nuclear Fra-1 staining (p=1.000), b) with cytoplasmic Fra-1 staining (p=0.678) and c) with nuclear and/or cytoplasmic Fra-1 staining (p=1.00). All p values calculated from two-tailed Fisher's exact test.

3.3 Comparison of Fra-1 immunohistochemical staining of Human Muscle-Invasive and Non-Invasive Bladder Tumours

A comparison of Fra-1 staining between muscle invasive tumours and non-muscle invasive tumours is shown in Tables 3.3.1 and 3.3.2, taking into account nuclear (3.3.1) and nuclear and/or cytoplasmic staining (3.3.2) in the non-muscle invasive group of tumours. As seen earlier (Section 3.1), all muscle invasive tumours which were positive for Fra-1 demonstrated nuclear staining. Regardless of the intracellular Fra-1 localisation, there is a statistically significant difference in Fra-1 positivity between non-invasive and invasive bladder tumours (two-tailed Fisher's exact test).

Therefore, the incidence of Fra-1 positivity is higher in invasive than non-invasive bladder tumours.

	Fra-1 negative	Fra-1 positive
Non-invasive	30	22
Invasive	21	83

Table 3.3.1 Comparison of Fra-1 staining between non-invasive and invasive bladder tumours, when only nuclear staining is considered in the non-invasive tumours. Two-tailed Fisher's exact $p<0.001$

	Fra-1 negative	Fra-1 positive
Non-invasive	20	32
Invasive	21	83

Table 3.3.2 Comparison of Fra-1 staining between non-invasive and invasive bladder tumours, when nuclear and cytoplasmic staining is considered in the non-invasive tumours. Two-tailed Fisher's exact $p=0.02$

3.4 Characterisation of Human Bladder Cancer Cell Lines

Fra-1 expression was studies in six bladder cancer cells lines, HT1376, J82, RT4, RT112, T24 and UMUC3 (American Type Culture Collection and the European Collection of Cell Cultures). RT4 and RT112 were derived from low grade tumours (G1 and G2 respectively), whereas the remaining four cell types were derived from higher grade (G3) tumours.

Morphologically, they fall into two categories (Table 3.4.1, Figure 3.4.1), one with epithelial appearances (round cells, forming tight cell-cell contacts and islands of cells in culture), and the other with mesenchymal appearances (fusiform cells which are relatively quickly growing, appear motile and do not form clusters). To confirm that the division of the cell lines into these two groups is not purely on morphological grounds, Western Blot (Figure 3.4.3)

and immunofluorescence (Figure 3.4.2 a&b) analyses were undertaken for the epithelial marker E-cadherin and the mesenchymal marker vimentin. In epithelial cells, we observed the typical presence of E-cadherin in the cell membrane whereas there is no detectable E-cadherin in the mesenchymal cells. Conversely, vimentin staining is present, as expected, in the cytoplasm of the mesenchymal cells, but not in the group of epithelial cell lines (except for low levels of vimentin detected in the RT4 cell line). The results of Western Blot analysis correlates with the immunofluorescence data except for RT4 cells, which do not appear to express vimentin (Figure 3.4.3), in contradiction to the immunocytostaining. Two possible reasons exist for this, firstly that the vimentin immunocytostaining is non-specific, or that low levels of vimentin are expressed, but below the level of detection on this Western Blot.

As will be seen throughout this text, this difference in epithelial versus mesenchymal characterisation is important, not only when considering the role and regulation of Fra-1, but it also has a direct bearing on some of the techniques used to manipulate the cell lines, for example the difference in behaviour to electroporation (Section 2.2).

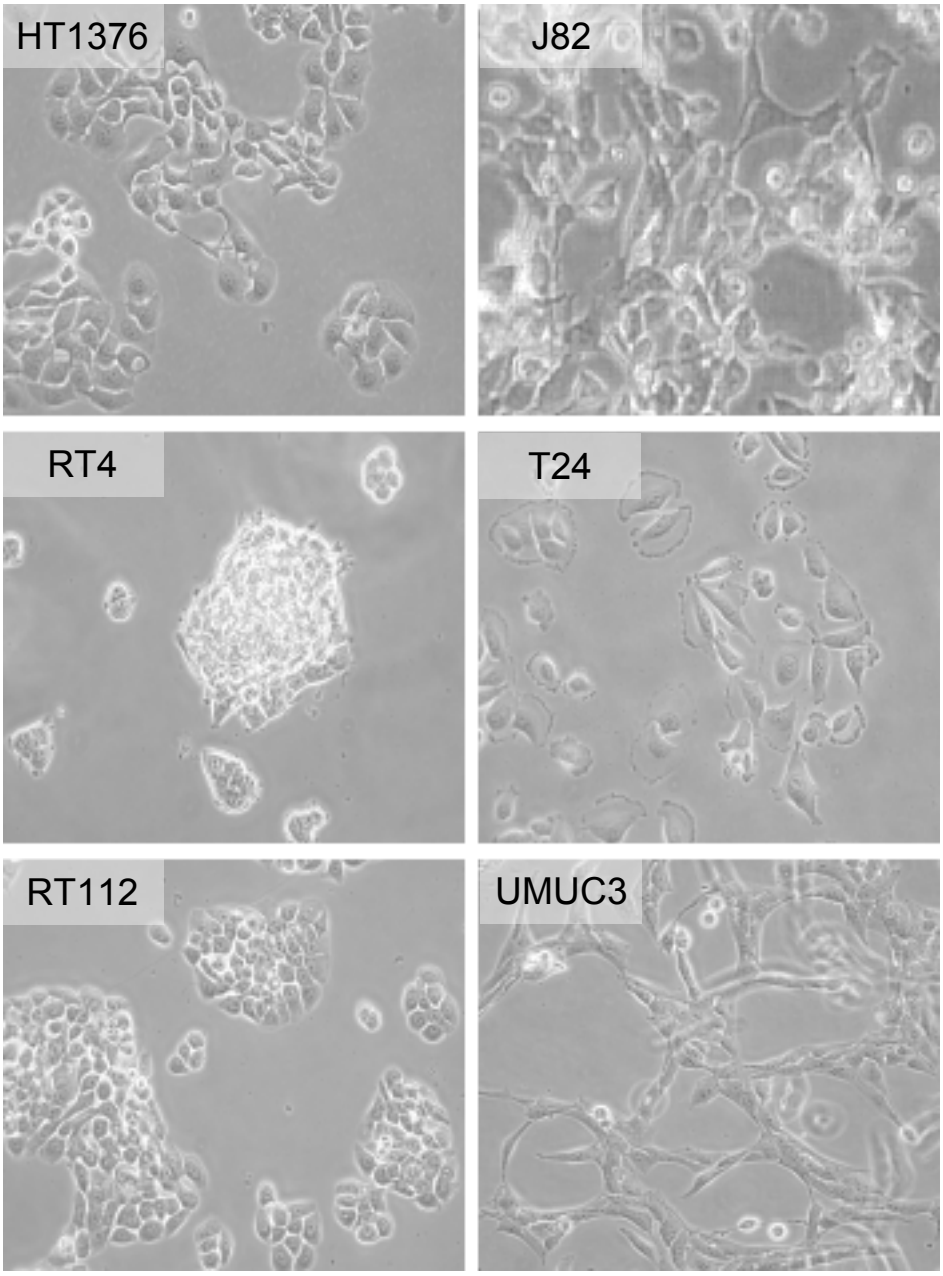

Figure 3.4.1 Morphological appearances of six bladder cancer cell lines. In the left-hand column are the "epithelial" cell lines, in the right-hand column are the "mesenchymal" cell lines

Epithelial	Mesenchymal
HT1376	J82
RT4	T24
RT112	UMUC3

Table 3.4.1 Distribution of bladder cancer cell lines by their morphological and E-cadherin/Vimentin staining characteristics

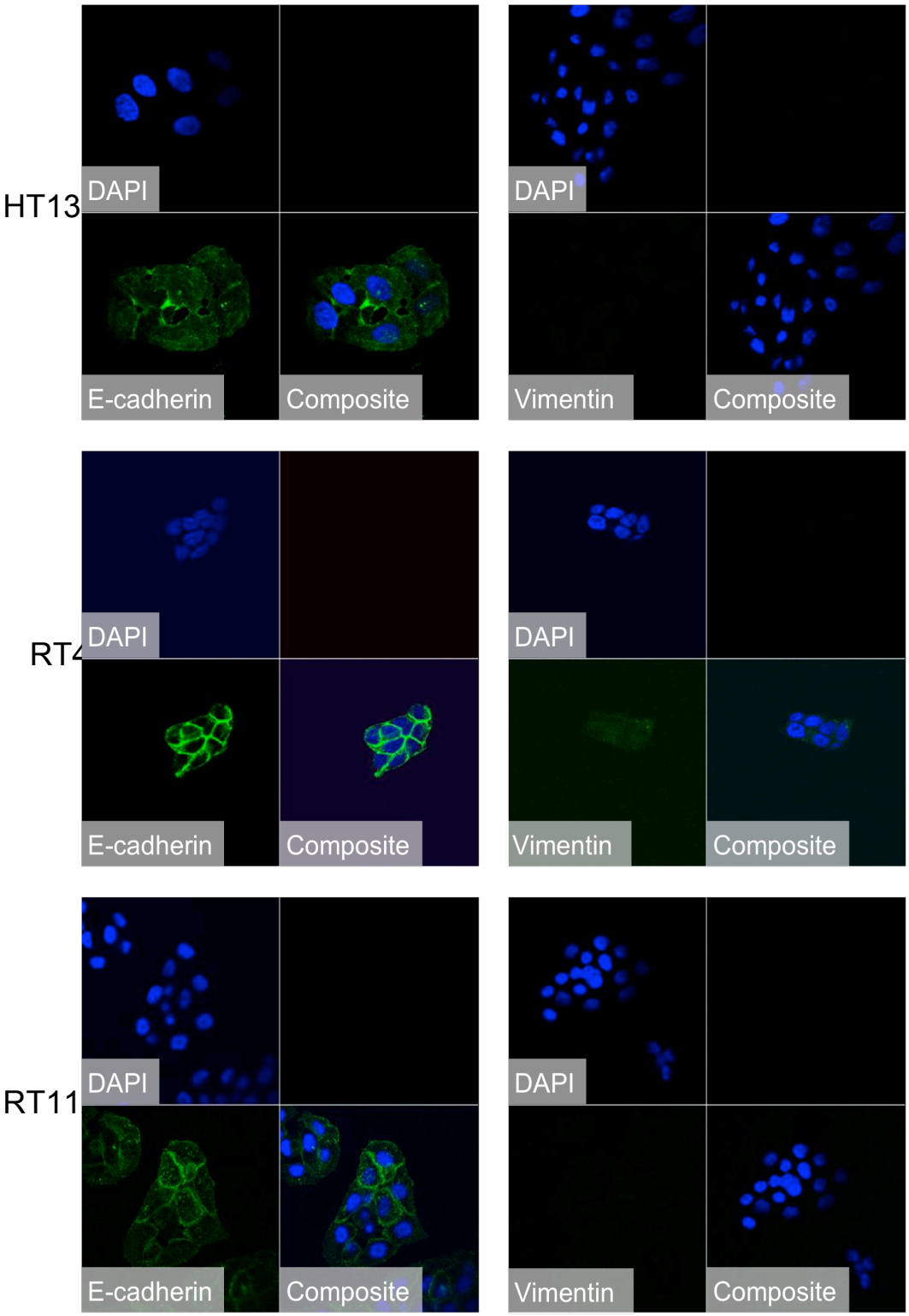

Figure 3.4.2a Confocal microscopy images of DAPI, E-cadherin and Vimentin immunocytostaining of HT1376, RT4 and RT112 cell lines (Primary antibody: Vimentin 1:200 or E-cadherin 1:400, Secondary antibody: Alexa-Fluor 488 donkey anti-mouse 1:1000)

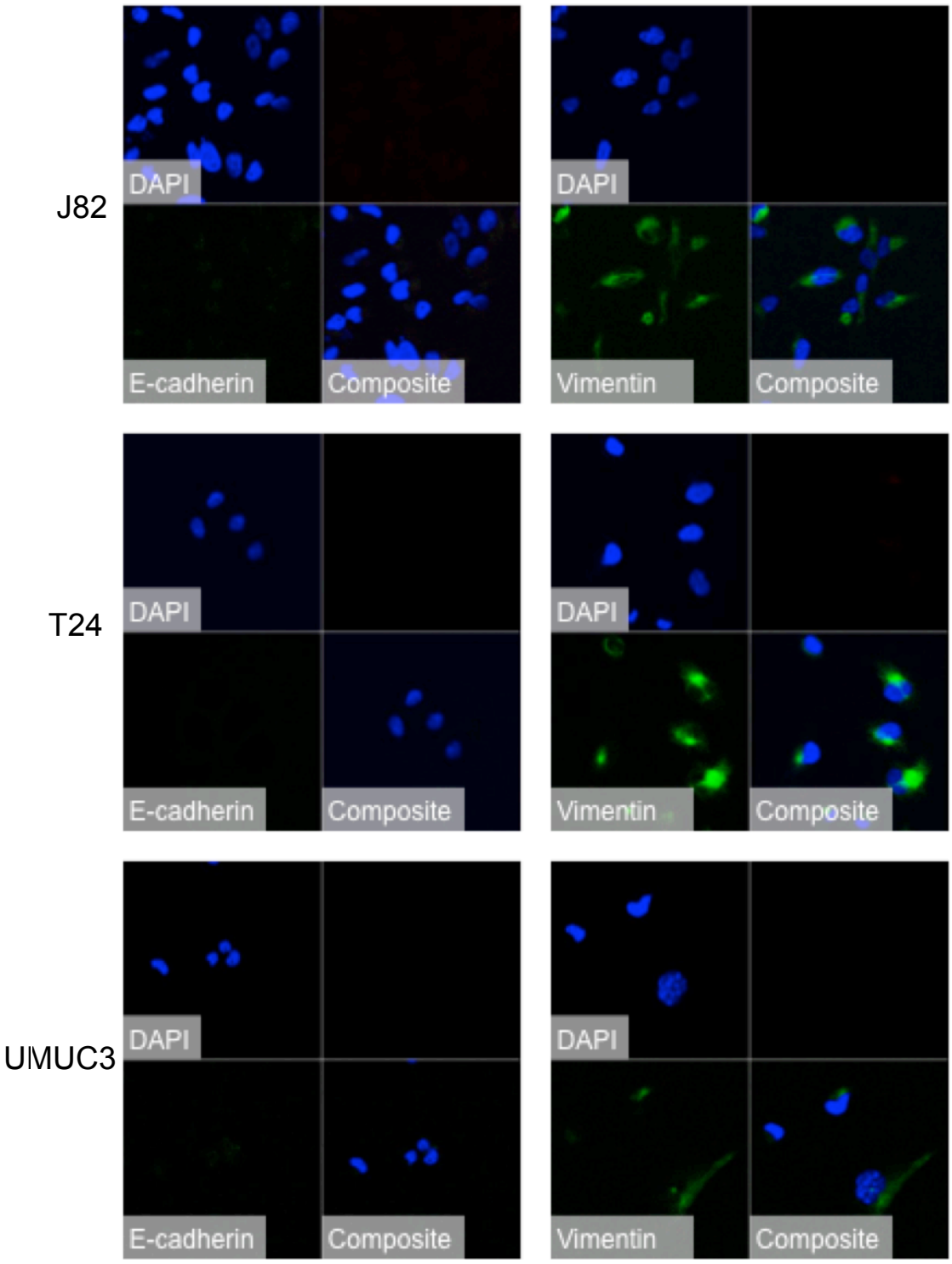

Figure 3.4.2b Confocal microscopy images of DAPI, E-cadherin and Vimentin immunocytostaining of J82, T24 and UMUC3 cell lines (Primary antibody: Vimentin 1:200 or E-cadherin 1:400, Secondary antibody: Alexa-Fluor 488 donkey anti-mouse 1:1000)

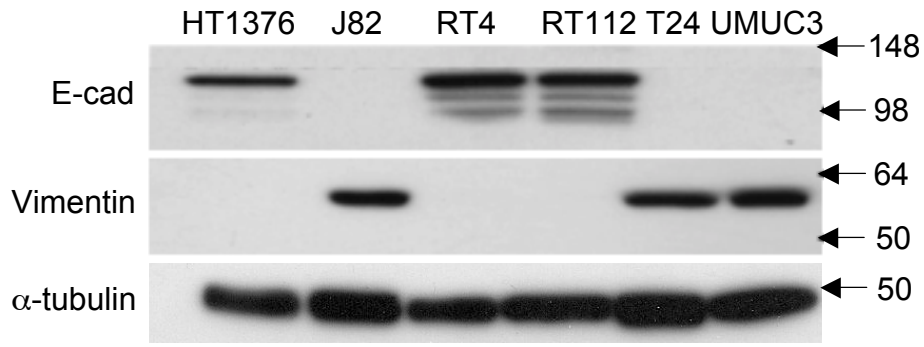

Figure 3.4.3 Western blot of six bladder cancer cell lines for E-cadherin (1:2000) and Vimentin (1:500), both anti-mouse secondary antibody (1:5000), and α-tubulin (1:5000, secondary anti-mouse 1:5000). Figures on the right are molecular weight (kDa).

3.5 Fra-1/*fosl1* expression in bladder cancer cell lines

3.5.1 Fra-1 expression

Fra-1 expression in bladder cancer cell lines was investigated firstly using Western Blot analysis. Subconfluent cell monolayers were harvested as described previously (Section 2.8) and subjected to Western Blot analysis, probing with rabbit anti-Fra-1 antibody as shown in Figure 3.5.1, using α-tubulin as a control for protein loading. This data shows that Fra-1 is expressed in J82, T24 and UMUC3 cell lines, but not in HT1376, RT4 and RT112 cell lines; the data therefore showing Fra-1 expression in mesenchymal but not epithelial bladder cancer cell lines (Section 3.4).

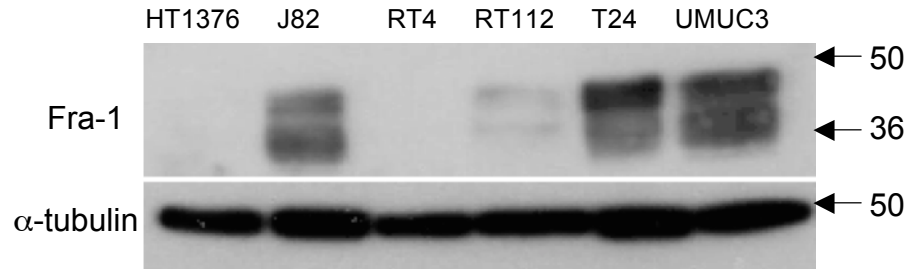

Figure 3.5.1 Western blot of six bladder cancer cell lines for Fra-1 (1:500, secondary anti-rabbit 1:5000) and α-tubulin (1:5000, secondary anti-mouse 1:5000). Figures on the right are the molecular weight (kDa).

3.5.2 *fosl1* mRNA transcripts in bladder cancer cells

We next examined *fosl1* mRNA levels and compared this to Fra-1 protein levels. All six cell lines were grown to sub-confluence and RNA isolated as per Section 2.4. cDNA was then generated from 0.75 μg of RNA using SuperScript III Reverse Transcriptase, and random hexamers as primers (Section 2.5.3). Approximately 10 ng cDNA was then used as the template for a PCR reaction to investigate *fosl1* RNA levels in the six cell lines. *Gapdh* was used as a control gene, and Reddymix Extensor PCR Master Mix 1 was used as the source of DNA polymerases (Section 2.6.3). 25 cycles of PCR were used, 94ºC (1 min), 60ºC (45 sec), 68ºC (1 min), and the primers used (all 20mers) were:

5'*fosl1*: tcacccccagcctggtcttc
3'*fosl1*: cccaagctggctctactgtg
5'*gapdh*: tcttccaggagcgagatccc
3'*gapdh*: caccaccctgttgctgtagc

The *fosl1* sequence is shown in Appendix A1.1, with the 5' primer located at 873-892 and the 3' primer located at 1152-1171; this pair of primers should therefore produce a fragment 299 bases long.

The *gapdh* sequence is shown in Appendix A1.2; the 5' primer 302-321 and the 3' primer 1031-1050, giving a fragment 749 bases long.

Figure 3.5.2 shows the resulting agarose gel, visualised with ethidium bromide under UV light (wavelength 302 nm), having been run along

with a 123 bp DNA marker. This demonstrates that mRNA levels of *fosl1* are higher in mesenchymal J82, T24 and UMUC3 cell lines than in the epithelial HT1376, RT4 and RT112 cell lines. However, *fosl1* mRNA is present in the epithelial cell lines, albeit at low levels; whereas Fra-1 protein is not detectable in HT1376 and RT4 cell lines (and barely in RT112 cells). One reason for this may be that there is regulation of Fra-1 levels at a protein level, as well as at the mRNA level; this is investigated further during this work.

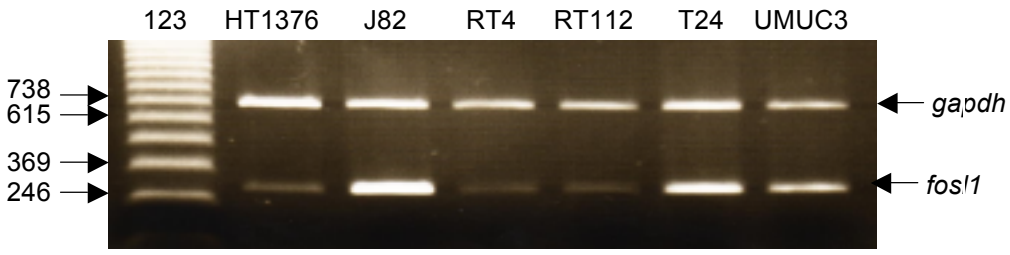

Figure 3.5.2 Minigel showing mRNA levels of *fosl1* (with *gapdh* as control) in six bladder cancer cell lines.

3.5.3 Fra-1 immunocytostaining in bladder cancer cells

Samples of each of the six bladder cancer cell lines were allowed to grow to 30-50% confluency before being fixed and permeabilised as described in Section 2.9.1. Previous work (not shown) had demonstrated an optimal anti-Fra-1 antibody concentration to be 1:200, diluted in D-MEM cell culture medium containing 10% FCS, to block non–specific staining (Section 2.9.2). The secondary antibody used was Alexa Fluor 594 goat anti-rabbit antibody (1:1000). Cells were then visualised with a Zeiss confocal microscope, and are shown in Figure 3.5.3. Mesenchymal cell lines J82, T24 and UMUC3 all have strong nuclear Fra-1 staining, and

appear to have some cytoplasmic staining, although it is unclear whether this is background staining, or a 'real' phenomenon of Fra-1 being present in the cytoplasm. No staining is seen in RT112 cells; faint cytoplasmic staining is seen in HT1376 and RT4 cells, although it is not clear if this is true Fra-1 staining or if it background staining. Correlating this data with the Western Blot data (Section 3.5.1), where, from the epithelial group of cell lines, very low levels of Fra-1 were detected in RT112 cells only, this would suggest that this appearance on immunocytostaining is due to background staining only.

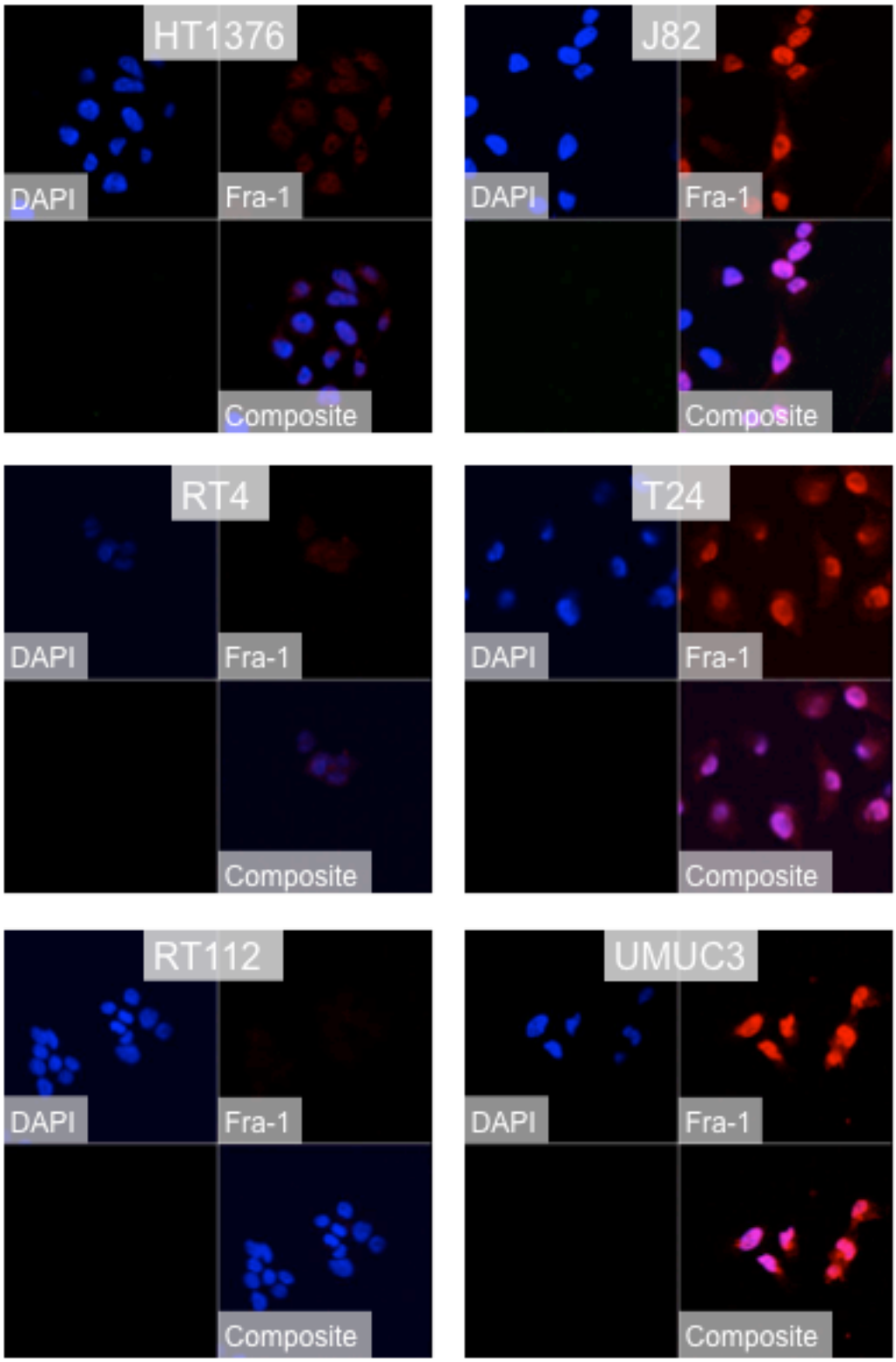

Figure 3.5.3 Immunofluoresence analysis of Fra-1 expression in six bladder cancer cell lines. Nuclei were stained with DAPI.

3.6 Summary of Fra-1 in bladder cancer cells

Fra-1 is present at readily detectable levels (at mRNA level and at protein level with both Western Blot and immunocytostaining) in J82, T24 and UMUC3 cell lines; these cell lines have mesenchymal characteristics.

fosl1 is detectable only at low levels HT1376, RT4 and RT112 cells. Fra-1 is not detectable in HT1376 and RT4 cells, and only detectable at very low levels in RT112; cell lines which have epithelial characteristics.

From a comparison of the mRNA data and the Western Blot data, there is a clear difference between Fra-1 levels in the two groups of cell lines. However, on straightforward visual analysis it may be felt that the difference between the groups at the protein level is somewhat greater than that at the mRNA level. There could be one of several factors involved in this difference, or indeed a combination of factors, including regulation of translation from mRNA to protein and regulation of Fra-1 protein levels at a post-translational level (see Section 1.8)

We have detected nuclear Fra-1 in both tumour tissues and cultured bladder cells. In addition, we have observed its occasional cytoplasmic localisation suggesting that Fra-1 may have a role outside the nucleus.

One criticism of the data above with regard to the cytoplasmic localisation of Fra-1 is that the immunocytostaining in the cytoplasm could be due to

crossreactivity of the anti-Fra-1 antibody used in this study. To address this criticism, we next transfected all six cell lines with the HA-tagged full length Fra-1 construct (the generation of this construct is described in detail in Section 4.1) or an HA-tagged p73-alpha construct (which is localised exclusively to the nucleus [138], a gift from Dr Mario Rossi, Medical Research Council, Toxicology Unit, University of Leicester), and stained them with an anti-HA antibody (Santa-Cruz). Anti-HA staining of J82 (Figure 3.6.1) and T24 cells (not shown) which have been transfected with HA-tagged Fra-1 and HA-tagged p73, clearly demonstrates that HA-Fra-1 appears throughout the cell, whereas HA-p73 is localised to the nucleus. Given that the same transfection technique was used for both vectors, and the same protein tag was used to detect both Fra-1 and p73 proteins, we conclude that localisation of Fra-1 in the cytoplasm is not an artefact in our experimental system. These data are consistent with the reports of Chiappetta *et al*. [94] and Ma *et al*. [92] who detected Fra-1 in the cytoplasm of tumour cells in thyroid and non-small cell lung carcinoma respectively.

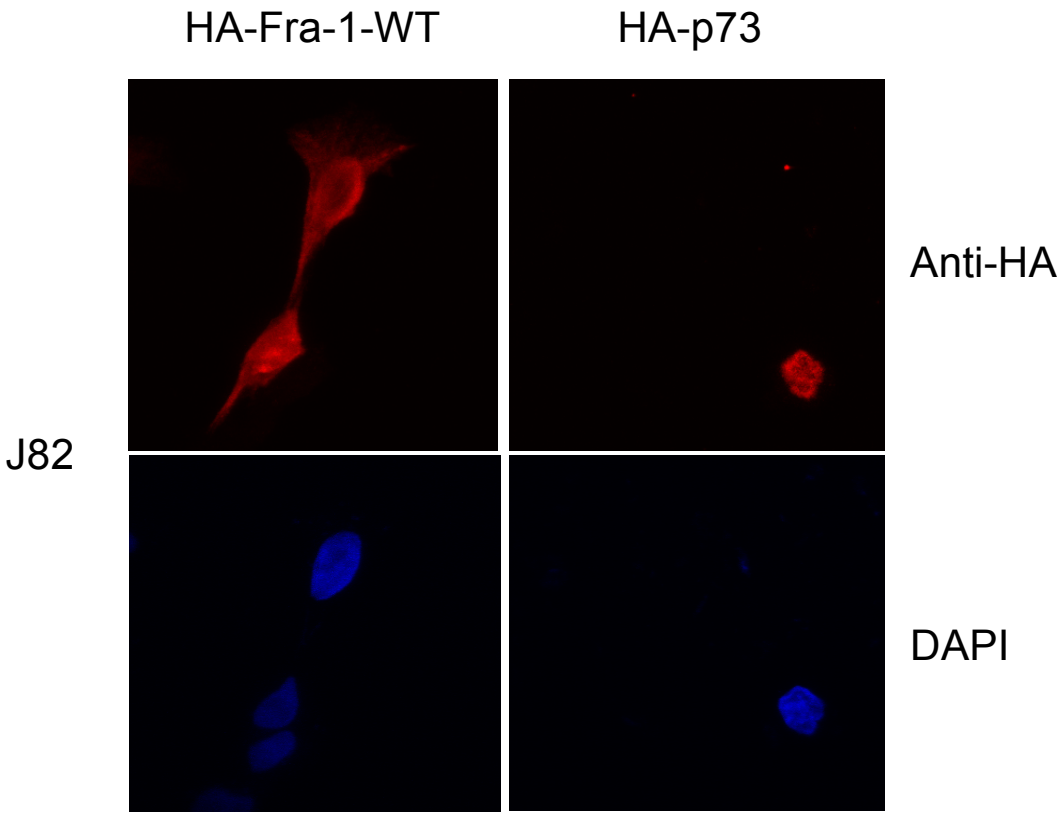

Figure 3.6.1 Immunofluoresence analysis of J82 cells transfected with either HA-Fra-1WT or HA-p73 and stained with Anti-HA and DAPI to demonstrate subcellular localisation of transfected proteins

Chapter 4 – Results 2

Regulation of Fra-1 in Bladder Cancer Cells

4.1 Generation of a Haemagglutinin (HA)-tagged Fra-1 expression vector

To further investigate factors involved in the regulation of Fra-1 levels within bladder cancer cells, including both features of the Fra-1 protein itself and additional regulatory proteins, it was necessary to generate an expression vector which was capable of being transfected into bladder cancer cell lines and expressing Fra-1 protein (use of this expression vector has already been demonstrated in Section 3.6). As this form of Fra-1 (which I will now refer to as exogenous Fra-1) is exempt from the usual transcriptional and translational controls which endogenous *fosl1*/Fra-1 is subject to, it allows further investigation of post-translational events that regulate Fra-1 levels. It has been previously shown that the N-terminus of Fra-1 can be deleted without significantly influencing Fra-1 stability (although this leads to functional inactivation), whereas deletion of the Fra-1 C-terminus has no effect on Fra-1 function, but increases protein stability, thereby leading to a marked increase in Fra-1 protein accumulation [136]. To allow us to distinguish between endogenous and exogenous Fra-1, the expression vector also encodes a Haemagglutinin (HA) tag; as we are interested in the regulation of Fra-1 stability (hypothesized to be regulated more so by the C-terminus than the N-terminus, given the degree of sequence homology between c-Fos and Fra-1 towards the C-terminus, and that Ser^{362} and Ser^{374} of c-Fos are important in the ERK/RSK-mediated regulation of c-Fos [71]), it was therefore considered appropriate to insert the HA-tag at the N-terminus of Fra-1, so that it is

unlikely to interfere with regulatory motifs within the C-terminus and also allow us to modify proposed regulatory areas within the C-terminus.

The pCGN vector (see Figure 4.1.1, reproduced from Fiordalisi *et al*. [139]) was selected to form the basis for our HA-Fra-1 expression vector. The vector was already in use within our laboratory (in this case expressing an N-terminal HA-tagged ß-catenin construct) and incorporates an N-terminal HA tag and includes a sequence encoding for Ampicillin resistance. As described below, the HA-Fra-1WT expression vector encoding full-length Fra-1 was generated by excising the ß-catenin insert and inserting (in the first instance) a full-length insert encoding Fra-1.

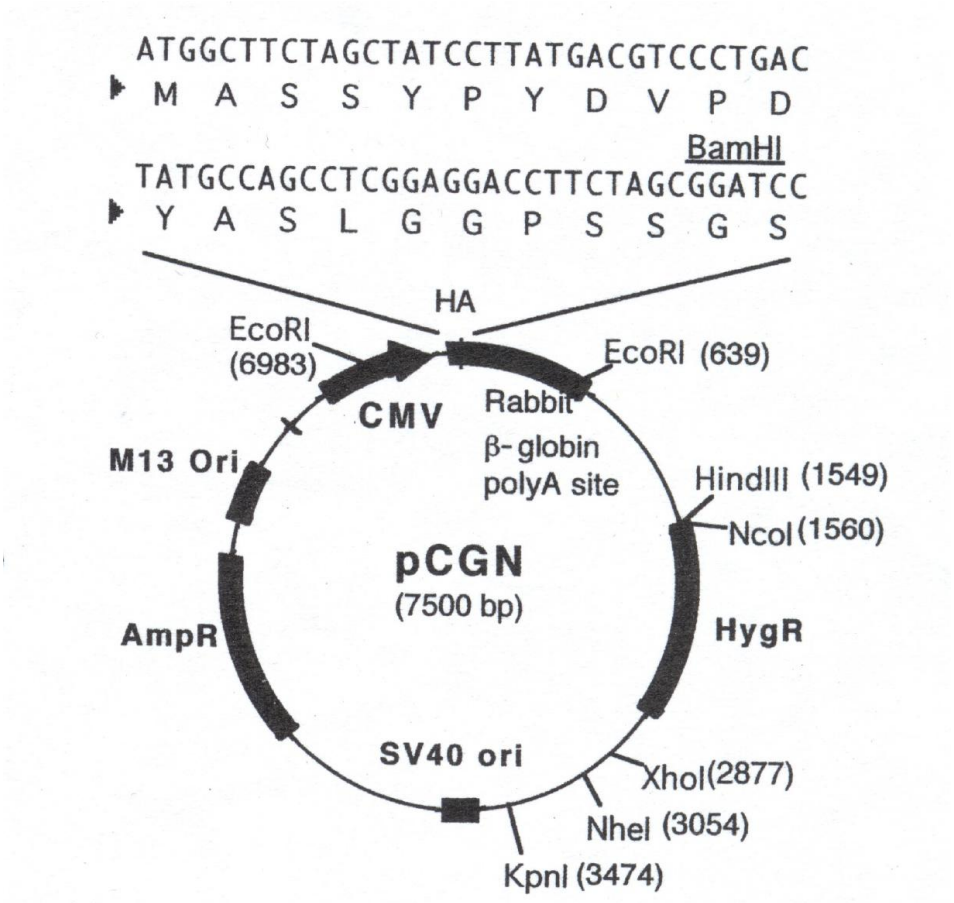

Figure 4.1.1 pCGN vector map (reproduced from Fiordalisi *et al*. 2001). Fra-1 was inserted adjacent to the HA-tag between *Xba*I (5') and *Bam*HI (3') restriction sites.

4.1.1 Generation of an mRNA template for *fosl1* amplification

The first step in producing the pCGN-HA-Fra-1WT vector was to isolate RNA which could be used as a template from which *fosl1* DNA could be amplified using PCR.

RNAs from J82 and RT112 cells were isolated using TRIzol® as described in Section 2.4. Prior to isolation, all cells had been starved of serum for 24 hours and for each cell type, one flask containing approximately 4 x 10^6 cells was treated with 20% foetal calf serum for four hours, and a similar number of cells in a second flask continued to be incubated in serum-free media. Following isolation, to assess RNA quality and accuracy of concentration calculation, 10 μg of the RNAs were subjected to gel electrophoresis as described in Section 2.4; the results of this are shown in Figure 4.1.2.

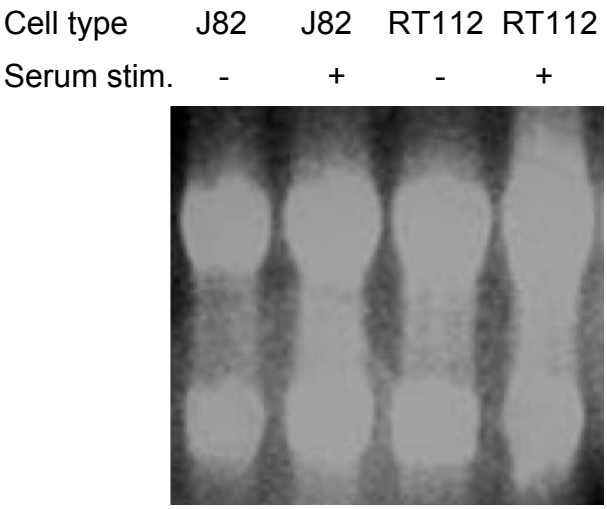

Figure 4.1.2 1.2% agarose, 6.4% formaldehyde gel electrophoresis with 10 μg RNA loaded per lane. mRNA was isolated from either J82 or RT112 bladder cancer cells with or without stimulation with 20% FCS.

4.1.2 Generation of pCGN-HA-Fra-1WT using *rTth* DNA polymerase

The next step in producing the pCGN-HA-Fra-1WT vector was to generate cDNA from this RNA produced in Section 4.1.1 and then amplify the cDNA which encodes *fosl1*. At the same time restriction sites for *Xba*I (5') and *Bam*HI (3') were incorporated into the final product by the design of the amplification oligonucleotides. Already in use in our laboratory was the combined reverse transcriptase/DNA polymerase EZ *rTth* RNA PCR kit (GeneAmp, Section 2.5.1).

Because of initial difficulties with amplifying *fosl1* using oligonucleotides designed to anneal directly to the start and stop codons with leading or trailing *Xba*I or *Bam*HI restriction sites respectively (data not shown), we performed a first amplification step where oligonucleotides which annealed a distance upstream and downstream of the start/stop codons were used; this PCR product being known as "Long *fosl1*", and was 1027 bp in length.

Long *fosl1* 5': GAACCCAGCAGCCGTGTACC
anneals at 145-164 of *fosl1* (Appendix A1.1)

Long *fosl1* 3': CCCAAGCTGGCTCTACTGTG
anneals at 1152-1171 of *fosl1* (Appendix A1.1)

1.2 μg of J82 (serum-stimulated) mRNA was amplified using the method in Section 2.5.1, using the "Long *fosl1*" oligonucleotides with the following thermal profile:

60º	40 min	
94º	1 min	
94º	20 sec	} x 40 cycles
63º	2 min	
63º	7 min	
4º	thereafter	

The result of this PCR is shown in Figure 4.1.3. This produced two predominant products (between 369 and 492 bp and between 984 and 1107 bp; there is an additional product of lesser quantity which is just shorter than 984 bp. The product of our interest is the larger product of between 984 and 1107 bp which should be "Long *fosl1*" with a length of 1027 bp. "Long *fosl1*" was isolated from the PCR reaction using agarose gel electrophoresis (Section 2.6) and the 1027 bp band was excised and DNA eluted according to Section 2.7.3).

Full length, wild-type *fosl1* with 5' *Xba*I and 3' *Bam*HI restriction sites was the produced using a further PCR reaction with "Long *fosl1*" as the template and the following oligonucleotides as primers:

5'*fosl1Xba*I: GATCTAGAttccgagacttcggggaaccc

3'*fosl1Bam*HI: AAGGATCCctcaggcgcctcacaaagcgag

(lower cases represent *fosl1* sequence)

(underlined bases represent *Xba*I and *Bam*HI sites)

Taq polymerase was used (Section 2.6.1) in this reaction as we had produced the cDNA template earlier, with the following thermal profile:

94°	2 min	
65°	30 sec	
72°	2 min	
94°	20 sec	} x 40 cycles
72°	2 min	
72°	7 min	
4°	thereafter	

This reaction produced a fragment with the expected length of 839 bp. This fragment was then digested with *Pst*I (recognition site CTGCA|G) which cuts *fosl1* four times, at 339, 588, 630 and 651 (these figures are relative to the numbering given in Appendix A1.1, not the position within *fosl1* itself). As a control, *fosl1* was digested with *Kpn*I (recognition site GGTAC|C) which should not (and in Figure 4.1.4 is shown not to) cut *fosl1*.

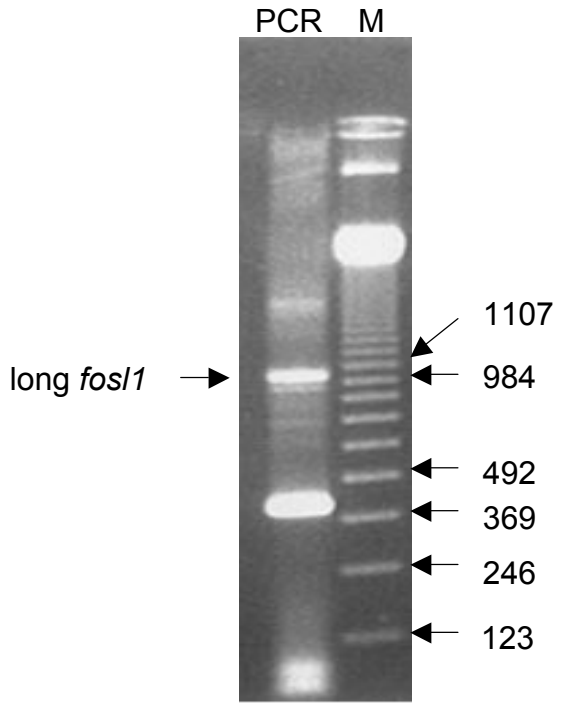

Figure 4.1.3 1.2% agarose + EtBr gel electrophoresis showing results from PCR of J82 (serum stimulated) RNA with 'long *fosl1*' oligonucleotides, 'long *fosl1*' being present as a 1027 bp product (uppermost bright band). M = 123 bp DNA ladder.

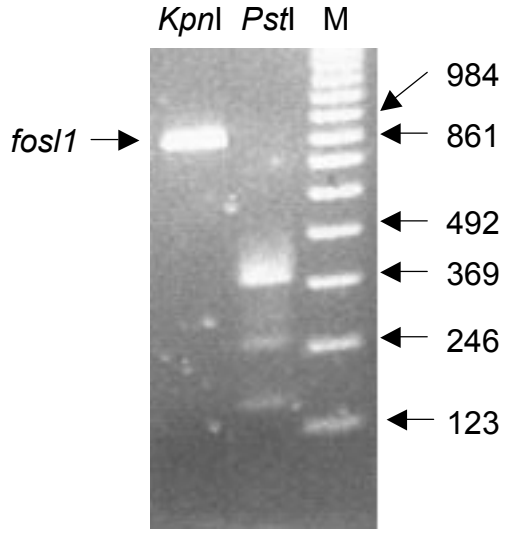

Figure 4.1.4 1.2% agarose + EtBr gel electrophoresis showing results of digesting eluted *fosl1* PCR product with either *Kpn*I or *Pst*I. M = 123 bp DNA ladder

This leads to fragments of 21, 42, 157, 249 and 370 bp, as shown in Figure 4.1.4, confirming that we have amplified *fosl1*. It is also noted that the elution was clean, isolating only one PCR product (*fosl1*) demonstrated by the single band seen in the *Kpn*I (undigested) lane.

To prepare the pCGN vector and the Fra-1 insert for ligation, they were both digested with *Bam*HI and *Xba*I (recognition sites G|GATCC and T|CTAGA respectively) and during the process, the ß-catenin insert was excised from our pCGN vector. 2.4 μg of pCGN-ß-catenin was digested with 16 units of *Xba*I using 1x One-phor-all buffer for two hours at 37ºC (Section 2.7.2). 12 μl of the *fosl1* amplification reaction was similarly treated, in a total reaction volume of 25 μl. Because *Xba*I and *Bam*HI activity in One-phor-all buffer is different, after two hours of incubation with *Xba*I, *Xba*I was inactivated by heating to 65ºC for 10 minutes, and

then additional One-phor-all buffer was added (bringing the total concentration to 2x), along with 20 units of *Bam*HI and then incubated for a further two hours at 37ºC. This reaction was then terminated by heating to 65ºC for ten minutes. The products of these reactions were then subjected to agarose gel electrophoresis, their bands excised and DNA then eluted from the gel (Section 2.7.3). To assess the success of electrophoretically separating the fragments, elution from the gel, and to assess the relative concentrations, an aliquot of the resulting DNAs were subjected to further electrophoresis (Figure 4.1.5).

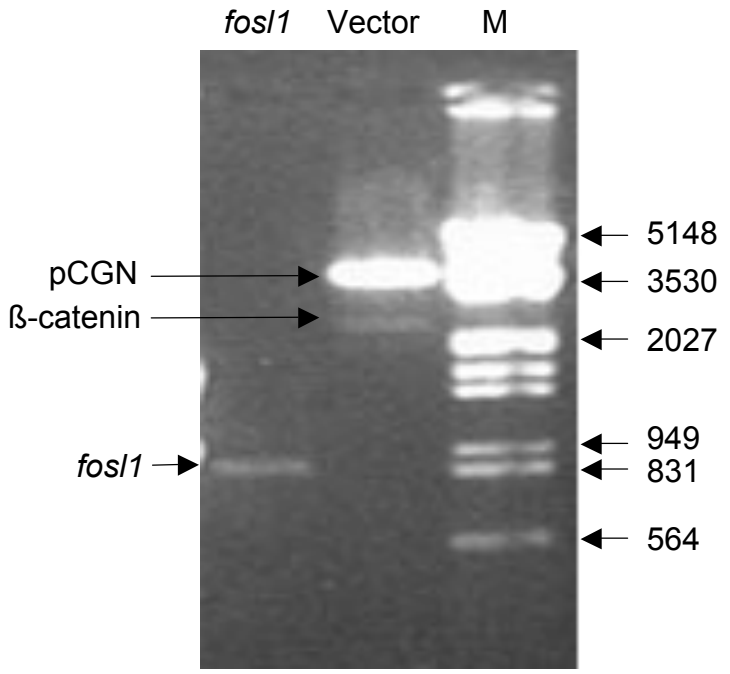

Figure 4.1.5 1.2% agarose + EtBr gel electrophoresis showing the results of digesting the *fosl1* insert and the pCGN-ß-catenin vector with *Bam*HI and *Xba*I. M= λDNA/*Eco*RI *Hind*III digest

The prepared *fosl1* insert and pCGN vector were then ligated and the products subjected to agarose gel electrophoresis as per Section 2.7.4. Chemically competent *E. coli* were then transformed with the ligation reactions (Section 2.3.1) and allowed to incubate overnight at 37ºC. Single colonies were then separated transferred into 2 ml Luria Broth with 100 μg/ml ampicillin and incubated overnight at 37ºC.

Vector DNA was isolated from these amplified clones using the QiaPrep Spin Miniprep Kit (Section 2.3.3) and digested with *Bam*HI and *Xba*I. Unlike the earlier digestion with *Bam*HI and *Xba*I were the digestion was performed in two stages to maximise efficiency, because here we were just screening clones for the presence of *fosl1*, therefore efficiency is not as important, the reaction was carried out in one step, and for a shorter time. The resultant products were then run on a 1.2% agarose gel (Section 2.6, Figure 4.1.6) and demonstrated the *fosl1* insert in four of the twelve isolated clones. Seven out of the twelve clones appeared to contain ß-catenin, probably due to incomplete excision of the insert from the vector by *Bam*HI and *Xba*I, with one end of the insert left attached to the vector. Concentrations of the pCGN-HA-Fra-1 vector DNA were calculated (Section 2.3.2) and adjusted to 62.5 ng/μl for sequencing (Section 2.7.4).

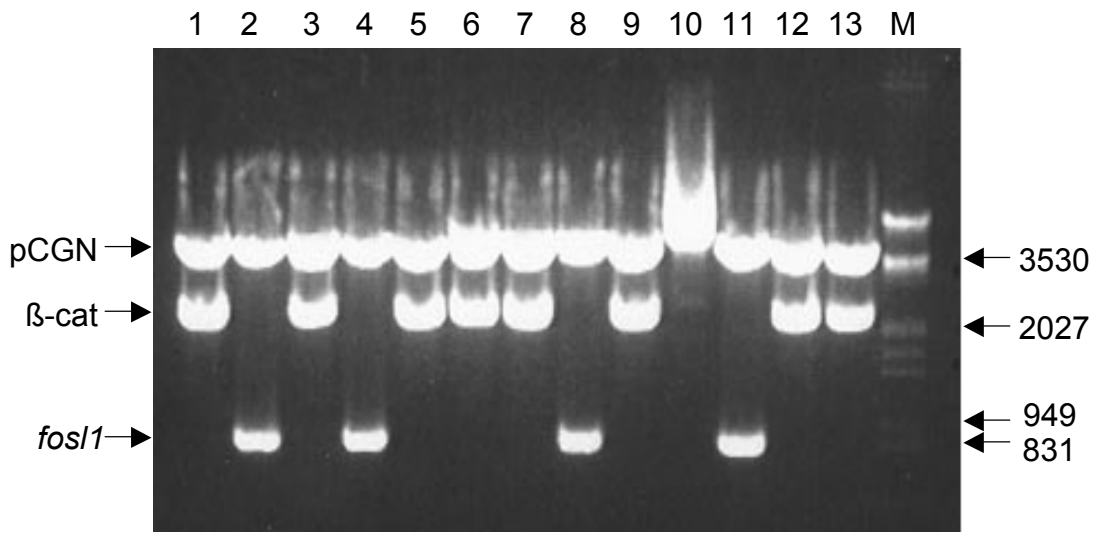

Figure 4.1.6 1.2% agarose + EtBr gel electrophoresis showing results of digesting DNA isolated from clones 1-12 with *Bam*HI and *Xba*I. Lane 13: original pCGN-HA-ß-catenin vector. M = λDNA/*Eco*RI *Hind*III digest

4.1.3 Sequencing results for pCGN-HA-Fra-1 (*rTth* DNA polymerase)

Both the converted sequencing data, and the raw sequencing data were compared with the predicted *fosl1* sequence. Unfortunately, all four clones contained significant mutations rendering them unusable. An example of the mutations present in one clone is:

218	a -> g	agc -> ggc	Ser -> Gly
223	*c -> t*	*tcc -> tct*	*Ser -> Ser*
287	a -> t	aag -> tag	Lys -> STOP
326	a -> g	agt -> ggt	Ser -> Gly
371	a -> t	agc -> tgc	Ser -> Cys
430	*a -> g*	*gga -> ggg*	*Gly -> Gly*
543	c -> t	gcg -> gtg	Ala -> Val
603	a -> g	aaa -> aga	Lys -> Arg
616	*g -> a*	*gag ->gaa*	*Glu -> Glu*
794	t -> g	tcc -> gcc	Ser -> Ala
851-853	ccc -> cc	Frameshift	
913 + 947	further point mutations but unable to assess alteration in amino acid sequence because of prior frameshift		

Note 1: positions refer to the map given in Appendix A1.1, not the position within *fosl1*, and it is noted that some mutations in DNA sequence do not give rise to mutations in protein sequence (highlighted in italics)

Note 2: There are no published mutations described in *fosl1*

Note 3: Further work (see below) generates a Fra-1 vector with no amino acid mutations, and as this further work used the same mRNA template, the mutations listed above have been generated by our techniques, rather than being newly described *fosl1* mutations.

4.1.4 Generation of pCGN-HA-Fra-1WT vector using a dedicated reverse transcriptase and DNA polymerase

One possible reason for the failure of the above experiment to produce a mutation-free vector was the use of a combined reverse transcriptase/DNA polymerase which required two PCR steps, thereby increasing the likelihood of introducing errors. Our next step, therefore was to use a dedicated reverse transcriptase (Superscript III) to generate cDNA, and then use *Taq* polymerase in a single PCR-step.

3.2 μg total RNA (RT112, serum-stimulated) was used as the template, with the 3' "long *fosl1*" primer as the oligonucleotide, along with 200 units Superscript III (Section 2.5.2). This product was then used as the template in the PCR step, using the following thermal profile:

94º	2 min	
65º	30 sec	
72º	2 min	
94º	20 sec	x 30 cycles
72º	2 min	
72º	7 min	
4º	thereafter	

A successful reaction was confirmed by running an aliquot of the PCR product on an agarose gel and then the *fosl1* product was eluted from the PCR reaction using phenol/chloroform extraction (Section 2.7.1). It was then digested with *Bam*HI and *Xba*I in parallel with the pCGN-HA-ß-catenin vector (Section 2.7.2). The products from this digest were then subjected to agarose gel electrophoresis to allow separation of the *fosl1* insert and the opened pCGN-HA vector (Section 2.7.3). Ligation of the prepared *fosl1* insert and pCGN-HA vector was then performed as in Section 2.7.4. Many colonies were produced from the subsequent transformation of *E. coli* and DNA from a number of these was then isolated using the QiaPrep Spin Miniprep kit (Section 2.3.3) and the products digested with *Bam*HI and *Xba*I (as in Section 2.7.2). This demonstrated that four out of six clones contained a fragment with a molecular weight consistent with that of the *Bam*HI/*Xba*I digested *fosl1* insert (835 bp). One of these clones was then sent for sequencing as described previously (Section 4.1.2).

Unfortunately, sequencing revealed seven mutations within the *fosl1* portion of the pCGN-HA-Fra-1 vector:

756	a -> g	agc -> aac	Ser -> Asn
783	t -> c	gta -> gca	Val -> Ala
788	t -> c	tgt -> cgt	Cys -> Arg
825	a -> g	gag -> gcg	Glu -> Ala
843/4	ca -> ag	aca -> aag	Thr -> Lys
916	*t -> c*	*cct -> ccc*	*Pro -> Pro*
933	g -> a	cgc -> cac	Arg -> His

Note: positions refer to the map given in Appendix A1.1, not the position within *fosl1*, and it is noted that some mutations in DNA sequence do not give rise to mutations in protein sequence (highlighted in italics).

All of these mutations (six of which lead to a change in protein sequence) are in the 3' portion of the *fosl1* insert. Because of this, two options were then available to us. One was to send one or more of the other *fosl1* clones for sequencing in the hope that they are free of mutations, it was not guaranteed that one of the other clones would however be free of mutations. The other option was to excise the 3' portion of *fosl1* from the pCGN-HA-Fra-1WT vector, clone a smaller fragment from the cDNA generated earlier using Superscript III Reverse Transcriptase and then ligate this into the vector.

4.1.5 Cloning a new, unmutated 3' portion of *fosl1*

There were two strong arguments for following the second suggestion described above, i.e. excise the 3' end of *fosl1* and introduce a newly cloned fragment. Firstly, as above, there was no guarantee that the other

clones were mutation free, and secondly, one reason for generating the Fra-1 vector was to allow us to manipulate the Fra-1 C-terminus to assess the effect on protein stability. To do this, we would be using essentially the same technique, i.e. excising the 3' end of *fosl1* from the pCGN-HA-Fra-1WT vector and cloning in a manipulated fragment. On the basis of these arguments, the decision was made to clone in a new 3' fragment from existing cDNA. By dealing with a smaller fragment, rather than the entire length of *fosl1*, it also enabled us to select a higher fidelity DNA polymerase, *Pfu* DNA polymerase.

Firstly, it was necessary to identify a single restriction site within the 3' region of *fosl1* which was located such that the entire mutated region of *fosl1* would be excised, and that this excised region also incorporated potential sites of interest for later manipulation. The enzyme selected must also only cut once within the *fosl1* sequence, should not cut at any sites within the pCGN-HA vector, and ideally use the same reaction buffer as *Bam*HI which would be used to cut the 5' end. To select such an enzyme, NEBcutter (http://tools.neb.com/NEBcutter2/index.php) was used and identified the restriction enzyme *Sbf*I as a suitable candidate. *Sbf*I generates sticky ends, and has a recognition sequence CCTGCA|GG which is present at 583-590 within *fosl1* (Appendix A1.1).

For the initial PCR of *fosl1* cDNA, the following oligonucleotides were used, generating a fragment of 437 bp length:

5'*fosl1Sbf*I: cgacttcctgcaggcggagactg

3'*fosl1Bam*HI: AAGGATCCctcaggcgcctcacaaagcgag

(lower cases bases represent *fosl1* sequence)

(underlined bases represent *Sbf*I and *Bam*HI sites)

2 μl *fosl1* cDNA was amplified using the protocol in Section 2.6.2 using the above oligonucleotides and the following thermal profile:

94º	1 min	
94º	45 s	x 35 cycles
68º	45 s	
72º	1 min	
72º	10 min	
4º	thereafter	

The product of this reaction was confirmed on agarose gel electrophoresis to have a molecular weight consistent with the *fosl1Sbf*I*Bam*HI fragment (437 bp) and phenol/chloroform extraction was then performed (Section 2.7.1), followed by a one step digestion with *Bam*HI and *Sbf*I (compared with the two steps used previously for *Bam*HI and *Xba*I), using NEBuffer4 as the sole reaction buffer. In parallel, pCGN-HA-Fra-1WT was similarly digested. These digestion products were then subjected to agarose gel electrophoresis and vector and inserts were excised and eluted from the agarose gel (Section 2.7.3). Aliquots of the elution products were then further exposed to agarose gel electrophoresis to confirm the presence of the product and to assess relative proportions (Figure 4.1.7).

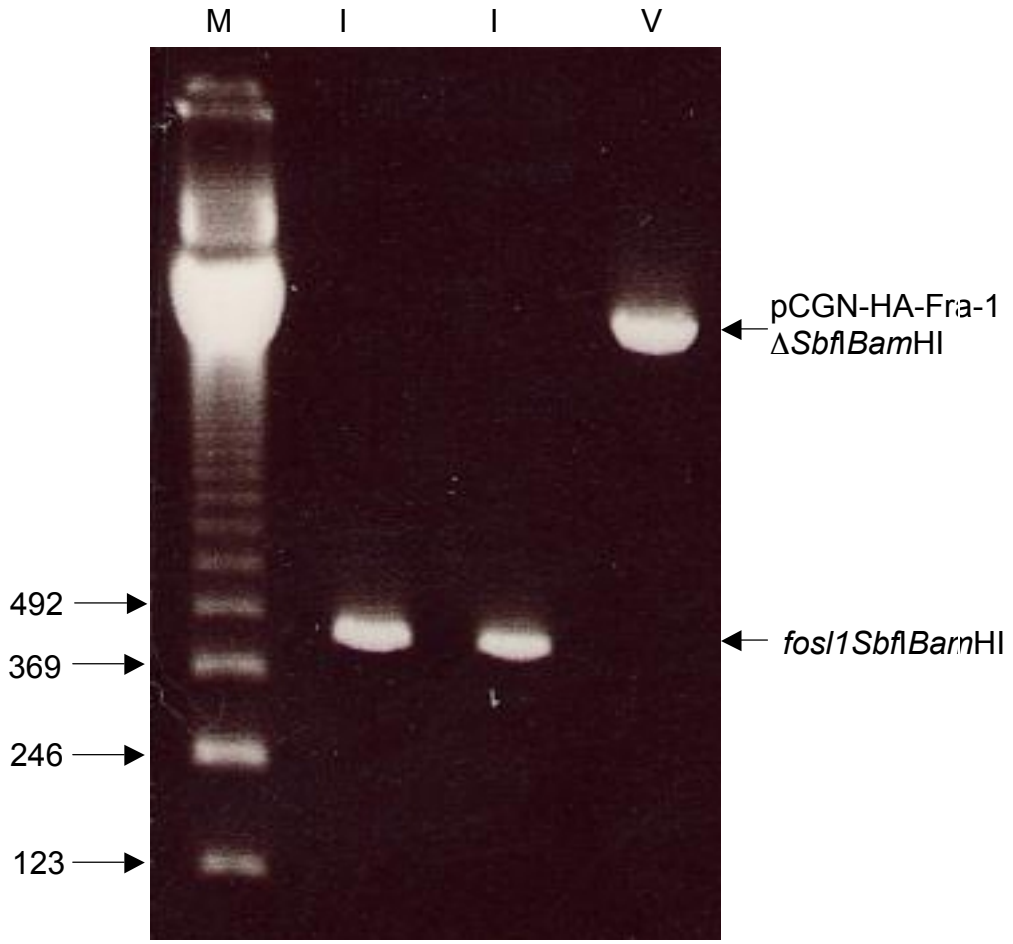

Figure 4.1.7 1.2% agarose + EtBr gel electrophoresis showing the result of digestion and elution of *fosl1Sbf*I*Bam*HI (I, in duplicate) and pCGN-HA-Fra-1WT(mut) (V) with *Bam*HI and *Sbf*I. M = 123 bp ladder.

The pCGN-HA-Fra-1Δ*Sbf*I*Bam*HI vector and *fosl1Sbf*I*Bam*HI inserts were then ligated (Section 2.7.4) and then subjected to agarose gel electrophoresis to confirm successful ligation. *E. coli* were then transformed (Section 2.3.1) with the ligated samples, subsequent colonies amplified and then the DNA isolated using the Qiaprep Spin Miniprep kit (Section 2.3.3) and digested with *Sbf*I and *Bam*HI (Section 2.7.2). The resulting DNA was subjected to agarose gel electrophoresis confirming that a fragment consistent with *fosl1Sbf*I*Bam*HI (437 bp) is present,

although it is not possible from this to determine whether or not this is the mutated fragment or the non-mutated fragment. The DNA was then sent to PNACL for sequencing (Section 2.7.4) which confirmed the presence of a wild-type Fra-1 containing no mutations, along with an N-terminal HA tag. This vector is subsequently referred to as pCGN-HA-Fra-1WT.

4.1.6 Expression of pCGN-HA-Fra-1WT in HEK 293 cells

To confirm that the pCGN-HA-Fra-1WT vector was capable of leading to the expression of HA-Fra-1WT in mammalian cells, it was first further amplified using a large scale amplification (Section 2.3.2) to generate quantities suitable for transfection. Once this amplification and isolation was performed, the Human Embryonic Kidney cell line HEK 293 was used to assess expression of the vector. HEK 293 cells were already used within our laboratory and were easy to culture and very readily transfectable using the electroporation techniques described earlier; our previous data (not shown) demonstrated that HEK 293 cells had greater transfection efficiency than any of the mesenchymal bladder cancer cell lines (J82, T24 and UMUC3) and were therefore deemed suitable for preliminary experiments.

2 x 10^6 HEK 293 cells were transfected (Section 2.2) with 1 μg pEGFP-C1 (encoding Enhanced Green Fluorescent Protein) and 5 μg pCGN-HA-Fra-1WT (or no Fra-1 construct as control) and cultured for forty-eight hours. High transfection efficiency was noted (as assessed by EGFP expression at epifluorescence microscopy) and then cells lysed and

20.5 μg of protein subjected to Western Blot analysis on a 10% SDS-PAGE gel (Section 2.8). Two membranes were produced in parallel, one to be probed with anti-Fra-1 antibody and the other with anti-HA antibody. Figure 4.1.8 confirms that pCGN-HA-Fra-1WT can be expressed in 293 cells, and that it can be detected with both anti-Fra-1 and anti-HA antibodies.

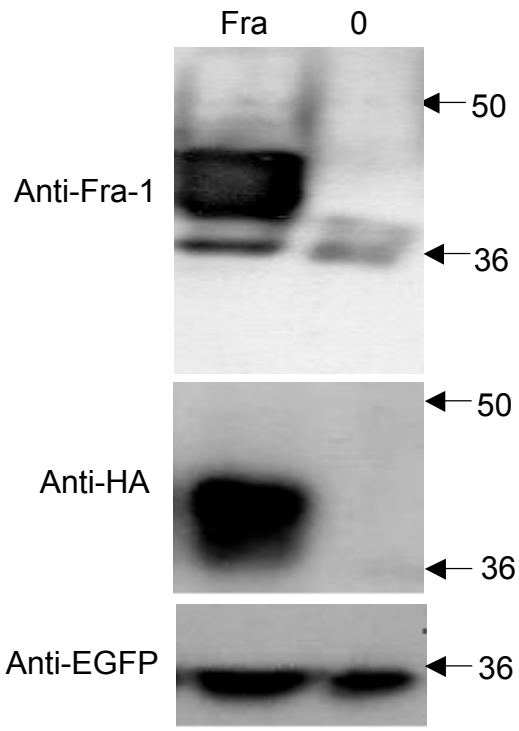

Figure 4.1.8 Western Blot of HEK 293 cells transfected with pCGN-HA-Fra-1WT and pEGFP-C1 (Fra lane) or just EGFP-C1 (0 lane). Anti-Fra-1 (1:500), anti-HA (1:500), anti-EGFP (1:300), all secondary anti-rabbit (1:5000). MW in kDa shown on right

4.2 Effect of C-terminal deletion on Fra-1 levels in bladder cancer cell lines

Andersen *et al*. [136] have previously demonstrated that a C-terminal truncated Fra-1 construct causes an increase in Fra-1 activity and they hypothesise that this increase is due to an increase in protein stability due to the deletion of the C-terminal PEST motif, which targets proteins for degradation by the proteasome; Acquaviva *et al*. [140] demonstrated that just a tripeptide component (PTL motif) of the C-terminal PEST motif is important in promoting degradation of c-Fos, although there are other factors within the C-terminus that also regulate protein stability.

The C-terminus of Fra-1 contains not only this PTL motif (in red below), but also putative RSK-mediated (Ser^{252} below in green) and ERK-mediated (Ser^{265} below in blue) phosphorylation sites.

...C^{244}SSAHRKSSSSSGDPSSDPLGSPTLLAL^{271}

4.2.1 Effect of 24 and 50 amino acid C-terminal truncations

To investigate the significance of these motifs/amino acids on the stability of Fra-1, our first step was to create Fra-1 expression vectors with the C-terminal 50 and 24 amino acids deleted (the 24 amino acid deletion is shown above underlined). These were created in a similar fashion to the final step of making the pCGN-HA-Fra-1WT vector (Section 4.1.5), in that the *fosl1Bam*HI*Sbf*I fragment was excised from the pCGN-HA-Fra-1WT vector and the truncated fragment (which was amplified using 10 ng of the pCGN-HA-Fra-1WT vector as template) was

spliced in. The same PCR reaction was used as in Section 4.1.5, but with T_m adjusted to 65ºC. Primers used for this reaction were 5'*fosl1Sbf*I and either 3'*fosl1*Δ24*Bam*HI or 3'*fosl1*Δ50*Bam*HI giving fragments of length 355 bp (Δ24) or 279 bp (Δ50):

5'*fosl1Sbf*I: cgacttcctgcaggcggagactg

3'*fosl1*Δ24*Bam*HI: gtaaggatccTCAagctgaggcacaaggctc

3'*fosl1*Δ50*Bam*HI: gtaaggatccTCAcatgagtgtgggggtgtg

(TCA represents STOP codon)

(Underlined bases represent *Sbf*I and *Bam*HI recognition sites)

An aliquot of each of these PCR reactions were then subjected to agarose gel electrophoresis, confirming successful amplification (Figure 4.2.1). An identical protocol to that used in Section 4.1.5 was then used to splice this truncated fragment into the pCGN-HA-Fra-1WT donor vector. Following confirmation of the incorporation of a non-mutated fragment into the vector from DNA sequencing, the plasmid was amplified and then transfected into our panel of six bladder cancer cells. These cells were then lysed and Western Blot analysis was then performed staining for total Fra-1 (using anti-Fra-1 antibody), exogenous Fra-1 (using anti-HA antibody) and EGFP as a transfection and loading control (Figure 4.2.2).

Figure 4.2.2 clearly shows that both the wild-type and truncated Fra-1 vectors can be expressed by all bladder cancer lines, and we see the expected increase in electrophoretic migration with the truncated forms

due to their lower molecular weight. Deletion of the C-terminal 24 and 50 amino acids both lead to a similar increase in protein levels (presumably through increasing protein stability) when compared with full-length Fra-1, again in all cell lines; however, this increase appears greater in the epithelial cell lines (HT1376, RT4 and RT112) than in the mesenchymal lines. In Section 3.5.2 it was noted that *fosl1* mRNA was detectable in the epithelial cell lines, whereas minimal Fra-1 protein was detected, suggesting that Fra-1 is relatively unstable in these cell lines. Figure 4.2.2, Figure 4.2.3 and Section 3.5.2 therefore suggest that in the epithelial cell lines, Fra-1WT is much less stable than in mesenchymal cell lines, and that this is likely due to regulation at the protein level, and that the C-terminus plays a key role (as it does in Fra-1 stability in the mesenchymal cell lines).

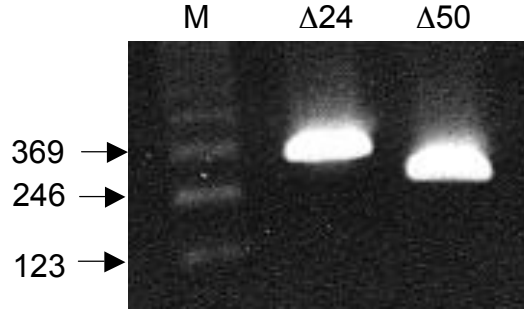

Figure 4.2.1 1.2% agarose + EtBr gel electrophoresis showing results of PCR of the Δ24 and Δ50 fragments of Fra-1. M = 123 bp DNA ladder.

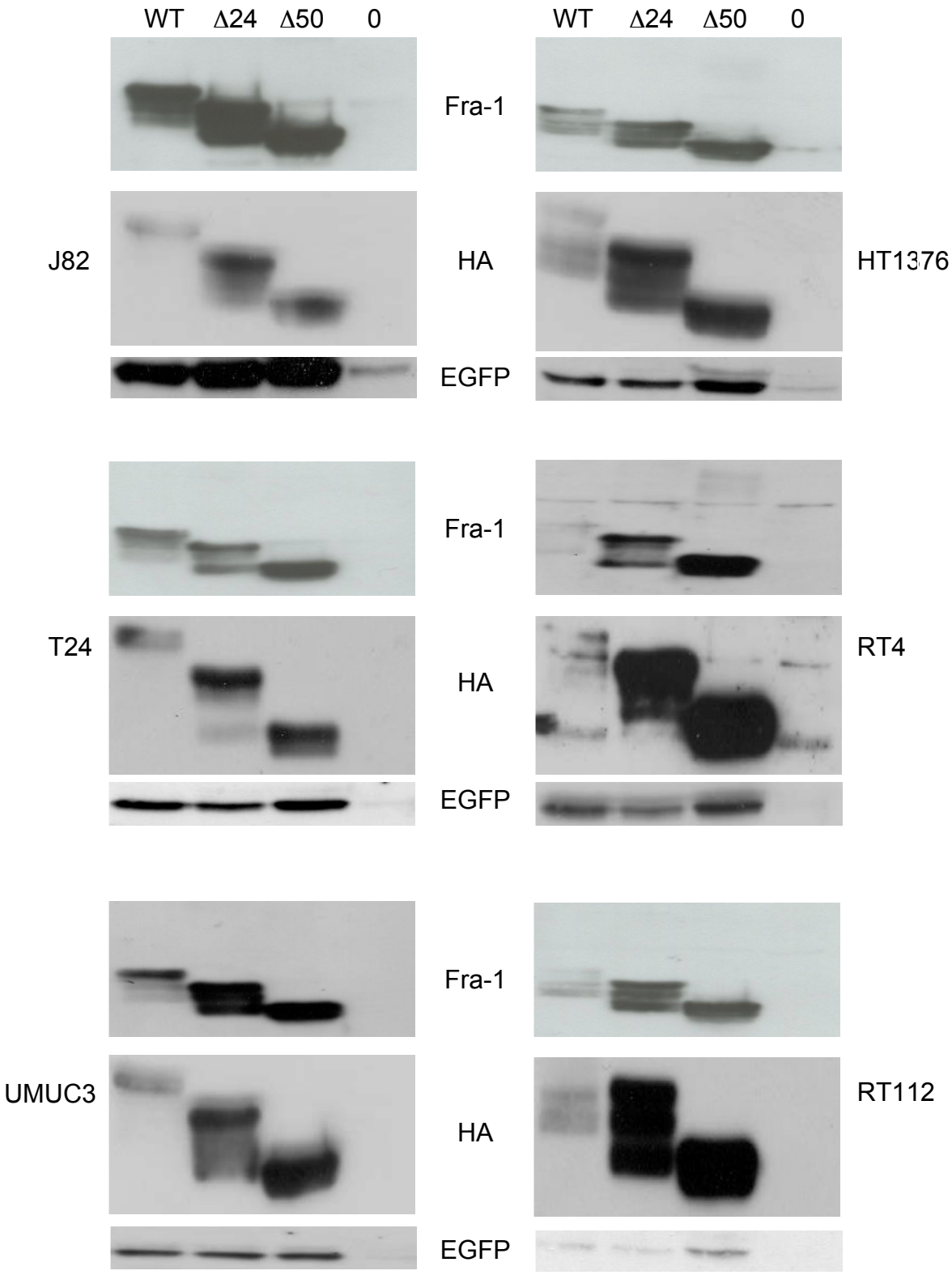

Figure 4.2.2. Western Blots showing expression of full length (WT) and C-terminal truncated (Δ24 and Δ50) Fra-1 in bladder cancer cell lines. Anti-Fra-1 (1:500), anti-HA (1:500), anti-EGFP (1:300), all secondary anti-rabbit (1:5000). MW markers not shown for clarity.

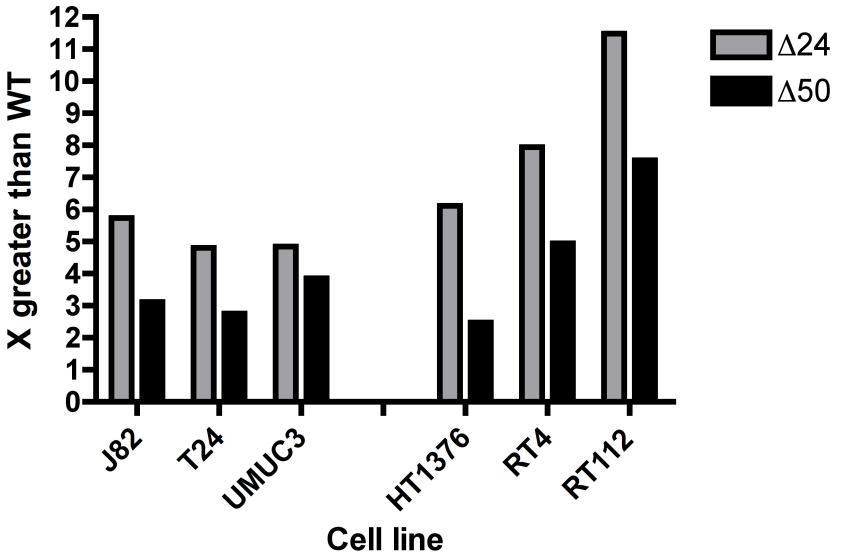

Figure 4.2.3. Densitometric analysis of HA-Fra-1 levels in six bladder cancer cell lines (from Figure 4.2.2.) comparing truncated Fra-1 (Δ24 and Δ50) with full-length Fra-1. Values shown are normalised to the EGFP expression and expressed as a multiple of WT staining.

4.2.2 Effect of 3, 5, 7 and 17 amino acids C-terminal truncations

We have demonstrated that deleting 24 or 50 amino acids from the Fra-1 C-terminus leads to increase in protein levels and therefore the next step is to create further truncated forms of Fra-1 with progressively smaller deletions to further map the C-terminus.

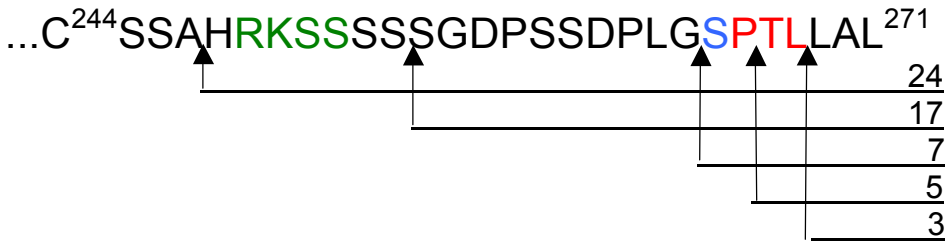

The next series of truncated forms consisted of deletions of the C-terminal 17, 7, 5 and 3 amino acids. The 17 amino acid deletion was chosen because between it and the 24 amino acid deletion is the RSK consensus

sequence RXXS (shown in green), therefore deleting 17 amino acids leaves the RSK consensus sequence present, whilst deleting further putative C-terminal regulatory sites. A 7 amino acid deletion removes the ERK-consensus sequence SP (shown in red and blue), whilst a 5 amino acid deletion destroys the PTL motif (shown in red) which has been previously shown in c-Fos to be important in the regulation of protein stability. Our final deletion is of just three amino acids, leaving the PTL motif intact. The oligonucleotides used for the creation of these truncated forms are:

3'*fosl1*Δ17*Bam*HI:	gtaaggatccTCAgctgctgctactcttgcg
3'*fosl1*Δ17S253A*Bam*HI:	gtaaggatccTCAgctggcgctactcttgcg
3'*fosl1*Δ7*Bam*HI:	gtaaggatccTCAgccaaggggtcagagga
3'*fosl1*Δ5*Bam*HI:	gtaaggatccTCAtggagagccaaggggtc
3'*fosl1*Δ3*Bam*HI:	gtaaggatccTCAgagggttggagagccaag

The same protocol as for the creation of Δ24 and Δ50 was used and sequencing was performed to confirm the correct sequence. J82 cells were then transfected with our panel of truncated Fra-1 forms and then Western Blot analysis was performed using the same protocol as for the Δ24 and Δ50 truncations. The result of this is shown in Figure 4.2.4 and demonstrates that deleting as little as the C-terminal three amino acids causes a marked increase in Fra-1 protein levels when compared with wild-type. This clearly shows that the C-terminus is vital in regulating Fra-1 protein levels, presumably by regulating stability, but gives little more information than that. With just three amino acids deleted, the putative RSK, ERK and PTL regulatory sequences are still present but

either the C-terminal three amino acids are part of a regulatory process which has greater effect on Fra-1 protein stability than the other three motifs above, or by deleting these three amino acids, we are somehow interfering with the recognition or binding of the additional regulatory proteins at the three (or perhaps more, as yet undescribed) putative regulatory sites.

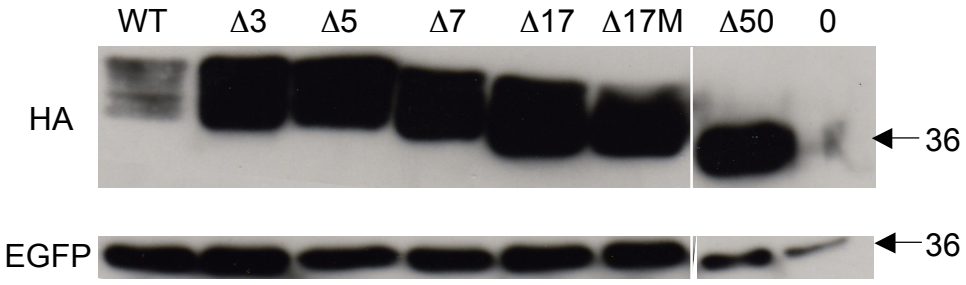

Figure 4.2.4 Western Blot of J82 cells transfected with WT, Δ3, Δ5, Δ7, Δ17, Δ17S253A (Δ17M) and Δ50 variants of the pCGN-HA-Fra-1 plasmid, with pEGFP transfected in all lanes to monitor transfection efficiency. Anti-Fra-1 (1:500), anti-HA (1:500), anti-EGFP (1:300), all secondary anti-rabbit (1:5000). MW in kDa shown on the right.

4.2.3 ^{35}S-pulse chase labelling of Fra-1WT and Fra-1Δ3

The work above has demonstrated an increase in Fra-1 protein levels when the C-terminus is truncated, even by as few as three amino acids. It is highly likely that this is due to stabilisation of the protein, but to confirm this, ^{35}S-pulse chase labelling was performed of Fra-1WT and Fra-1Δ3 in RT4 and J82 cells (Section 2.12). Figure 4.2.5 shows the PhosphoImager image following exposure of the screen to the SDS-PAGE gel from an experiment using Fra-1WT and Fra-1Δ3 in J82 cells. It can be seen from this that Fra1Δ3 is the more stable protein; this is confirmed when this data is further analysed using ImageQuant TL

software (Figure 4.2.6a&b). When comparing RT4 and J82 cells, after eight hours there is a similar proportion of Fra-1WT to Fra-1Δ3; however, Fra-1WT levels appear to drop more rapidly to reach a plateau in RT4 cells, with approximately 20% of the starting amount of Fra-1WT present at three hours in RT4 cells compared with approximately 35% in J82 cells; the reason for this is unclear. It can also be seen that Fra-1 again has the multiple band pattern described later and that the less electrophoretically mobile band (thought to be the hyperphosphorylated form of Fra-1 – see Section 4.3) of Fra-1WT is the predominant form after eight hours; this is not evident with Fra-1Δ3, presumably because the effect on stability of the Δ3 deletion overrides the effect of Fra-1 phosphorylation on stability.

This work therefore confirms that the increase in Fra-1 levels seen on Western Blot when the C-terminus is deleted is due to an increase in protein stability, indicating that the C-terminus has a role in the regulation of Fra-1 protein stability.

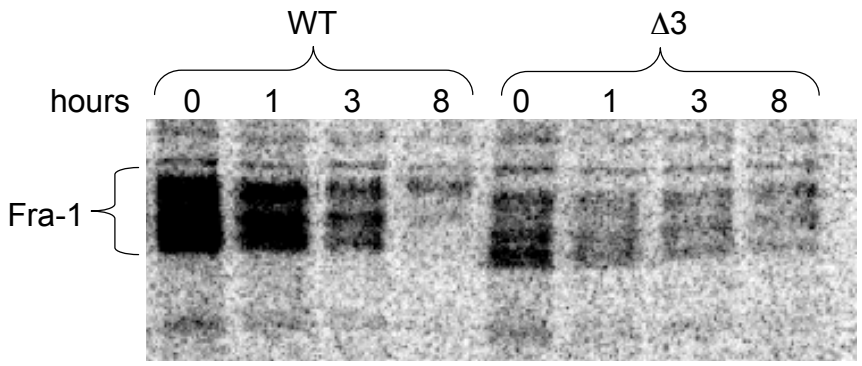

Figure 4.2.5. ^{35}S-pulse chase labeling of Fra-1WT (WT) and Fra-1Δ3 (Δ3) in J82 cells. Pulse time of one hour, chase time in hours given above each lane.

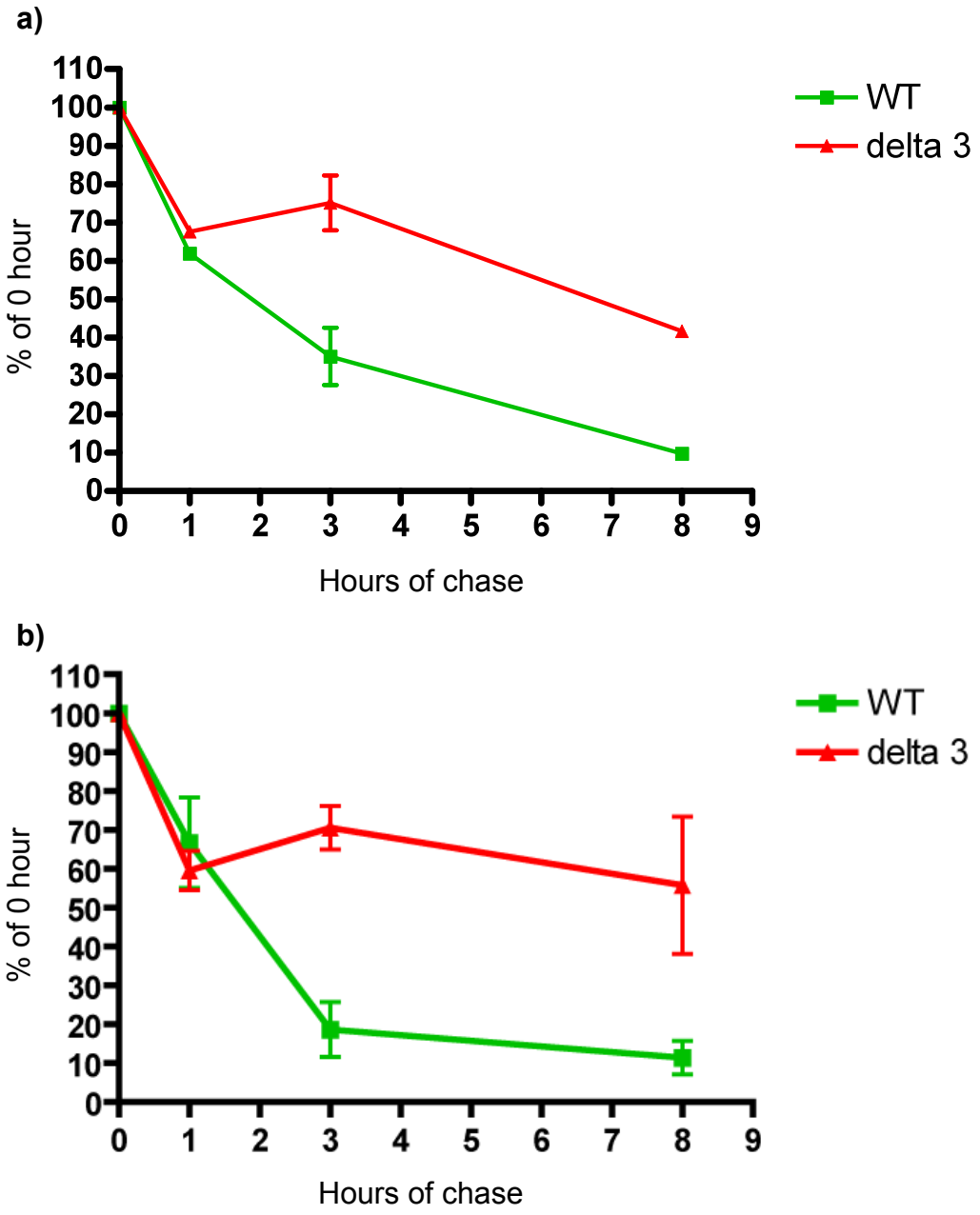

Figure 4.2.6. ^{35}S-pulse chase labeling of Fra-1WT (WT) and Fra-1Δ3 (Δ3) in J82 cells (a) and RT4 cells (b). Percentage of protein remaining at given time point compared with starting amount (100%). n=3 for all timepoints except 3 hours (for which n=2)

4.3 Phosphorylation of Fra-1

The data above has confirmed that the C-terminus is crucial in regulating Fra-1 stability but it gives no further information on the particular amino acid(s) involved in this. Given previous work discussed earlier with c-Fos demonstrating the presence of ERK and RSK phosphorylation sites within the C-terminus whose sequence is conserved across the Fos family of proteins, it would therefore seem appropriate to investigate phosphorylation of Fra-1 to ascertain whether the corresponding amino acid(s) are phosphorylated.

...C^{244}SSAHRKSSSSSGDPSSDPLGSPTLLAL^{271}

Within the C-terminal 24 amino acids of Fra-1, there are eight serine residues (shown in red) and one threonine residue (shown in green), all of which are potential candidates for phosphorylation. To further investigate the role of phosphorylation of Fra-1 in regulating protein stability, we first need to confirm that Fra-1 is phosphorylated and then identify the individual amino acid(s) that are phosphorylated. When this is achieved, it will be possible to assess the role that these phosphorylated residues have on regulating protein stability by creating further mutated expression vectors, mutating the serine(s) or threonine residues to either alanine (to block phosphorylation) or aspartic acid (mimicking phosphorylation).

Western Blot studies of Fra-1 often demonstrate three species with differing electrophoretic mobility. To date, no splice variants, or mutants of Fra-1 have been discovered, thereby suggesting that these species are due to post-translational modification(s) of Fra-1, one possibility being phosphorylation.

Previous work has demonstrated that phosphorylation of c-Fos, Fra-2, JunD and Fra-1 [74, 75, 141, 142] leads to a decrease in electrophoretic mobility.

To confirm that Fra-1 is phosphorylated, ^{32}P-phospholabelling of Fra-1 was performed, followed by immunopreciptation and gel electrophoresis. Firstly, 2 x 10^6 cells were transfected with either 1 μg EGFP alone, 5 μg pCGN-HA-Fra-1WT + 1 μg EGFP, 5 μg pCGN-HA-Fra-1Δ7 + 1 μg EGFP, or 5 μg pCGN-HA-Fra-1Δ24 + 1 μg EGFP (Section 2.2) and then incubated overnight in a 6 well plate. Phospholabelling was then performed with 1 mCi of ^{32}P-orthophosphate as per Section 2.11.1, but without EGF stimulation. Immunoprecipitation with anti-HA antibody (Roche) was performed (Section 2.11.2) followed by SDS-PAGE electrophoresis and transfer to Protran Nitrocellulose Transfer membrane (2.11.3). Autoradiography was then performed and the resulting image is shown in Figure 4.3.1. This demonstrates that WT, Δ7 and Δ24 forms of Fra-1 are all phosphorylated. We also see the increase in electrophoretic mobility with Δ7 and Δ24 due to their lower molecular weights.

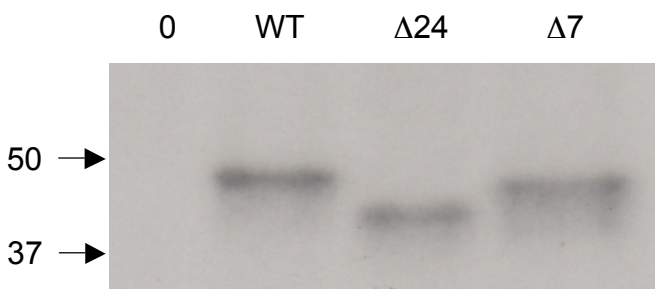

Figure 4.3.1 Autoradiograph following 10% SDS-PAGE demonstrating ^{32}P-phospholabelling of wild-type, Δ7 and Δ24 variants of Fra-1.

4.3.1 Effect of dephosphosphorylation of Fra-1 on electrophoretic mobility

To confirm that Fra-1 is phosphorylated in human bladder cancer cells, and also to confirm that the multiple species seen on Western Blot are due to phosphorylation, 20 μg of protein lysate from J82 cells (Section 2.8.2) was treated with calf intestinal phosphatase (CIP) (Section 2.8.4). The resulting samples were subjected to conventional Western Blot analysis and stained for Fra-1 and α-tubulin. Figure 4.3.2 demonstrates that treatment with CIP modifies the appearance of Fra-1 on WB, with the disappearance of the more slowly migrating species, and an increase in the amount of the faster migrating species. This suggests that 1) Fra-1 is phosphorylated, 2) the multiple bands seen on WB for Fra-1 are due to different phosphorylation states of Fra-1, and 3) the more rapidly migrating band is dephosphorylated Fra-1 and that phospho-Fra-1 species migrate more slowly. This is also supported by the ^{32}P-phospholabelling experiment in Figure 4.3.1 where the uppermost band is by far the most prominent, suggesting that this is the more heavily phosphorylated species – it must be remembered that in this experiment it is not only the amount of protein present that determined the strength of the signal, but the amount of phosphorylation, and therefore radioactivity, that determines the signal. It also appears that there may be some residual phosphatase activity within the cell lysates using this particular lysis and treatment protocol, as in Figure 4.3.2 it is seen that lysates incubated for one hour in the absence of CIP appear to lose the most slowly migrating species, with an increase in the faster migrating species, whereas if samples are left on ice for one hour, three species are seen on Fra-1 WB. To confirm that this

is the case, and that this alteration in appearance is not due to other modifications of Fra-1, the experiment was repeated, but in the presence or absence of the phosphatase inhibitor sodium orthovanadate (Na_3VO_4). Figure 4.3.3 shows that when incubated on ice for one hour, there is no difference in the WB appearance of Fra-1. If samples are incubated for one hour at 37ºC in the absence of CIP, there is a partial loss of the phospho-Fra-1 species in the orthovanadate untreated sample, but the treated sample appears unchanged compared with the ice-incubated control. In the CIP treated samples, the orthovanadate-untreated sample produces an appearance on WB of a single band, whereas in the orthovanadate-treated sample (where endogenous phosphatase activity and CIP activity is inhibited by the orthovandate), the appearance is that of phospho-Fra-1 as seen in the ice-incubated control. Figure 4.2.2 also demonstrates an alteration in appearance of Fra-1 on WB when the C-terminal 50 amino acids are deleted, when compared to WT or a smaller deletion (e.g. 24 amino acids), such that one or possibly two of the three species are lost, indicating either loss of the relevant phosphorylatable amino acids between the C-terminal 50 and 24 amino acids, or loss of recognition site(s) for the relevant protein kinases.

This data therefore confirms previous findings that Fra-1 is phosphorylated and that it is phosphorylation that gives rise to the three-band appearance of Fra-1 on WB, with the hypo/non-phosphorylated species being the more rapidly migrating.

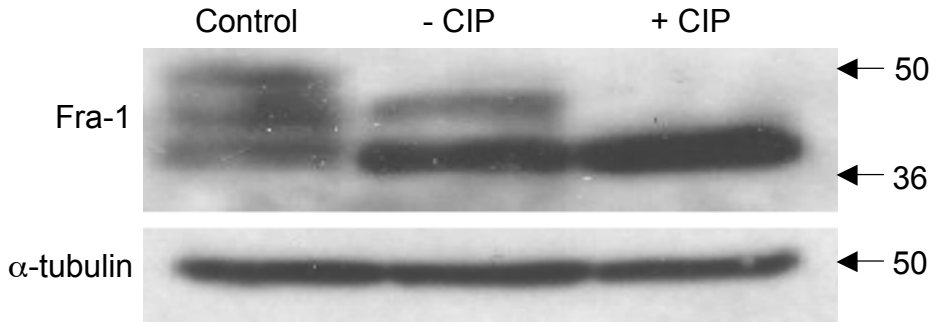

Figure 4.3.2 WB showing the effect of CIP treatment on Fra-1 appearance on WB. Fra-1 1:500, secondary anti-rabbit 1:5000, α-tubulin 1:5000, secondary anti-mouse 1:5000. MW in kDa shown on right.

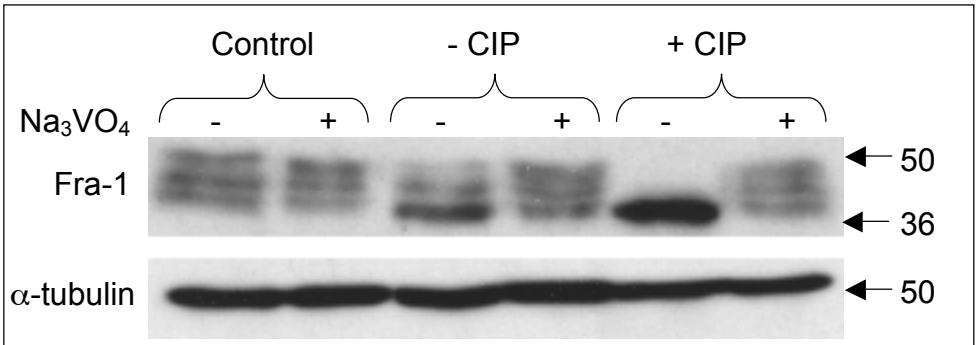

Figure 4.3.3 WB showing the effect of sodium orthovanadate treatment and CIP treatment on Fra-1. Fra-1 1:500, secondary anti-rabbit 1:5000, α-tubulin 1:5000, secondary anti-mouse 1:5000. MW in kDa shown on right.

4.3.2 Effect of phosphorylation of Fra-1 on electrophoretic mobility and Fra-1 levels

Treatment with CIP to dephosphorylate Fra-1 leads to an increase in electrophoretic mobility as shown in Section 4.3.1. It would therefore be logical to confirm that the reverse is true, i.e. that phosphorylation of Fra-1 causes a decrease in electrophoretic mobility. To investigate this, J82 cells which had been serum starved for 48 hours were stimulated with EGF (100 $ng \cdot ml^{-1}$). As discussed in Section 1.8, the regulation of Fra-1 is

at both transcriptional and post-translational levels. It would be expected that stimulation of ERK with EGF would have a biphasic response with regards to Fra-1, the first being due to direct phosphorylation of Fra-1 (a post-translational modification) and then a more delayed response due to changes in transcription. Therefore this experiment, as well as confirming EGF-stimulated phosphorylation of Fra-1 (presumably by ERK), was also designed to investigate changes in Fra-1 level over a longer time period (which could be due to either the effect of an early post-translational modification or changes in transcription).

Figure 4.3.4 shows the results of this experiment in J82 cells looking at changes in endogenous Fra-1. Firstly, it can be clearly seen that after ten minutes of EGF stimulation, both ERK and RSK are activated; RSK activation reduces by around two hours, but the ERK activation is more prolonged, and remains elevated even at eight hours. (Note that the control lane for P-RSK staining contains artifact, and that P-RSK staining is the lower of the two areas of signal – this was confirmed in other experiments (data not shown). Fra-1 is phosphorylated within ten minutes of EGF stimulation (presumably by an ERK-dependent mechanism) – this is shown by the decrease in electrophoretic mobility of Fra-1. It is not possible to determine from this experiment whether there is any significant change in Fra-1 level at 10 minutes. Clearly, with longer stimulations (between 2 and 8 hours), Fra-1 levels are increased; this is due to either the effect of phosphorylation on stabilising Fra-1 protein or by the increased production of Fra-1 via an increase in transcription.

Further experiments (Section 4.3.8) use transfected Fra-1 which removes the effect of transcriptional changes due to EGF stimulation, and demonstrate that accumulation of exogenous Fra-1 (i.e. EGF will have no effect on its transcription) increases with EGF stimulation.

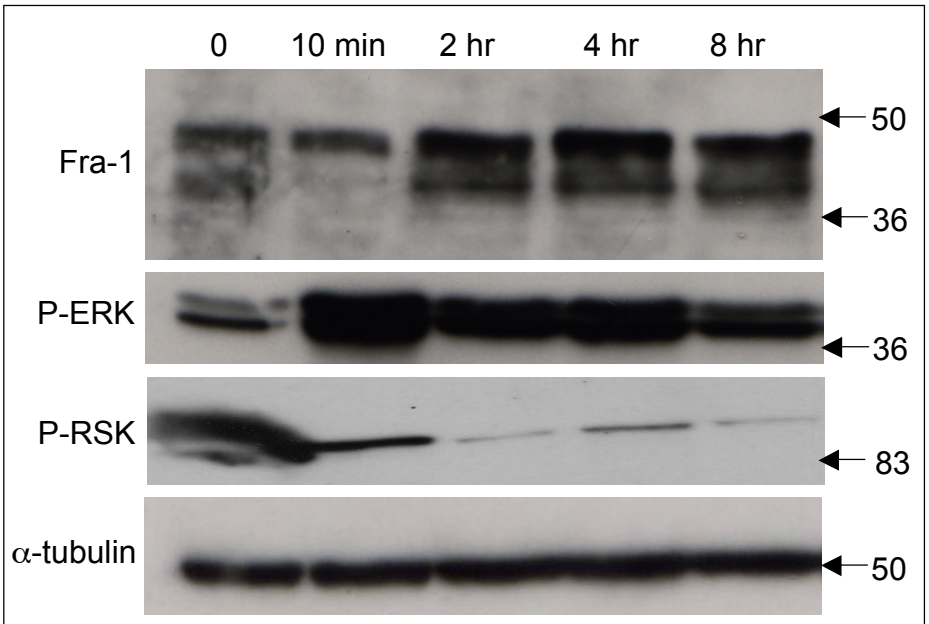

Figure 4.3.4 WB showing the effect of EGF stimulation on Fra-1, P-ERK and P-RSK levels in J82 cells. Fra-1 1:500, P-ERK 1:1000, P-RSK 1:1000 all secondary anti-rabbit 1:5000, α-tubulin 1:5000, secondary anti-mouse 1:5000. MW in kDa shown on right.

4.3.3 Phosphoaminoacid analysis of Fra-1

To investigate whether serine, tyrosine or threonine residues are phosphorylated in Fra-1, we attempted to correlate anti-Fra-1 antibody staining with anti-phosphoserine, anti-phosphotyrosine and anti-phosphothreonine staining on Western Blot (Figure 4.3.5). Basic Western Blot analysis leads to electophoresis of many proteins, many of which will be phosphorylated, and this will result in what should appear to be non-specific (but is actually specific binding to many proteins) staining; this is useful as a positive control for staining. To assess Fra-1 phosphorylation, Fra-1 firstly needs to be immunoprecipitated (using anti-HA antibody against the N-terminal HA tag). J82 cells were transfected with 1 μg EGFP (control), 1 μg EGFP + 5 μg pCGN-HA-Fra-1WT or 1 μg EGFP + 5 μg pCGN-HA-Fra-1Δ50 (Section 2.2). Following overnight incubation, cells were lysed and either subjected to standard WB analysis (Section 2.8) or firstly immunoprecipitated with anti-HA antibody, and then WB analysis was performed. This experiment fails to demonstrate any Fra-1 phosphorylation; anti-phosphothreonine and anti-phosphoserine antibodies failed to give any demonstrable signal, whereas anti-phosphotyrosine gave some signal but failed to demonstrate any significant staining in the region of Fra-1. The absence of Fra-1 phospho-amino acid staining is more likely due, in this experiment, to technical reasons rather than the real absence of Fra-1 phosphorylation.

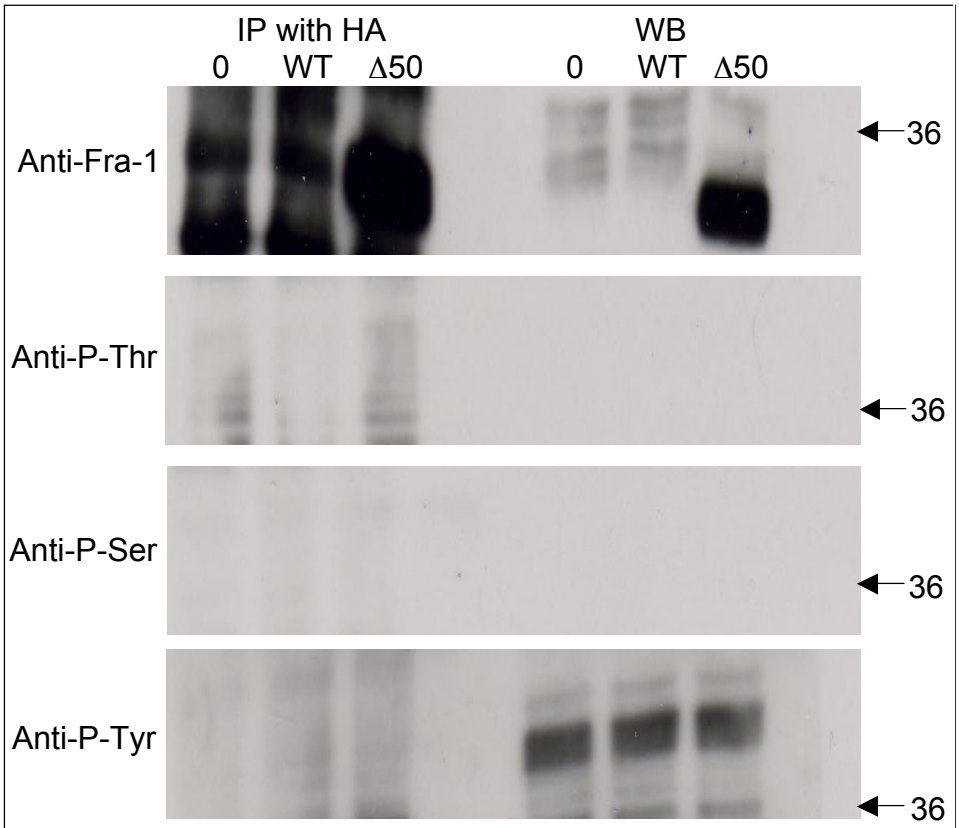

Figure 4.3.5 10% SDS PAGE of control (0), HA-Fra-1WT (WT) and HA-Fra-1Δ50(Δ50) stained for Fra-1 (1:500), P-Thr (1000), P-Ser (1:200) and P-Tyr (1:1000). Left hand panel has been immunoprecipitated with HA for HA-Fra-1 prior to electrophoresis. Anti-P-tyr secondary anti-mouse (1:5000), all others secondary anti-rabbit 1:5000. MW in kDa shown on right.

4.3.4 Phosphomapping of Fra-1

To determine which individual amino acids within Fra-1 are phosphorylated, it was decided to generate Fra-1 phosphomaps, rather than to create a large panel of vectors with potential phosphorylation sites mutated (as another group were doing at the same time as this work was being performed [143]). Fra-1 contains numerous serine, threonine and tyrosine residues, many of these will not be phosphorylated *in vitro* or *in*

vivo and mutating them will not give us the required information. It would be much more logical to define the phosphorylation sites using phosphomapping and then perform targeted mutations of these sites to determine whether phosphorylation has any effect on protein stability.

Our phosphomapping protocol involves trypsinisation of the immunoprecipitated ^{32}P-labelled Fra-1. Trypsinisation hydrolyses peptide bonds on the carboxyl side of lysine (K) and arginine (R) residues. The predicted tryptic digest of Fra-1 (generated from the sequence analysis tools at http://expasy.org/tools/peptidecutter/) is shown below (with serine, tyrosine and threonine residues shown in red) and reveals nine tryptic peptides, one of which (251-271) contains both the RSK and ERK consensus sequences, and the PTL motif:

4-34	DFGEPGPSSGNGGGYGGPAQPPAAAQAAQQK
35-84	FHLVPSINTMSGSQELQWMVQPHFLGPSSYPRPLTY PQYSPPQPRPGVIR
85-93	ALGPPPGVR
95-107	RPCEQISPEEEER
128-139	ELTDFLQAETDK
150-156	EIEELQK
161-173	LELVLEAHRPICK
180-249	EGDTGSTSGTSSPPAPCRPVPCISLSPGPVLEPEALH TPTLMTTPSLTPFTPSLVFTYPSTPEPCASAAHR
251-271	SSSSSGDPSSDPLGSPTLLAL

^{32}P-phosphomapping of J82 cells transfected with either pCGN-HA-Fra-1WT or pCGN-HA-Fra-1Δ3 was performed using the protocol in Section 2.11 and the resulting phosphomaps are shown in Figure 4.3.6 with electrophoresis being performed along the X-axis and chromatography along the Y-axis. There is a clear difference between the two maps, with three phosphopeptides (ringed in red) having migrated differently under chromatography, indicating an alteration in hydrophobicity of the fragments between Fra-1WT and Fra-1Δ3. The only difference between the two protein sequences, however, is the deletion of the C-terminal three amino acids:

251-271 SSSSSGDPSSDPLGSPTLLAL	Fra-1WT
251-268 SSSSSGDPSSDPLGSPTL	Fra-1Δ3

All three of these amino acids (leucine x 2 and alanine) are hydrophobic, which fits with this hypothesis.

It would also be reasonable to hypothesise at this point that these three phosphopeptides all represent the C-terminus (251-268/271) but clearly there has been modification to it to generate three, rather than one phosphopeptide on the map; phosphorylation may be one such modification.

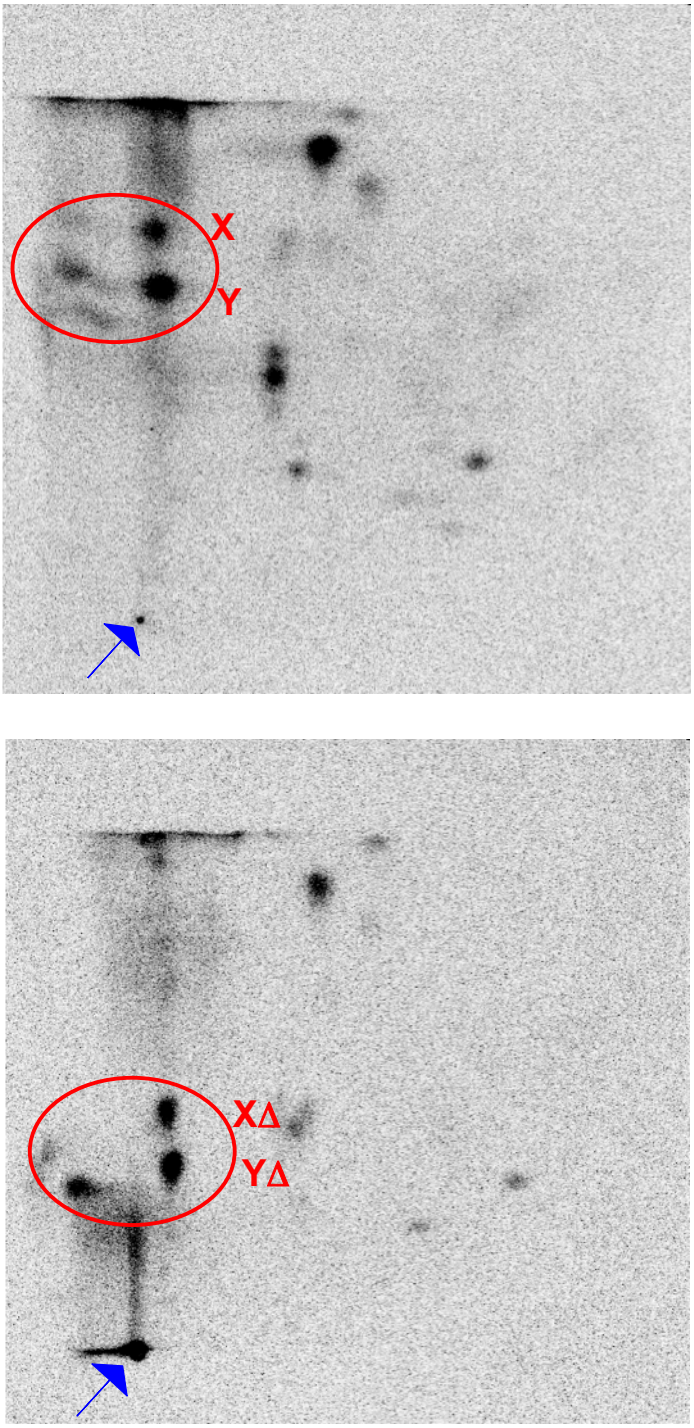

Figure 4.3.6 ^{32}P-phosphomaps showing tryptic digests of Fra-1WT and Fra-1Δ3. Blue arrow denotes origins of electrophoresis (X-axis) and chromatography (Y-axis). For explanation of annotations in red, see text

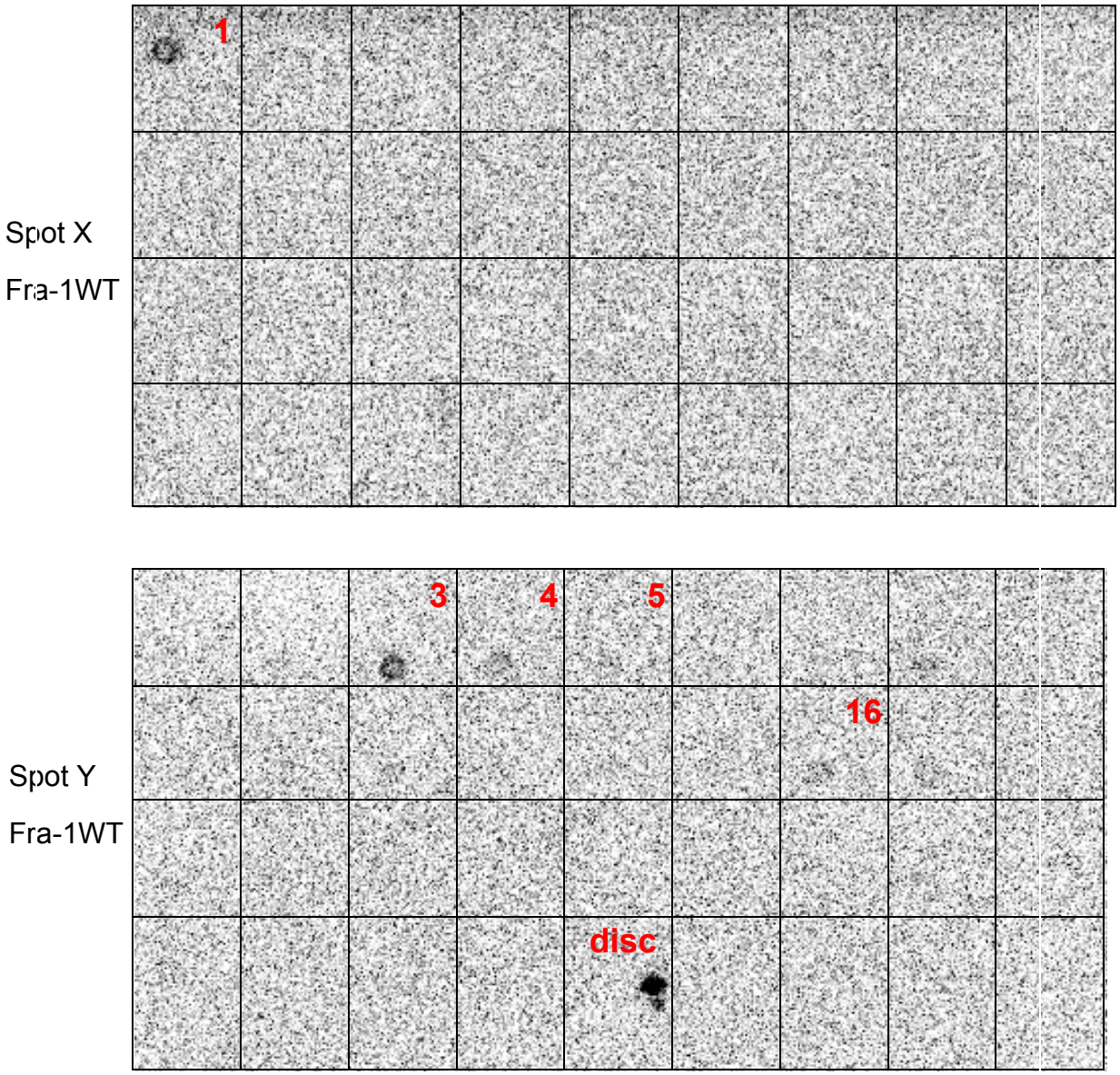

Figure 4.3.7a Maps showing the results of Edman degradation of Spot X and Spot Y from the Fra-1WT phosphomap. Numbers indicate the position within the phosphopeptide of the particular residue. 'disc' is the Sequelon-AA disc post Edman processing, showing residual activity in the Spot Y map.

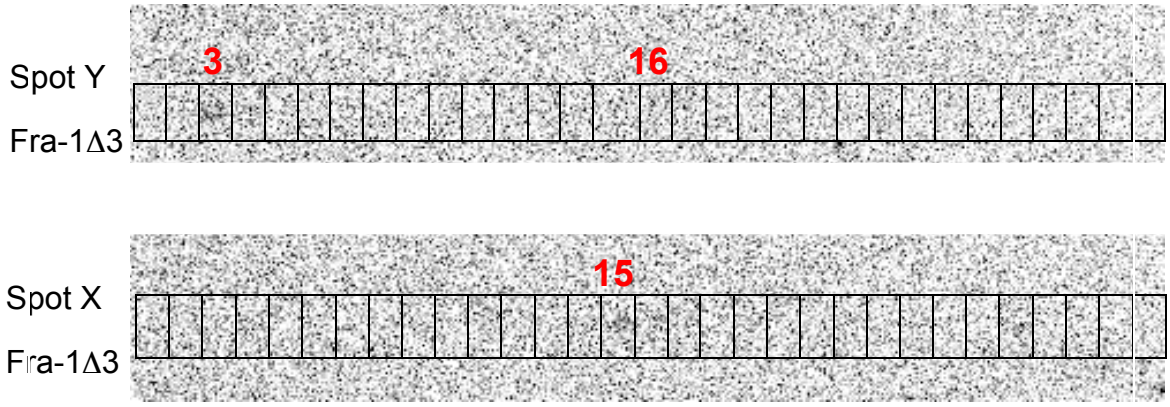

Figure 4.3.7b Maps showing the results of Edman degradation of Spot X and Spot Y from the Fra-1Δ3 phosphomap. Numbers indicate the position within the phosphopeptide of the particular residue. Note that Spot Y is shown above Spot X in this figure; the opposite to Figure 4.3.7a

The four phosphopeptides marked in Figure 4.3.6 (X, Y, XΔ and YΔ) were then excised from the TLC plate and processed for Edman degradation (Section 2.11.6). The resulting Edman maps are shown in Figures 4.3.7a&b. For Fra-1WT the Edman degradation demonstrates phosphoamino acids at position 1 for phosphopeptide X and positions 3, 4, 5 and 16 for phosphopeptide Y (although positions 4 and 5 gave a very faint signal). For Fra-1Δ3, phosphopeptide XΔ has a phosphoamino acid at position 15 and YΔ has a phosphoamino acid at position 3, with a further possible phosphoamino acid at position 16.

This firstly suggests that there are two different phospho-species of the C-terminal phosphopeptide, namely that which is represented by X and XΔ which is mono-phosphorylated (and appears to be phosphorylated at different sites, possibly due to the effect of the C-terminal three amino

acid deletion, and that which is represented by Y and YΔ, which appear to be bi-phosphorylated (at least), and probably at the same sites.

However, when the Edman maps are compared with the predictive sequence of the C-terminus (below), there is a problem with this hypothesis. If the sequence of the predicted tryptic phosphopeptide is examined, residue 16 (in Y and YΔ) cannot be phosphorylated – it is a proline residue.

251-271 S S S S S G D P S S D P L G S P T L L A L
1 2 3 4 5 9 10 15 17

One assumption with regard to this hypothesis (and its possible failure) is that the predicted tryptic phosphopeptide sequence is correct. If the sequence is looked at in more detail, it is noted that immediately before Ser^{251} is the lysine residue (Lys^{250}) which is cleaved from the C-terminus during the trypsin digestion. Immediately before Lys^{250} is the arginine residue Arg^{249}, which will also be cleaved by trypsin digestion, from Lys^{250}. In this situation, it is known that Lys^{250} may not necessarily be cleaved from the C-terminal fragment, and therefore the C-terminal fragment as predicted above is partly incorrect, in that Lys^{250} should be present at the N-terminus. This means that our tryptic digest will contain both Lys^{250}-containing and Lys^{250}-deficient C-terminal phosphopeptides. If this is the case, it can be seen that our hypothesis based on the Edman maps holds and that phosphopeptide X contains amino acids 251-271 (i.e.

no Lys^{250}) and that phosphopeptide Y contains amino acids 250-271 (i.e. contains Lys^{250}):

251-271 S S S S S G D P S S D P L G S P T L L A L
1 2 3 4 5 9 10 15 17

250-271 K S S S S S G D P S S D P L G S P T L L A L
2 3 4 5 6 1011 16 18

Further analysis of this data also supports the hypotheses being generated during this interpretation. If phosphopeptide Y is doubly phosphorylated, it should move to the left relative to phosphopeptide X because of the phosphate moiety carrying a negative charge, however it does not. The reason for this is that phosphopeptide Y contains the polar amino acid Lys^{250} which carries a positive charge, thereby cancelling out the negative charge carried by the additional phosphate moiety. Furthermore, if hydrophobicity is considered, the addition of the hydrophilic Lys^{250} in the Y phosphopeptide should inhibit migration during chromatography, compared with the X phosphopeptide, which in fact it is seen to do.

Whilst the C-terminus contains numerous potentially phosphorylated serine residues, it also contains a single threonine residue that could also be phosphorylated. To confirm that just serine residues were phosphorylated, phosphoamino acid analysis was performed on Spot Y from Fra-1Δ3 (Section 2.11.7, Figure 4.3.8). This demonstrates that the

only detectable phospho-amino acid was serine, which also fits with our hypothesis.

To summarise, this data demonstrates that the C-terminus of Fra-1 can be phosphorylated at Ser^{251}, Ser^{252} and Ser^{265}. It also suggests that Ser^{251} is only phosphorylated in Fra-1WT, and never in Fra-1Δ3, and if Ser^{251} is phosphorylated, no other phosphorylation is present within the C-terminus. This raises the question of whether phosphorylation of Ser^{251} blocks phosphorylation of other C-terminal amino acids?

4.3.5 Effect of mutation of Ser^{251}, Ser^{252} and Ser^{265} on Fra-1 stability

We have demonstrated that Fra-1 appears to be phosphorylated at Ser^{251}, Ser^{252} and Ser^{265}, it is now therefore appropriate to assess the effect of phosphorylation at these sites on protein stability. To assess this, a further series of pCGN-HA-Fra-1 constructs were made, mutating Ser^{251}, Ser^{252} and/or Ser^{265} to either alanine (to mimic the non-phosphorylated state) or aspartate (to mimic the phosphorylated state). These mutations were performed in the context of both Fra-1WT and Fra-1Δ3 to examine whether any effect of phosphorylation is independent or dependent on the presence of the full-length C-terminus; the following combinations of mutations were created:

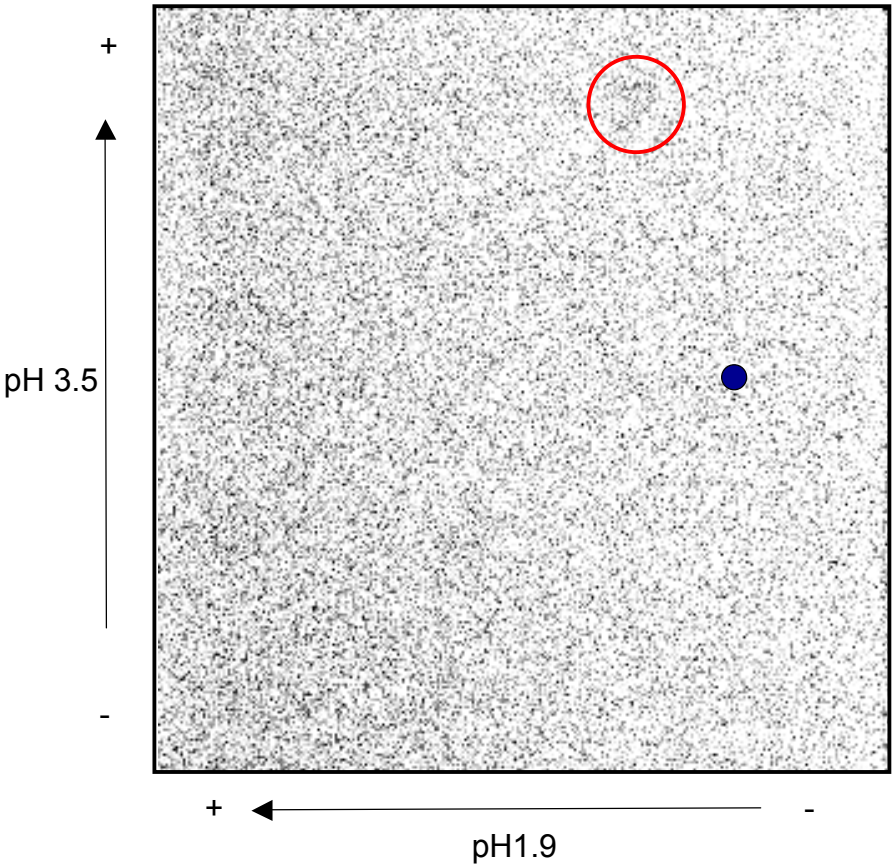

Figure 4.3.8 Phosphoamino acid analysis of Fra-1Δ3 spot Y. Circled area of signal correlates with ninhydrin-stained region on the same TLC plate consistent with the electrophoretic mobility of phosphoserine (migrates furthest on both axes compared with phosphothreonine and phosphotyrosine).

pCGN-HA-Fra-1WT-S251A

pCGN-HA-Fra-1WT-S251D

pCGN-HA-Fra-1Δ3-S251A

pCGN-HA-Fra-1Δ3-S251D

pCGN-HA-Fra-1WT-S252A-S265S

pCGN-HA-Fra-1WT-S252A-S265A

pCGN-HA-Fra-1WT-S252S-S265A

pCGN-HA-Fra-1WT-S252D-S265A

pCGN-HA-Fra-1WT-S252D-S265D

pCGN-HA-Fra-1WT-S252S-S265D

To create the WT-S252S-S265A and WT-S252S-S265D mutants, a similar protocol to the one used to generate the pCGN-Ha-Fra-1 C-terminal deletion mutants was used (Sections 4.2.1 and 4.2.2). 10 ng of pCGN-HA-Fra-1WT vector was used as the template, and the T_m was 56ºC. Primers used were:

5'*fosl15'ofSbfI*:	cttgtgaacagatcagcc
3'*fosl1S265A*:	aggatccTCAcaaagcgaggagggttggagcgccaag
3'*fosl1S265D*:	aggatccTCAcaaagcgaggagggttggatcgccaag

Following successful amplification, the two vectors were confirmed to contain the appropriate mutation by sequencing as described previously

(Section 2.7). To confirm that the protein products of these constructs could be detected, they were transfected into J82 cells and Western Blot analysis performed (Sections 2.2 and 2.8, and Figure 4.3.9)

To then create the S252A and S252D mutants, three PCR reactions were required for each construct. For all three reactions, the PCR program was as for Section 4.2.1, with a T_m of 56ºC. In the first two reactions, the template was the same, either pCGN-HA-Fra1WT-S252S-S265A, pCGN-HA-Fra-1WT-S252S-S265D or pCGN-HA-Fra-1WT (10 ng).

In the first reaction, the primers were:

3'*fosl1Bam*HI: aaggatccctcaggcgcctcacaaagcgag

and either

5'*fosl1S252A*: catcgcaagagtagcgccagcagcggagac

or

5'*fosl1S252D*: catcgcaagagtagcgacagcagcggagac

In the second reaction, the primers were:

5'*fosl15'ofSbfI*: cttgtgaacagatcagcc

and either

3'*fosl1S252A*: gtctccgctgctggcgctactcttgcgatg

or

3'*fosl1S252D*: gtctccgctgctgtcgctactcttgcgatg

The third reaction utilised the product of the first two reactions with the primers:

3'*fosl1Bam*HI: aaggatccctcaggcgcctcacaaagcgag

5'*fosl15'ofSbfI*: cttgtgaacagatcagcc

The resulting vectors were sent for sequencing as before to confirm the insertion of the correct mutation and then J82 cells were transfected and Western Blot analysis performed (Figure 4.3.9).

The final set of mutants created were of Ser^{251} to either alanine or aspartate in the presence of either full-length Fra-1 or the Δ3 Fra-1 truncation. These were created in the same way as the S252 mutants immediately above, using either pCGN-HA-Fra-1WT or pCGN-HA-Fra-1Δ3 as the template (10 ng) for the first two reactions, and the products of reactions one and two as the template for the third reaction, with the following primers:

First Reaction

3'*fosl1Bam*HI: aaggatccctcaggcgcctcacaaagcgag (full length)

or

3'*fosl1*Δ3*Bam*HI: gtaaggatccTCAgagggttggagagccaag (Δ3)

and either

5'*fosl1S251A*: catcgcaagagtgccagcagcagcggagac

or

5'*fosl1S251D*: catcgcaagagtgacagcagcagcggagac

Second Reaction

5'*fosl15'ofSbfI*: cttgtgaacagatcagcc

and either

3'*fosl1S251A*: gtctccgctgctgctggcactcttgcgatg

or

3'*fosl1S251D*: gtctccgctgctgctgtcactcttgcgatg

Third Reaction

5'*fosl15'ofSbfI*: cttgtgaacagatcagcc

and either

3'*fosl1Bam*HI: aaggatccctcaggcgcctcacaaagcgag (WT)

or

3'*fosl1*Δ3*Bam*HI: gtaaggatccTCAgagggttggagagccaag (Δ3)

The vectors produced were then sent for sequencing and, when the sequence was confirmed as correct, transfected into J82 cells and Western Blotting was performed (Figure 4.3.10)

With regard to Ser^{251}, in the full-length Fra-1 setting (the phosphomapping experiments above suggested that it was only full-length Fra-1 that was phosphorylated at Ser^{251}), if Ser^{251} is phosphorylated (WT D), there is little difference in Fra-1 level (hence little difference in stability). However, if Ser^{251} is not phosphorylated (WT A), Fra-1 levels are higher, which does not agree with our earlier findings that phosphorylation of Fra-1 (by ERK)

stabilises Fra-1. It is proposed that Ser^{252} is phosphorylated by RSK (via ERK activity) and that this should stabilise Fra-1; this data suggests that Ser^{251} may be phosphorylated by a different mechanism and that, in contrast to the effect of ERK-mediated phosphorylation, which appears to stabilise Fra-1, phosphorylation at this site reduces stability. If the WT A lane is looked at in detail in Figure 4.3.10, it can also be seen that not only are Fra-1 levels higher than in WT, but that the faster migrating (less phosphorylated) species of Fra-1 is more prominent, which also suggests that dephosphorylation at Ser^{251} stabilises Fra-1.

If the C-terminal three amino acids are deleted and the same mutations applied, the effect of dephosphorylation at Ser^{251} is reversed, i.e. Fra-1 levels fall. Phosphorylation at Ser^{251} in the presence of the deletion has no significant effect. This is an interesting finding because phosphomapping failed to demonstrate any phosphorylation at Ser^{251} in the presence of the deletion, therefore one would not necessarily expect any change in Fra-1 levels when this site was 'dephosphorylated' by mutating to alanine, given the increase in levels due to the C-terminal deletion; the reason for this finding is not yet clear.

The next step is to assess the effect of phosphorylation/dephosphorylation at Ser^{252} and Ser^{265}, and this is shown in Figure 4.3.9.

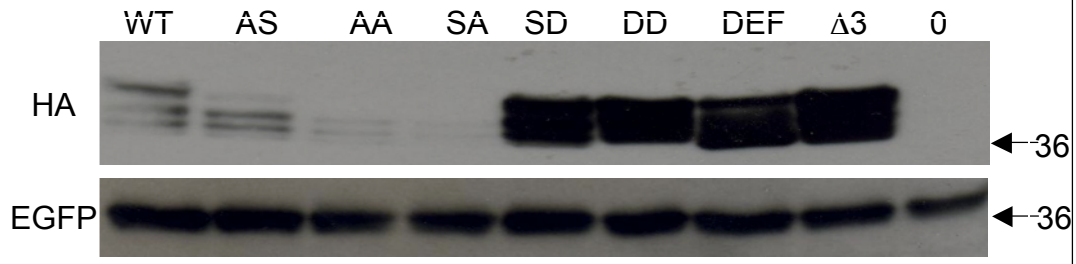

Figure 4.3.9 Western Blot analysis of J82 cells transfected with full length Fra-1 WT or full length Fra-1 with Ser^{252} -> Ala (AS), Ser^{252} and Ser^{265} both to Ala (AA), Ser^{265} -> Ala (SA), Ser^{265} -> Asp (SD), Ser^{252} and Ser^{265} both to Asp (DD). Also shown is Fra-1Δ3 and full length Fra-1 with an ERK-docking DEF motif mutated (DEF, Phe^{235} -> Ala). All transfections were performed along with EGFP to monitor transfection efficiency. Anti-HA (1:500), anti-EGFP (1:300), all secondary anti-rabbit (1:5000). MW in kDA shown on right

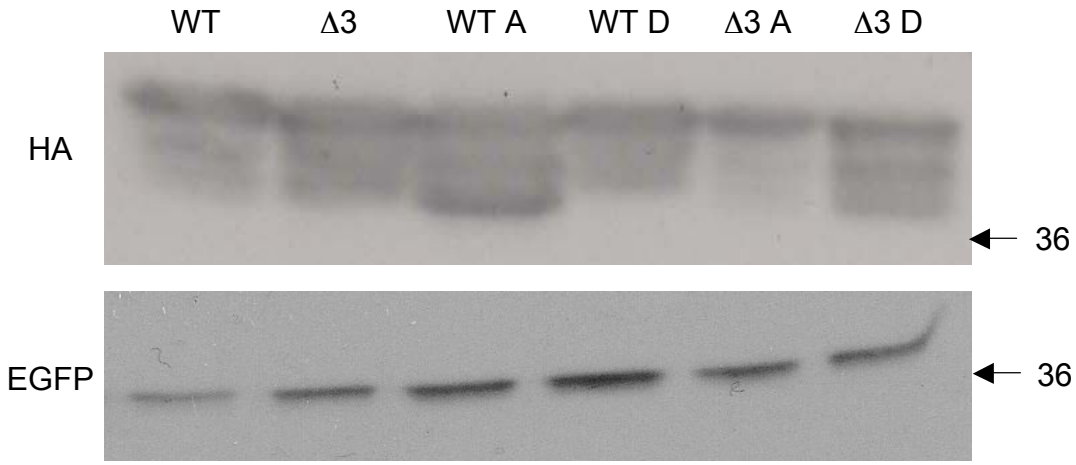

Figure 4.3.10 Western Blot analysis of J82 cells transfected with WT or Δ3 Fra-1 mutants in the presence of either Ser^{251}-> Ala (A) or Ser^{251}-> Asp (D), along with EGFP to monitor transfection efficiency. Anti-HA (1:500), anti-EGFP (1:300), all secondary anti-rabbit (1:5000). MW in kDA shown on right

As expected Δ3 is present at higher levels than WT. If Ser^{252} is dephosphorylated (AS), Fra-1 levels are lower, with loss of the hyperphosphorylated, slower migrating band. Dephosphorylation of Ser^{265} (SA) results in even lower levels of Fra-1, again with loss of the hyperphosphorylated species. This effect of dephosphorylation of Ser^{265} appears to be greater than the effect of Ser^{252}; dephosphorylation of both Ser^{252} and Ser^{265} (AA) leads to no difference in Fra-1 levels when compared to dephosphorylation of Ser^{265} (SA) alone.

Phosphorylation of Ser^{265} (SD) and Ser^{252} and Ser^{265} (DD) both generate the expected increase in Fra-1 levels, with all three Fra-1 Western Blot phospho-species appearing prominently.

Fra-1 contains an ERK-docking DEF motif (^{235}FTYP), homologous to ^{343}FTYP in c-Fos [114]. Mutation of the site Phe^{235} -> Ala in an otherwise wild-type Fra-1 increases Fra-1 protein levels; this is an unexpected finding. Murphy *et al*. [114] suggest that although the homologous sites to Ser^{252} and Ser^{265} in c-Fos are phosphorylated by ERK-dependent mechanisms, this is independent of the DEF-motif; rather phosphorylation of these two residues 'primes' c-Fos such that docking of ERK causes further c-Fos phosphorylation (at Thr^{325} and Thr^{331}, which modifies c-Fos transcriptional activity. Their findings suggest that ERK binding of the DEF motif has no effect on c-Fos stability, but does affect c-Fos function. Our experiments with the DEF mutant do not investigate function, but do clearly show that absence of ERK binding via mutation of the DEF motif

leads to an increase in Fra-1 levels; in contradiction, one may have hypothesized that this mutation should reduce Fra-1 levels. This is further investigated below by stimulating/inhibiting ERK in the presence/absence of Fra-1 mutations (Sections 4.3.6 and 4.3.7).

4.3.6 Effect of MAPK activity and inhibition of the proteasome on endogenous Fra-1 levels

Data presented in Section 4.3.2 demonstrates that Fra-1 accumulation is increased by stimulating J82 cells with EGF. To confirm that this EGF-mediated increase in Fra-1 accumulation is MEK dependent, J82 cells were pre-treated with the selective MEK-1 and MEK-2 inhibitor U0126 [144] prior to EGF stimulation (Figure 4.3.11). This demonstrates that in non-EGF-stimulated cells, Fra-1 levels are reduced by pre-treatment with U0126 (lane 1 vs. lane 3). If cells are treated with EGF, Fra-1 levels increase (lane 5 vs. lane 1) but not if co-treated with U0126 (lane 7 vs. lane 5). This demonstrates that the EGF-mediated increase in Fra-1 accumulation occurs via a MEK-dependent pathway.

Previous work in c-Fos [70] and Fra-1 [60, 143] demonstrated that these proteins are degraded by the proteasome. Figure 4.3.11 also demonstrates that Fra-1 levels are regulated by proteasomal degradation. When J82 cells were pre-treated with the proteasome inhibitor lactacystin [145], Fra-1 levels were significantly elevated (especially the hyperphosphorylated, slower migrating species; lane 1 vs. lane 2).

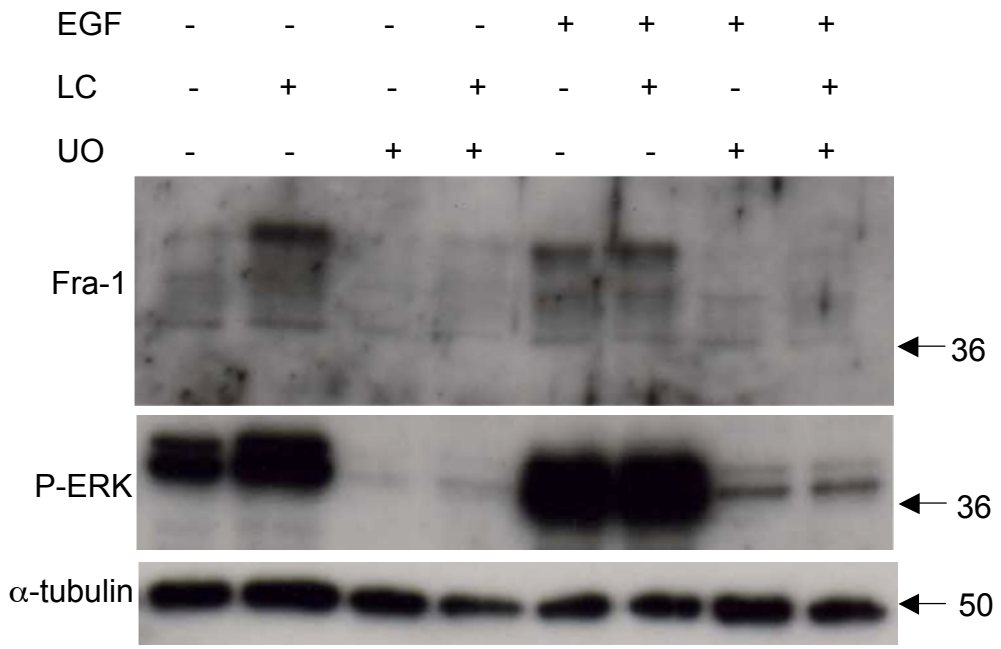

Figure 4.3.11 Western Blots of J82 cells pre-treated with Lactacystin (LC, 5 μM) and/or U0126 (UO, 30 μM) for 16 hours prior to stimulation with EGF (100 ng/ml) for two hours. Fra-1 1:500, P-ERK 1:1000, α-tubulin 1:5000, secondary anti-mouse 1:5000. MW in kDa shown on right

If, however, cells are also pre-treated with U0126, there is no lactacystin-mediated accumulation of Fra-1 (lane 4 vs. lane 3). In cells stimulated with EGF, there is no further increase in Fra-1 levels when pre-treated with lactacystin (lanes 5 and 6) which concurs with data from Vial [60]. They demonstrated that in BE colon carcinoma cells (containing mutations in both KRAS and BRAF) which have approximately five-times greater MAPK activity than their other colon carcinoma cell line HCT-116 (containing only a KRAS mutation), treatment with lactacystin does not cause further accumulation in Fra-1, whereas there is further accumulation of Fra-1 in lactacystin-treated HCT-116 cells.

This suggests that in J82 cells, endogenous Fra-1 levels are regulated both by the proteasome and MEK, and that proteasomal regulation is itself MEK-dependent. When interpreting this data, it must however be borne in mind that Fra-1 levels are a result of both production and degradation of Fra-1; it is known that *fosl1* mRNA accumulation is increased by MEK stimulation [60, 74] and in this experiment we are measuring endogenous Fra-1 levels, therefore with these experimental conditions we may be modifying both the production and degradation of Fra-1. To exclude the effect of transcriptional modification of Fra-1 levels, the same experiment was repeated in J82 cells transfected with pCGN-HA-Fra-1WT and pCGN-HA-Fra-1Δ7) (Section 4.3.7).

4.3.7 Effect of MAPK activity and inhibition of the proteasome on exogenous Fra-1 levels

To exclude any effect of MAPK modulation of Fra-1 accumulation via transcriptional regulation of *fosl1*, J82 cells were transfected with either pCGN-HA-Fra-1WT or pCGN-HA-Fra-1Δ7 and subjected to the same conditions as in Section 4.3.6. The resulting Western Blots are shown in Figures 4.3.12a & b.

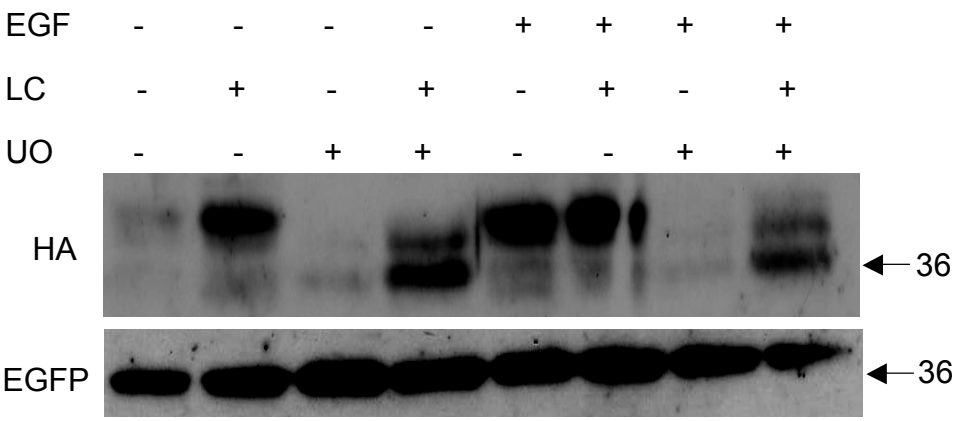

Figure 4.3.12a Western Blot analysis of J82 cells transfected with HA-Fra-1WT, and then treated with Lactacystin (LC, 5 μM) and/or U0126 (U0, 30 μM) for 16 hours prior to stimulation with EGF (100 ng·ml^{-1}) for two hours. Transfection efficiency was monitored by co-transfection with EGFP. Anti-HA (1:500), anti-EGFP (1:300), all secondary anti-rabbit (1:5000). MW in kDA is shown on the right.

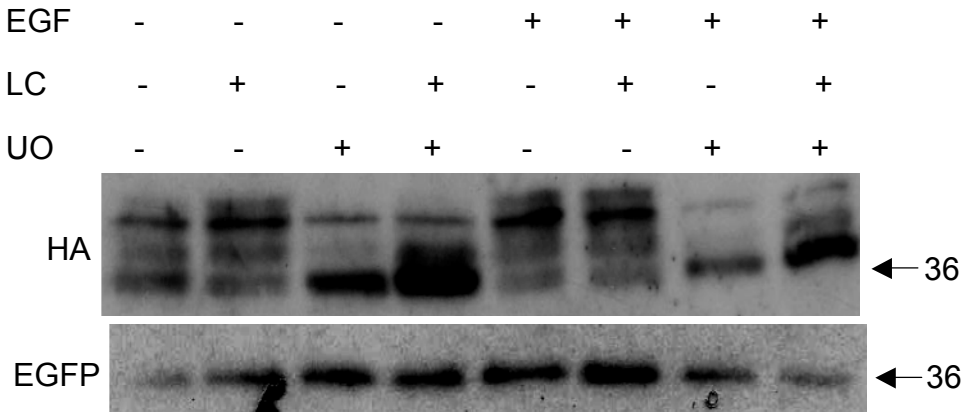

Figure 4.3.12b Western Blot of J82 cells transfected with HA-Fra-1Δ7, and then treated with Lactacystin (LC, 5 μM) and/or U0126 (U0, 30 μM) for 16 hours prior to stimulation with EGF (100 ng·ml^{-1}) for two hours. Transfection efficiency was monitored by co-transfection with EGFP. Anti-HA (1:500), anti-EGFP (1:300), all secondary anti-rabbit (1:5000). MW in kDA is shown on the right

If a comparison of the Western Blots for HA-Fra-1WT (Figure 4.3.12a) and endogenous Fra-1 (Figure 4.3.11) is performed, it can be seen that lactacystin again causes an increase in Fra-1 levels. However, whereas U0126 inhibited any lactacystin-mediated endogenous Fra-1 increase (Figure 4.3.11, lane 4), HA-Fra-1WT levels are increased in cells treated concurrently with lactacystin and U0126. The balance between different Fra-1 phospho-species in HA-Fra-1WT transfected J82 cells treated with lactacystin is modified (as expected) by MEK inhibition with U0126. This therefore suggests that Fra-1 levels are regulated post-transcriptionally by both MEK-dependent phosphorylation and the proteasome, and transcriptionally by MEK-dependent mechanisms.

To investigate the effect of the C-terminus on MEK-dependent and proteasomal Fra-1 regulation, the experiment was repeated with J82 cells transfected with HA-Fra-1Δ7 (Figure 4.3.12b). Lactacystin fails to cause any increase in HA-Fra-1Δ7 (lane 2 vs. lane 1). MEK inhibition appears to drive HA-Fra-1Δ7 into the hypo-phosphorylated form; it is difficult therefore to say whether total HA-Fra-1Δ7 accumulation is altered (lane 3 vs. lane 1). Lactacystin does appear, however, to cause an increase in HA-Fra-1Δ7 accumulation in the presence of MEK inhibition (lane 4 vs. lane 3). EGF treatment does not appear to cause a significant increase in HA-Fra-1Δ7 levels (lane 5 vs. lane 1), although it may increase the relative levels of the hyperphosphorylated Fra-1 phospho-form. Again, lactacystin causes no increase in HA-Fra-1Δ7 accumulation when also treated with EGF (lanes 1,2,5 and 6). Altogether, this suggests that the

C-terminus is important for proteasomal degradation. It is difficult to say from this data whether MEK inhibition reduces HA-Fra-1Δ7 levels because of the change in the relative quantities of the different Fra-1 phospho-forms; to investigate this point further, a further experiment would need to be performed to treat these samples with calf intestinal phosphatase (CIP) (Section 4.3.1) so that the overall HA-Fra-1Δ7 level could be measured.

4.3.8 Effect of Ser^{252} and Ser^{265} mutations on EGF and lactacystin modulation of Fra-1 levels in J82 cells

The above experiments confirm that both EGF and lactacystin treatment increase wild-type Fra-1 accumulation; either treatment individually appears to have little effect on overall Fra-1 levels in the presence of the deletion of the C-terminal seven amino acids. The next experiment (Figures 4.3.13a-c) examines the impact of Ser^{252} and Ser^{265} on EGF- and lactacystin-mediated regulation.

Figure 4.3.13a demonstrates the effect of MEK stimulation/inhibition and proteasomal inhibition on J82 cells transfected with wild-type Fra-1 (a repeat of the experiment shown in Figure 4.3.12a). The blot shown appears to show minimal Fra-1 in the untreated lane (lane 1); this is a feature of the exposure given when developing the blot (identical exposures were used for Figure 4.3.13b&c, with identical amounts of protein loaded per blot).

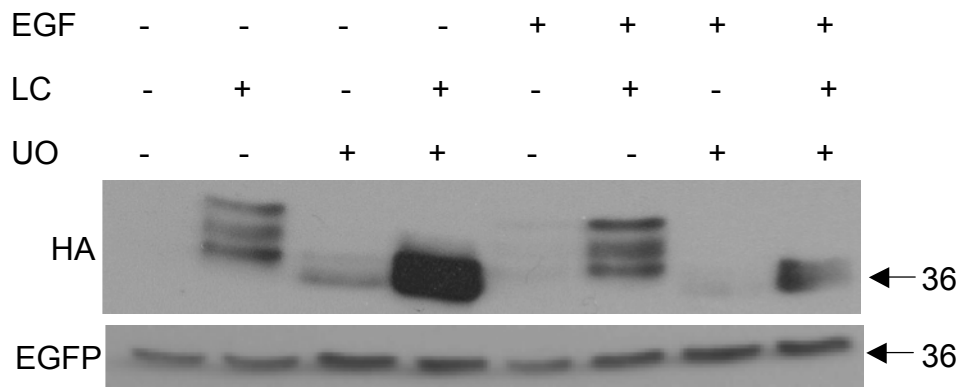

Figure 4.3.13a Western Blot of J82 cells transfected with HA-Fra-1ΔWT and then treated with Lactacystin (LC, 5 μM) and/or U0126 (U0, 30 μM) for 16 hours prior to stimulation with EGF (100 ng·ml^{-1}) for two hours. Transfection efficiency was monitored by co-transfection with EGFP. Anti-HA (1:500), anti-EGFP (1:300), all secondary anti-rabbit (1:5000). MW in kDA is shown on the right.

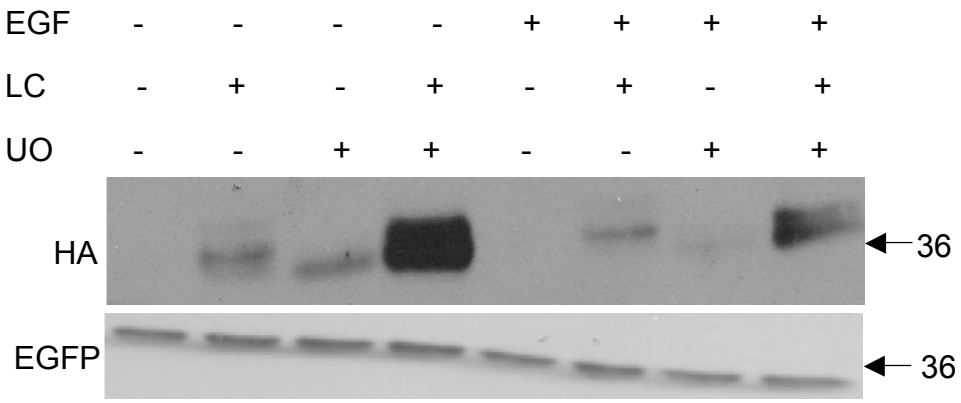

Figure 4.3.13b Western Blot of J82 cells transfected with HA-Fra-1DA and then treated with Lactacystin (LC, 5 μM) and/or U0126 (U0, 30 μM) for 16 hours prior to stimulation with EGF (100 ng·ml^{-1}) for two hours. Transfection efficiency was monitored by co-transfection with EGFP. Anti-HA (1:500), anti-EGFP (1:300), all secondary anti-rabbit (1:5000). MW in kDA is shown on the right.

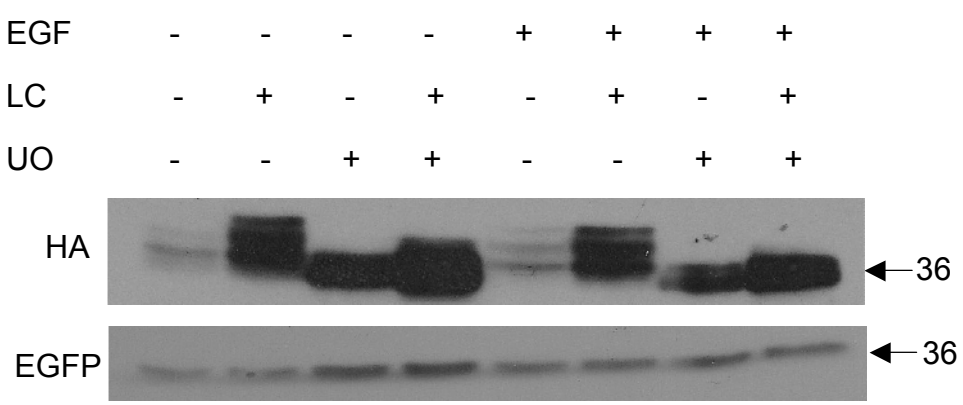

Figure 4.3.13c Western Blot of J82 cells transfected with HA-Fra-1SD and then treated with Lactacystin (LC, 5 μM) and/or U0126 (U0, 30 μM) for 16 hours prior to stimulation with EGF (100 ng/ml) for two hours. Transfection efficiency was monitored by co-transfection with EGFP. Anti-HA (1:500), anti-EGFP (1:300), all secondary anti-rabbit (1:5000). MW in kDA is shown on the right.

Figure 4.3.13a highlights the increase in Fra-1 levels caused by lactacystin treatment and suggests that MEK inhibition with U0126 may cause an increase in Fra-1 levels (there was little apparent difference in Fra-1 levels in Figure 4.3.12a when treated with U0126, although the phosphorylation pattern, as expected, was modified). The reason for these differences between the experiments performed using the same conditions is unclear, and both sets of results have been found again on repeating the experiments.

Mimicking phosphorylation at Ser^{252} and dephosphorylation at Ser^{265} (Figure 4.3.13b, Fra-1DA) modifies the phosphorylation-dependent Western Blot appearance of Fra-1. Proteasomal inhibition with lactacystin increases Fra-1 levels; MEK inhibition with U0126 also increases Fra-1 levels; proteasomal and MEK inhibition combined lead to

a very substantial increase. Treatment with EGF may lead to a small decrease in Fra-1 levels.

Figure 4.3.13c demonstrates the effect of MEK and proteasomal inhibition in Fra-1SD (Ser^{252} unchanged, Ser^{265} mutated to Asp). This mutation has previously been shown to increase Fra-1 accumulation (Figure 4.3.9) and is confirmed in this experiment. Again, lactacystin increases Fra-1 accumulation; this suggests that Ser^{265} affects Fra-1 levels via a proteasomal-independent mechanism. Again we see that MEK inhibition causes an increase in Fra-1 levels; this effect is clearly independent of Ser^{265} which in this system is acting as if it were phosphorylated regardless of MEK inhibition. EGF treatment has no significant effect on Fra-1SD accumulation (it may, as possibly in Fra-1DA, Figure 4.3.13b slightly reduce Fra-1 levels). This suggests that phosphorylation of Ser^{265} can be promoted by EGF treatment through a MEK-dependent pathway.

The data shown in Section 4.3 suggest that the regulation of Fra-1 accumulation is both transcriptional and post-transcriptional. With regard to post-transcriptional regulation of Fra-1, this is not only at the level of Fra-1 phosphorylation itself but by regulation of other components of the pathway(s) responsible for regulating Fra-1. Certainly Fra-1 is degraded by the proteasome and this regulation can in some way be regulated by MEK. However, whereas the initial hypothesis was that MEK activation would increase Fra-1 levels and, therefore MEK inhibition would

decrease levels, we have data to suggest that this is not simply the case, and the MEK-dependent regulation of Fra-1 is perhaps very tightly controlled such that some MEK-regulated components of Fra-1 levels increase Fra-1 whereas some result in a decrease in Fra-1. This would fit with a hypothesis that a key protein (such as Fra-1) which can promote its own transcription would need to be very tightly controlled to prevent a small increase in its level from some external stimulus leading to an ongoing, rapidly spiralling increase in levels.

4.4 Phospho-Fra-1 Immunohistochemical analysis of human muscle-invasive bladder tumours

The first section of this thesis demonstrates, for the first time, that Fra-1 is present in the majority of human bladder tumours. The second section demonstrates that Fra-1 is phosphorylated at Ser^{252} and Ser^{265} and that these sites are important for the regulation of Fra-1 accumulation. To bring the project 'about circle' therefore, immunohistochemical analysis of muscle-invasive bladder tumours using a phospho-Fra-1 antibody was performed. Ten of the original muscle invasive bladder tumours (Section 3.1.1) which expressed Fra-1 were selected for parallel staining with anti-Fra-1 and an anti-P-Ser^{265}-Fra-1 antibody (a kind gift from Dr M. Piechaczyk [143]) (Figure 4.4.1). All ten Fra-1 positive bladder tumour sections also stained positive for P-Ser^{265}-Fra-1, indicating that this phosphorylated, stabilised form of Fra-1 plays a role in human muscle-invasive bladder cancer. It is also noted that all of these P-Ser^{265}-Fra-1 positive sections demonstrate nuclear staining and none demonstrated cytoplasmic staining, whereas some of the total-Fra-1 stained sections demonstrated cytoplasmic staining.

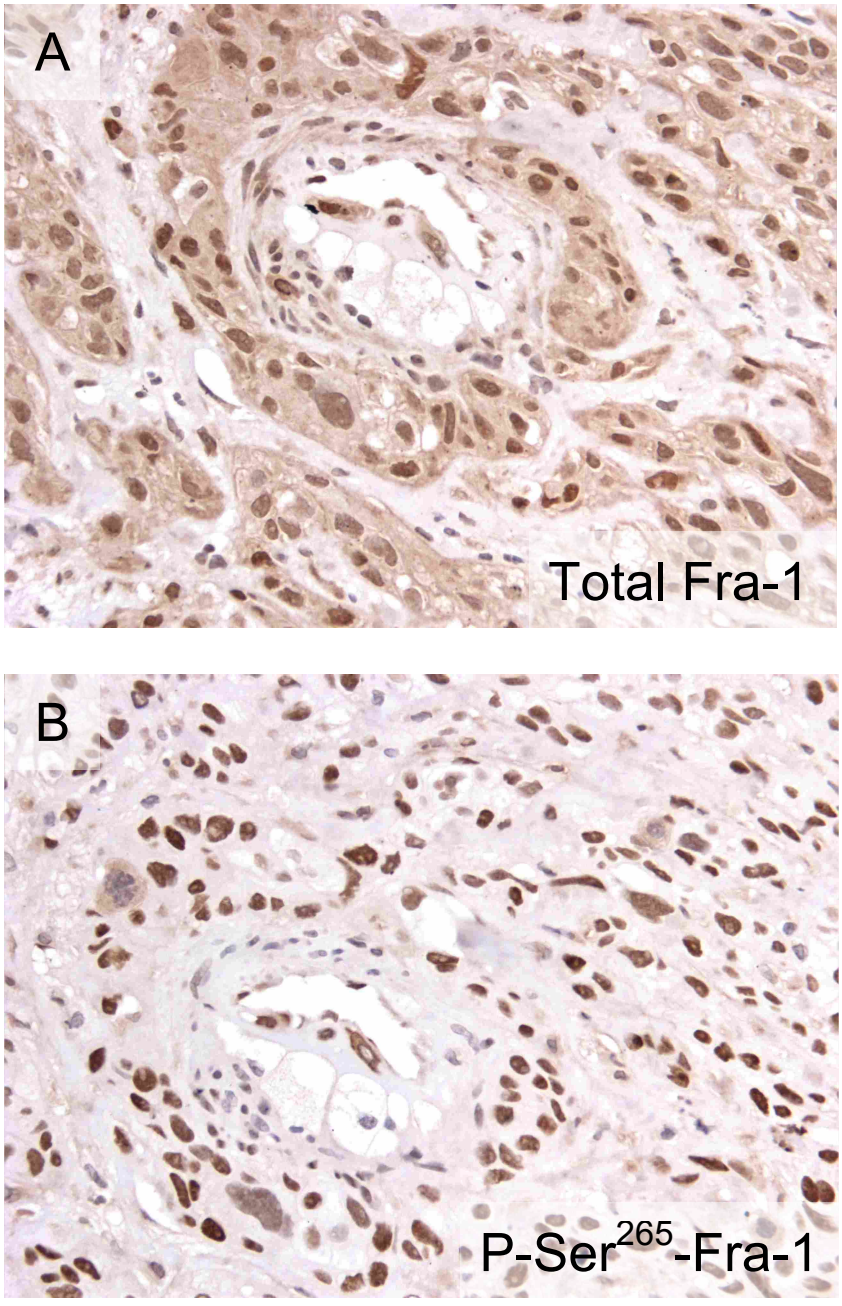

Figure 4.4.1 Examples of immunohistochemical staining for a) total Fra-1 and b) P-Ser^{265}-Fra-1.

Chapter 5

Discussion

In the introduction to this thesis, two main aims were described. The first aim was to investigate whether Fra-1 is present, and therefore may play a role, in human bladder cancer; the second aim being to investigate the regulatory mechanisms of Fra-1 in human bladder cancer cell lines. The findings with regard to these two aims will now be discussed, in turn, further.

5.1 Fra-1 is present in human bladder cancer

By immunohistochemical analysis, elevated Fra-1 expression has been detected in several tumour types including breast [93], thyroid [94], colon [95], oesophagus [96] and endometrium [97]. In addition, Fra-1 was upregulated in cell lines derived from mesothelioma [98, 99], glioblastoma multiforme [100] and nasopharyngeal carcinoma [101]. Work in breast carcinoma also demonstrated that Fra-1 expression was associated with higher grade tumours [93].

In addition to the fact that Fra-1 levels are elevated in a number of common human malignancies, there are five other factors to suggest that Fra-1 should be investigated in TCCB:

1. TCCB often harbours activating *ras* mutations which can signal via MAP Kinase to modify AP-1 activity.

2. FGFR3 mutations and overexpression in commonly found in TCCB. FGFR3 signals via *ras* to modify MAP Kinase activity.

3. Growth factor receptors c-Met and EGFR are positively associated with bladder cancer aggressiveness. EGFR signalling can activate AP-1.

4. Urokinase plasminogen activator is a specific transcriptional target of Fra-1 and is associated with poor prognosis in TCCB.

5. High levels of vascularisation are positively associated with TCCB aggressiveness. Fra-1 is essential for normal placental vascularisation and induces the expression of genes implicated in angiogenesis.

By immunohistochemical analysis, we have demonstrated that Fra-1 is highly expressed in superficial (62%, n=52) and muscle-invasive (80%, n=104) bladder tumours.

With regard to the muscle-invasive tumour group, whilst it should be remembered that this is a selected group of muscle-invasive tumours (i.e. those who for whatever clinical reason were treated with radiotherapy), it should not detract from the fact that Fra-1 is present in the majority of these tumours.

Whilst the age and gender characteristics of our cohort are similar to published radiotherapy series [13,14], our cohort does have a higher proportion of T3 tumours (38%) and a smaller proportion of T2 (49%) tumours, which one would expect to have an adverse impact on survival, and could represent a bias introduced via our patient selection.

To remove the risk of any cohort bias because of this selection, this study could be extending by analysing tumours from any patients with muscle-invasive disease, regardless of the treatment(s) they are to undergo.

In addition, we have not formally assessed benign transitional epithelium in this study due to the nature of the way that samples were obtained from patients only with known tumours. However, frequently tumour resections include an area of normal urothelium and when these areas have been seen in our samples, they appear not to contain Fra-1. To examine this further, benign tissue samples would have to be obtained, ideally from patients who have no history of transitional cell carcinoma of the urinary tract and subjected to the same formal histological analysis that we have already used.

One final limitation with the immunohistochemical analysis is that interpretation was only performed by one pathologist. This does introduce the possibility for intra-observer error. To reduce the risk of this, the study design could have included two pathologists. They would have independently analysed the sections, current research practice often including the generation of a Histoscore (which is a score given to a tumour section based on the sum

of the percentage of cells of the particular staining intensities multiplied by a factor for each staining intensity). This score from both pathologists can then be compared for each tumour to investigate inter-observer error.

More than 70% of non muscle-invasive bladder tumours contain mutations in *FGFR3* (as well as *FGFR3* often being overexpressed in such tumours); our finding that 62% of non muscle-invasive tumours express Fra-1 suggests that there is a mechanistic link between *FGFR3* status and Fra-1 levels via the MAP Kinase pathway. Further work to confirm this link would require identification of tumours with *FGFR3* mutations and correlation of these data with Fra-1 expression. In addition, the effect of novel FGFR3 inhibitors on Fra-1 (and even P-Ser^{265}-Fra-1) levels could be assessed.

Another interesting finding is that of cytoplasmic localisation of Fra-1. We show that Fra-1 is present both in the cytoplasm of human bladder tumour sections (Sections 3.1 and 3.2) and bladder cancer cell lines (Section 3.5.3). Cytoplasmic Fra-1 localisation has previously been shown in thyroid [94] and non-small cell lung carcinomas [92], as well as in breast [146, 147]. However, the data in breast is contradictory; Chiappetta *et al*. [146] show that Fra-1 is localised in the cytoplasm of benign fibroadenomas but not in carcinomas, whereas according to Song *et al*. [147], Fra-1 is present in the cytoplasm of breast carcinomas. This raises the obvious question of what, if any, role is Fra-1 having in the cytoplasm. Vial *et al*. [129] have suggested that Fra-1 may inhibit ß1-integrin activity either by regulating associated proteins or by a direct interaction with ß1-integrin. This is clearly another

interesting area for further investigation which may be started with immunoprecipitating cytoplasmic Fra-1 and followed by proteomic analysis of co-precipitated proteins. In addition, it should be possible to tag Fra-1 with, for example, EGFP and then track in real time the movement of Fra-1 throughout the cell to further investigate any discrete areas of intracellular localisation.

5.2 Fra-1 and Epithelial to Mesenchymal Transition (EMT)

Our data (Sections 3.4 and 3.5) demonstrates that the panel of six bladder cancer cell lines available in our laboratory can be divided into two groups based on their phenotypic appearance. Three cell lines (J82, T24 and UMUC3) have mesenchymal characteristics and express the mesenchymal marker vimentin, but not the epithelial marker E-cadherin, whilst the other three cell lines (HT1376, RT4 and RT112) have epithelial characteristics and express E-cadherin but not vimentin. Interestingly, Fra-1 expression is split into the same two groups, i.e. the mesenchymal cells express Fra-1 whereas the epithelial cells do not express significant levels of Fra-1.

Epithelial to mesenchymal transition is a vitally important event occurring both in normal development and the development of an invasive, malignant phenotype [122]. It is known that AP-1 can play a role in EMT; for example Davies *et al*. demonstrated that TGF-ß1 can promote EMT via ERK and p38 MAPK pathways and that this is inhibited by AP-1 inhibition [123]. More recent studies have demonstrated that Fra-1 plays a key role in EMT. ERK2 (but not ERK1) signalling can lead to EMT in breast and intestinal epithelial

cells via a Fra-1 dependent mechanism [125, 126]. These EMT pathways involve upregulation of a number of Fra-1 direct transcriptional targets including MMP-2 and MMP-9 [127, 148]. It has also been shown that RSK may play an important role in ERK/Fra-1 mediated EMT, in MCF10A cells by stimulating Fra-1 expression at the mRNA level and in MDCK cells by acting post-translationally on Fra-1, hypothetically by phosphorylating Ser^{252} [124].

Clearly our data does not prove that Fra-1 is indeed important in the development of EMT in bladder cancer cell lines. To further investigate the role of Fra-1 in EMT, further work could involve siRNA knockdown of Fra-1 in the J82/T24/UMUC3 cell group; this should, if the hypothesis is correct, lead to the inverse of EMT – mesenchymal to epithelial transition (MET). The opposite experiment could be performed in the HT1376/RT4/RT112 cell group; stably transfecting a Fra-1 construct and assessing whether the epithelial cells start to develop mesenchymal characteristics.

5.3 Regulatory mechanisms of Fra-1

5.3.1 Transcriptional regulation

fosl1 transcription is controlled by c-Fos via an AP-1 binding site in the first intron of the gene [68]. Casalino *et al*. [75] also show that this AP-1 binding site can be stably occupied by Fra-1 containing AP-1 complexes, suggesting that Fra-1 can promote *fosl1* transcription. Therefore manipulation of c-Fos and/or Fra-1 expression levels may affect *fosl1* transcription, hence modifying Fra-1 protein levels. MAP Kinase

stimulation has been shown to stabilise both c-Fos and Fra-1 proteins [60, 72, 73, 75]. This suggests that mitogenic stimulation or mutational activation of MAPK pathways may activate a positive autoregulatory loop involving transcriptional upregulation of *fosl1* and Fra-1 stabilisation. It is plausible to speculate that this loop represents a mechanistic basis for the accumulation of Fra-1 in cancer [75, 143]. However, our data showing that MEK inhibition results in accumulation of exogenous wild type Fra-1 and its mutants (Figures 4.3.12a and 4.3.13a) contradicts this hypothesis and implies that the control of Fra-1 abundance might be more complex than anticipated.

5.3.2 Post-translational regulation

By characterising the six bladder cancer cell lines (Section 3.4) we show that *fosl1* mRNA is present in all six, albeit at differing levels depending on whether they have mesenchymal or epithelial characteristics. However, Fra-1 protein is only detectable in the three mesenchymal-type cells (and to a small degree in RT112 cells) suggesting that post-translational regulation of Fra-1 might be involved.

Previously it has been demonstrated that Fra-1 levels are positively regulated by ERK1/2 activity in both physiological and pathological conditions [60, 61, 75, 116] and that Fra-1 appears on Western Blot as several bands with retarded mobility corresponding to different phosphorylated forms of the protein [75].

Experiments using calf intestinal phosphatase (CIP) (Section 4.3.1) clearly confirm that in bladder cancer cells the multi-band appearance of Fra-1 on Western Blot is due to phosphorylation, and that the hypo-phosphorylated form of Fra-1 is the more rapidly migrating species.

Next, we aimed to identify those Ser/Thr residues that undergo ERK-dependent phosphorylation resulting in Fra-1 stabilisation. It has been shown that the C-terminus of c-Fos is phosphorylated at Ser^{362} (by RSK1/2) and Ser^{374} (by ERK1/2) and that phosphorylation at these sites stabilises c-Fos [114, 116]. As discussed earlier, there is significant sequence homology between c-Fos and Fra-1, especially in the C-terminus, and the homologous amino acid residues in Fra-1 are Ser^{252} and Ser^{265}.

Andersen *et al*. [136] demonstrated that deleting the C-terminal 88 amino acids led to a marked increase in Fra-1 accumulation and hypothesised that this is due to the deletion of the C-terminal PEST motif which targets proteins for proteasomal degradation. We have mapped the effect of C-terminal deletions more closely by producing a series of smaller C-terminal deleted Fra-1 constructs and clearly show that deleting as little as the C-terminal three amino acids leads to a significant increase in Fra-1 accumulation (Section 4.2.2) and stability (Section 4.2.3). According to Acquaviva *et al*. just the tripeptide PTL motif within the PEST sequence in the homologous region of c-Fos is important in PEST-mediated regulation [140]. Our data however shows that the presence of this PTL

sequence does not necessarily promote degradation, as in the three amino acid deletion this sequence remains immediately at the C-terminus. Therefore, the absence of the adjacent leucine or leucine-alanine affects either protein folding or recognition of this sequence. It would be interesting to assess the effect of just one C-terminal amino acid deletion.

Sequence homology with c-Fos and the C-terminal deletion data therefore suggest that the C-terminus should be investigated further to identify critical amino acids which are involved in Fra-1 stability. Phosphomapping experiments (Section 4.3.4) identify Ser^{251}, Ser^{252} and Ser^{265} as amino acids which are phosphorylated in Fra-1. We performed mutation analysis of these amino acids to address the role of their phosphorylation in Fra-1 regulation. If Ser^{251} was mutated to alanine (to mimic the non-phosphorylated state), Fra-1 levels appeared to be higher than in wild-type. In contrast, mutations of both Ser^{252} and Ser^{265} to alanine reduced Fra-1 levels; whilst mutation of Ser^{252} and Ser^{265} to aspartate increased its stability. The effect of Ser^{252} and Ser^{265} mutation is to be expected because these residues are homologous to Ser^{362} and Ser^{374} in c-Fos. These residues are phosphorylated by RSK1/2 and ERK1/2 respectively resulting in c-Fos stabilisation [114, 149]. Whilst my work was in progress, the effect of phosphorylation at Ser^{252} and Ser^{265} of Fra-1 stability has been reported by Basbous *et al*. [143]. In agreement with our data, modulation of the phosphorylation state of Ser^{265} in mouse fibroblasts and colon cancer cells has a greater effect on Fra-1 stability than that of Ser^{252}.

The effect of the phosphorylation state of Ser^{251} is interesting and has not been reported elsewhere (in Basbous' article [143], Ser^{251} was not amongst their panel of phospho-mutant Fra-1 constructs). Mutation to alanine leads to an increase in Fra-1 accumulation, mainly due to an increase in the hypo-phosphorylated form as revealed by Western Blots (Figure 4.3.10). Our phosphomapping experiments also show that if Ser^{251} is phosphorylated (which does not appear to significantly alter accumulation of Fra-1) then no other amino acids in the C-terminus are phosphorylated. In addition, Ser^{251} phosphorylation is only seen in full-length Fra-1 and not in the Fra-1Δ3 mutant. It is not known which protein kinase phosphorylates Ser^{251} or if MEK activity has any influence over it. We suggest that this phosphorylation may inhibit MEK-dependent phosphorylation of Ser^{252} and Ser^{265} and counteract stabilisation of Fra-1 by MEK. Therefore, phosphorylation at Ser^{251} may represent a part of a signalling pathway negatively regulating Fra-1 expression and its physiological importance needs to be addressed in the future.

Unexpectedly, we have observed an increase in Fra-1 accumulation when MEK was inhibited with U0126 (Figures 4.3.13a, b & c). In U0126-treated cells, predominantly the accumulation of the hypophosphorylated form (which is though to be the least stable) was observed. Recent work has suggested that Fra-1 is interacting with TBP-1, a component of the 19S proteasome [150]. Whether the TBP-1/Fra-1 interaction or other components of the Fra-1 degradation

machinery are regulated by MEK is important for the better understanding of Fra-1 regulation and should be addressed in further studies.

C-Fos is known to be degraded by the proteasome [116, 140, 151], which is the major intracellular proteolytic pathway [152]. Most proteins are targeted for proteasomal degradation by being ubiquitinylated, however, c-Fos is one of a very small number of proteins that are able to be degraded by the proteasome without being ubiquitinylated [151, 153]. In addition to c-Fos, the list of these proteins includes ornithine decarboxylase [154] and cyclin-dependent kinase inhibitor 1 (p21) [155]. Interestingly, Sasaki suggest that whilst both nuclear and cytoplasmically located c-Fos are degraded by the proteasome, nuclear c-Fos is not ubiquitinylated whereas cytoplasmic c-Fos is.

Given the degree of sequence homology between c-Fos and Fra-1 it is reasonable to hypothesise that Fra-1 is also degraded via the proteasome, and this was first confirmed by Vial and Marshall [60]. Basbous *et al*. [143] have also confirmed proteasomal degradation using the proteasome inhibitor MG132. Our experiments with the proteasome inhibitor lactacystin also clearly show that Fra-1 is degraded via the proteasome (Sections 4.3.6-4.3.8). With regard to other proteolytic pathways, Ito *et al*. [156] showed that the cystine protease inhibitor E-64, the lysosome inhibitor chloroquine and calpain inhibitor ALLM did not affect c-Fos accumulation. We have examined chloroquine-mediated lysosomal inhibition and found no effect on Fra-1 accumulation (data not shown).

Like c-Fos, Fra-1 has been reported to undergo ubiquitinylation [157]. Notably, ubiquitinylation of Fra-1 is stimulated by MEK and results in an increase in the interaction between Fra-1 and histone deacetylase-1 (HDAC1), a crucial component of protein complexes responsible for transcriptional repression. Therefore, ubiquitinylation of Fra-1 may represent a mechanism controlling the balance between transcriptional activation and repression by Fra-1 [157]. The stability of a ubiquitinylation-deficient Fra-1 mutant, in which all lysines were converted into arginines, has been assessed in HeLa cells [143]. Consistent with the fact that Fra-1 ubiquitinylation is induced by a Fra-1-stabilising MEK pathway, the ubiquitinylation-deficient Fra-1 mutant was as stable as wild type Fra-1. These data are in agreement with the recently suggested biphasic model of ubiquitin-independent degradation of Fra-1 [150]. According to this model, the recognition of Fra-1 by a proteasome occurs through the Fra-1/TBP-1 interaction. The hydrophobic C-terminal domain facilitates the uptake and/or processing of Fra-1 by a proteasome. MEK-dependent phosphorylation antagonises the degradation by reducing the hydrophobicity of the C-terminal domain of Fra-1 and thereby stabilises the protein [150]. We co-transfected J82 cells with HA-Fra-1WT and His-tagged ubiquitin and performed immunoprecipitations either with anti-HA or anti-His antibodies, but have been unable to identify any ubiquitinylated Fra-1 species (not shown). We cannot state from this experiment alone that Fra-1 is not

ubiquitinylated in our system as the inability to detect it may be due to a flaw in our experimental methodology.

5.4 Clinical applications of Fra-1

Two clinical applications of Fra-1 were discussed in the introduction; firstly, whether Fra-1 could be used as a clinical target and secondly whether it could be used as a biomarker.

5.4.1 Fra-1 as a therapeutic target

This thesis adds to the data suggesting that Fra-1 could have a therapeutic role. Firstly, we have shown that Fra-1 is present in most transitional cell carcinomas of the bladder; especially in the more aggressive muscle-invasive group. We also show that the more stable phospho-Fra-1 is detectable in these tumours. In agreement with the existing literature, our data show that Fra-1 is regulated via both MAP Kinase and the proteasome. Many of the novel chemotherapeutic agents are targeting cell-surface receptors such as EGFR and FGFR3 which signal via MAP Kinase. However, EGFR inhibitors such as gefitinib and lapatinib have so far shown disappointing results. This can be explained by the fact that the myriad of intracellular signalling pathways and crosstalk between them exist, and the magnitude of any effect on receptor activity may be greatly diluted at the level of the end effector. It then becomes logical to target the end-effector, and Fra-1 appears to be a candidate for this in bladder cancer. A DNA vaccine targeting Fra-1 in murine models of breast and non-small cell lung cancer has already shown promise. Two

other strategies to target Fra-1 may include inhibiting phosphorylation at Ser^{265} and/or Ser^{252}, or even promoting phosphorylation of Ser^{251} (by an as yet unknown protein kinase); or Fra-1 knockdown by RNAi.

5.4.2 Fra-1 as a biomarker

Given that Fra-1 is expressed in both non-invasive and invasive bladder tumours; but not expressed in all of the invasive bladder tumours in our series, I do not feel that Fra-1 will improve the histopathological diagnosis of bladder cancer. We also find no statistically significant difference in Fra-1 staining across tumour grades, which could, if it were significant, aid in the risk-stratification of bladder tumours. In addition, because the muscle-invasive cohort is super-selected (i.e. just those patients who have had radiotherapy) and there is no long-term data for the non muscle-invasive cohort, there is not enough data here to either claim or deny a role to Fra-1 with regards to being a prognostic biomarker.

A more likely role of Fra-1 as a (predictive) biomarker is as a marker of MAP Kinase activity. We, and others have clearly shown that Fra-1 is regulated by MAP Kinase via C-terminal phosphorylation. We suggest that in the clinical setting, Fra-1 phosphorylated at Ser^{265} can be used as an indicator of active MAPK pathway. To investigate the role of Fra-1 as a predictive biomarker further, initially *in vitro* studies looking at Fra-1 and phospho-Fra-1 responses to chemotherapeutic agents targeting the MAPK pathway would need to be performed. If these studies still suggest a role for Fra-1, then immunohistochemical analyses of bladder tumours

with both anti-Fra-1 antibody and the anti-phospho-Ser^{265}-Fra-1 antibody would need to be performed both pre- and post-chemotherapy.

Abbreviations

AP-1	Activator Protein-1
ATF	Activating transcription factor
BCG	Bacillus Calmette-Guérin
bZIP	Basic and leucine zipper domain
cDNA	Complementary deoxyribonucleic acid
cAMP	3'-5' cyclic adenosine monophosphate
CIP	Calf intestinal phosphatase
CRE	cAMP response elements
DAPI	4',6-diamidino-2-phenyl-indole dihydrochloride
dATP	Deoxyadenosine triphosphate
dCTP	Deoxycytosine triphosphate
dGTP	Deoxyguanosine triphosphate
DMEM	Dulbecco's minimum essential medium
DMSO	Dimethylsulphoxide
DNA	Deoxyribonucleic acid
dNTP	deoxyribonucleotide triphosphate
DOX	Doxycycline
DTT	Dithiothreitol
dTTP	Deoxythymidine triphosphate
DXT	Radiotherapy
E. coli	*Eschericia coli*
EDTA	Ethylene diaminotetraacetic acid
EGF	Epidermal growth factor

EGFP	Enhanced green fluorescent protein
EGFR	Epidermal growth factor receptor
EMT	Epithelial to mesenchymal transition
ER	Oestrogen receptor
ERK	Extracellular signal-related kinase
ETS	E-twenty six
EtBr	Ethidium bromide
FBJ	Finkel Biskis Jinkins
FCS	Foetal calf serum
FGFR	Fibroblast Growth Factor Receptor
Fos	FBJ-derived osteosarcoma
Fra-1	Fos-related antigen-1
FTI	Farnesyltransferase inhibitor
GAPDH	Glyceraldehyde-3-phosphate dehydrogenase
GC	Gemcitabine and cisplatin
HA	Haemagglutinin
HEPES	4-(2-hydroxyethyl)-1-piperazineethanesulfonic acid
HER2	Human epidermal growth factor receptor 2
HMGI	High mobility group I
HPV	Human papilloma virus
ICD	International classification of diseases
IL	Interleukin
IMS	Industrial methylated spirit
kDa	kiloDaltons
Lef	Lymphoid enhancer factor

MAP Kinase	Mitogen activated protein kinase
MnOAc	Manganese acetate
MEM	Minimum essential medium
MMP	Matrix metalloproteinase
MOPS	3-(N-morpholino)propanesulfonic acid
mRNA	Messenger ribonucleic acid
MTIIa	Metallothionein IIa
mTOR	mammalian target of rapamycin
MVAC	Methotrexate, vinblastine, Adriamycin and doxorubicin
PAGE	Polyacrylamide gel electrophoresis
PAI	Plasminogen activator inhibitor
PBS	Phosphate buffered saline
PCR	Polymerase chain reaction
PDGFR	Platelet-derived growth factor receptor
PI3K	Phosphatidyl inositol 3-kinase
PMSF	Phenylmethanesulphonyl fluoride
PTEN	Phosphatase and tensin homolog
PVDF	Polyvinylidene fluoride
RIPA	Radio immuno-precipitation assay (buffer)
RNA	Ribonucleic acid
RSK	90-kDa Ribosomal S6 Kinase
siRNA	Small interfering RNA
SDS	Sodium dodecyl sulphate
SV40	Simian virus 40
TBS-T	Tris buffered saline with Tween-20

TCC	Transitional cell carcinoma
TCCB	Transitional cell carcinoma of the bladder
Tcf	T cell factor
TCF	Ternary complex factor
TEG	Tris/EDTA/ß-glycerophosphate buffer
TEMED	N,N,N',N'-tetramethylethylenediamine
TIMP	Tissue inhibitor of metalloproteinase's
TLC	Thin layer chromatography
tPA	tissue-type plasminogen activator
TPA	12-*O*-Tetradecanoylphorbol-13-acetate
TRE	TPA responsive elements
Tris	2-amino-2-hydroxymethyl-1,3-propanediol
TURBT	Transurethral resection of bladder tumour
UHL	University Hospitals of Leicester NHS Trust
uPA	urokinase plasminogen activator
uPAR	urokinase plasminogen activator receptor
VEGF	Vascular endothelial growth factor
VEGFR	Vascular endothelial growth factor receptor
WHO	World Health Organisation

Appendix 1

Protein and Gene Sequences

A1.1 Human Fra-1/*fosl1*

MFRDFGEPGPSSGNGGGYGGPAQPPAAAQAAQQKFHLVPSINTMSGSQEL
QWMVQPHFLGPSSYPRPLTYPQYSPPQPRPGVIRALGPPPGVRRRPCEQISPE
EEERRRVRRERNKLAAAKCRNRRKELTDFLQAETDKLEDEKSGLQREIEEL
QKQKERLELVLEAHRPICKIPEGAKEGDTGSTSGTSSPPAPCRPVPCISLSPGP
VLEPEALHTPTLMTTPSLTPFTPSLVFTYPSTPEPCASAHRKSSSSSGDPSSDP
LGSPTLLAL

1 acgggccaag gcggcgcgtc tcgggggtgg agcctggagg tgaccgcgcc gctgcaacgc

61 ccccaccccc cgcggtcgca gtggttcagc ccgagaactt ttcattcata aaaagaaaag

Long *fosl1* 5' (4.1.2)

121 actccgcacg gcgcgggtga gtcagaaccc agcagccgtg taccccgcag agccgccagc

5' *fosl1Xba*I (4.1.2)

181 cccgggc**ATG**ttccgagact tcggggaacc cggcccgagc tccgggaacg gcggcgggta

241 cggcggcccc gcgcagcccc cggccgcagc gcaggcagcc cagcagaagt tccacctggt

301 gccaagcatc aacaccatga gtggcagtca ggagctgcag tggatggtac agcctcattt

361 cctggggccc agcagttacc ccaggcctct gacctaccct cagtacagcc ccccacaacc

421 ccggccagga gtcatccggg ccctggggcc gcctccaggg gtacgtcgaa ggccttgtga

481 acagatcagc ccggaggaag aggagcgccg ccgagtaagg cgcgagcgga acaagctggc

5' *fosl1Sbf*I (4.1.5)

541 tgcggccaag tgcaggaacc ggaggaagga actgaccgac ttcctgcagg cggagactga

601 caaactggaa gatgagaaat ctgggctgca gcgagagatt gaggagctgc agaagcagaa

661 ggagcgccta gagctggtgc tggaagccca ccgacccatc tgcaaaatcc cggaaggagc

721 caaggagggg gacacaggca gtaccagtgg caccagcagc ccaccagccc cctgccgccc

781 tgtaccttgt atctcccttt ccccagggcc tgtgcttgaa cctgaggcac tgcacacccc

841 cacactcatg accacaccct ccctaactcc tttcaccccc agcctggtct tcacctaccc

901 cagcactcct gagccttgtg cctcagctca tcgcaagagt agcagcagca gcggagaccc

3' *fosl1Bam*HI (4.1.2)

961 atcctctgac ccccttggct ctccaaccct cctcgctttg **TGA**ggcgcct gagccctact

1021 ccctgcagat gccaccctag ccaatgtctc ctccccttcc cccaccggtc cagctggcct

1081 ggacagtatc ccacatccaa ctccagcaac ttcttctcca tccctctaat gagactgacc

Long *fosl1* 3' (4.1.2)

1141 atattgtgct tcacagtaga gccagcttgg ggccaccaaa gctgcccact gtttctcttg

1201 agctggcctc tctagcacaa tttgcactaa atcagagaca aaatatttcc catttgtgcc

1261 agaggaatcc tggcagccca gagactttgt agatccttag aggtcctctg gagccctaac

1321 cccttccaga tcactgccac actctccatc accctcttcc tgtgatccac ccaaccctat

1381 ctcctgacag aaggtgccac tttacccacc tagaacacta actcaccagc cccactgcca

1441 gcagcagcag gtgattggac caggccattc tgccgccccc tcctgaaccg cacagctcag

1501 gaggcgccct tggcttctgt gatgagctga tctgcggatc tcagctttga gaagccttca

1561 gctccaggga atccaagcct ccacagcgag ggcagctgct atttattttc ctaaagagag

1621 tatttttata caaacctacc aaaatggaat aaaaggcttg aagctgtgaa aaaaaaaaaa

1681 aaaaaaaaaa aaa

ATG represents the Start Codon (188-190)

TGA represents the Stop Codon (1001-1003)

Highlighted regions refer to primer binding sites as described in the Sections given

A1.2 Human Glyceraldehyde-3-phosphate dehydrogenase (GAPDH)

MGKVKVGVNGFGRIGRLVTRAAFNSGKVDIVAINDPFIDLNYMVYMFQYD
STHGKFHGTVKAENGKLVINGNPITIFQERDPSKIKWGDAGAEYVVESTGV
FTTMEKAGAHLQGGAKRVIISAPSADAPMFVMGVNHEKYDNSLKIISNASC
TTNCLAPLAKVIHDNFGIVEGLMTTVHAITATQKTVDGPSGKLWRDGRGAL
QNIIPASTGAAKAVGKVIPELNGKLTGMAFRVPTANVSVVDLTCRLEKPAK
YDDIKKVVKQASEGPLKGILGYTEHQVVSSDFNSDTHSSTFDAGAGIALND
HFVKLISWYDNEFGYSNRVVDLMAHMASKE

1 aaattgagcc cgcagcctcc cgcttcgctc tctgctcctc ctgttcgaca gtcagccgca

61 tcttcttttg cgtcgccagc cgagccacat cgctcagaca cc**ATG**gggaaggtgaaggtc

121 ggagtcaacg gatttggtcg tattgggcgc ctggtcacca gggctgcttt taactctggt

181 aaagtggata ttgttgccat caatgacccc ttcattgacc tcaactacat ggtttacatg

241 ttccaatatg attccaccca tggcaaattc catggcaccg tcaaggctga gaacgggaag

301 cttgtcatca atggaaatcc catcaccatc ttccaggagc gagatccctc caaaatcaag

361 tggggcgatg ctggcgctga gtacgtcgtg gagtccactg gcgtcttcac caccatggag

421 aaggctgggg ctcatttgca ggggggagcc aaaagggtca tcatctctgc cccctctgct

481 gatgccccca tgttcgtcat gggtgtgaac catgagaagt atgacaacag cctcaagatc

541 atcagcaatg cctcctgcac caccaactgc ttagcacccc tggccaaggt catccatgac

601 aactttggta tcgtggaagg actcatgacc acagtccatg ccatcactgc cacccagaag

661 actgtggatg gcccctccgg gaaactgtgg cgtgatggcc gcggggctct ccagaacatc

721 atccctgcct ctactggcgc tgccaaggct gtgggcaagg tcatccctga gctgaacggg

781 aagctcactg gcatggcctt ccgtgtcccc actgccaacg tgtcagtggt ggacctgacc

841 tgccgtctag aaaaacctgc caaatatgat gacatcaaga aggtggtgaa gcaggcgtcg

901 gagggccccc tcaagggcat cctgggctac actgagcacc aggtggtctc ctctgacttc

961 aacagcgaca cccactcctc caccttttgac gctggggctg gcattgccct caacgaccac

1021 tttgtcaagc tcatttcctg gtatgacaac gaatttggct acagcaacag ggtggtggac

1081 ctcatggccc acatggcctc caaggag**TAA**gacccctgga ccaccagccc cagcaagagc

ATG represents the Start Codon (103-105)

TGA represents the Stop Codon (1108-1110)

A1.3 Murine Fra-1/*fosl1*

MYRDYGEPGPSSGAGSPYGRPAQPPQAQAQTAQQQKFHLVPSIDSSSQELH
WMVQPHFLGPTGYPRPLAYPQYSPPQPRPGVIRALGPPPGVRRRPCEQISPE
EEERRRVRRERNKLAAAKCRNRRKELTDFLQAETDKLEDEKSGLQREIEEL
QKQKERLELVLEAHRPICKIPEGDKKDPGGSGSTSGASSPPAPGRPVPCISLS
PGPVLEPEALHTPTLMTTPSLTPFTPSLVFTYPSTPEPCSSAHRKSSSSSGDPS
SDPLGSPTLLAL

1	tgtctgtaga	ggcggcttgc	cacccgagca	gagggtcgtg	aagttccgag	cggaccggtc
61	cacagaggtt	catctggaga	ggtgggtccc	ctgcgaggtg	aaaggcgccg	ctgagacacg
121	cccccacccc	ccgtggtgca	agtggttcag	cccaagaact	tttcattcat	aaaaaagacc
181	agactccgag	aggcgcgagt	gagtcagaac	cgcagccgcc	aacgcggacc	ctaccgaaca
241	tccagcccag	ggc**ATG**tacc	gagactacgg	ggaaccggga	ccgagctccg	gggctggcag
301	cccgtacggt	cgccccgcgc	agcccccgca	agctcaggca	cagaccgccc	agcagcagaa
361	gttccacctt	gtgccaagca	tcgacagcag	cagccaggaa	ctgcactgga	tggtgcagcc
421	tcatttcctg	ggacccactg	gctatccccg	acctctggcc	tatccccagt	acagtccccc
481	tcagccccgg	ccaggagtca	tacgagccct	agggccacct	ccgggggtgc	gtcgcaggcc
541	ctgcgagcag	atcagcccag	aggaggaaga	gcgccgcagg	gtgagacgcg	agcggaacaa
601	gctagcagct	gctaagtgca	gaaaccgaag	aaaggagctg	acagacttcc	tgcaggcgga
661	gaccgacaaa	ttggaggatg	agaaatcggg	gctgcagcga	gagattgaag	agctgcagaa
721	gcagaaggaa	cgccttgagc	tggtgctgga	agcccatcgc	cccatctgca	aaatcccaga
781	aggagacaag	aaggacccag	gtggttctgg	cagcaccagc	ggtgctagca	gcccaccagc
841	ccccggccgc	ccagtgcctt	gcatctccct	ttctccagga	cccgtacttg	aaccggaagc
901	actgcatacc	cccacgctca	tgaccacacc	ctctctgact	ccttttactc	cgagtctggt

961 tttcacctat cctagcacac cagaaccttg ctcctccgct caccgaaaga gtagcagcag

1021 cagtggcgac ccctcctccg acccccctggg ctctcctaca ctcctggctt tg**TGA**ggcac

1081 ccagccacat cccttgctgg tgctactcca agccatcccc tttctcccat tgatccagca

ATG represents the Start Codon (254-256)

TGA represents the Stop Codon (1073-1075)

Appendix 2

Sayan AE, Stanford R, Vickery R, Grigorenko E, Diesch J, Kulbicki K, Edwards R, Pal R, Greaves P, Jariel-Encontre I, Piechaczyk M, Kriajevska M, Mellon JK, Dhillon AS & Tulchinsky E. Fra-1 controls motility of bladder cancer cells via transcriptional upregulation of the receptor tyrosine kinase AXL. Oncogene 2012 Mar 22;31(12):1493-503. Epub 2011 Aug 8

Paper page 1

Bibliography

1. National Statistics Online - Product - Cancer Registration Statistics England 2007 [Internet]. [cited 2010 Jun 14];Available from: http://www.statistics.gov.uk/downloads/theme_health/2007cancerfirstrelease.xls

2. National Statistics Online - Product - Mortality statistics: Deaths registered in England and Wales (Series DR) [Internet]. [cited 2010 Jun 14];Available from: http://www.statistics.gov.uk/downloads/theme_health/DR2007/DR_07_2007.pdf

3. Wein A, Kavoussi L, Novick A, Partin A, Peters C. Campbell-Walsh Urology. 9th ed.

4. Sylvester RJ, van der Meijden APM, Oosterlinck W, Witjes JA, Bouffioux C, Denis L, et al. Predicting recurrence and progression in individual patients with stage Ta T1 bladder cancer using EORTC risk tables: a combined analysis of 2596 patients from seven EORTC trials. Eur. Urol. 2006 Mar;49(3):466–465; discussion 475–477.

5. Sylvester RJ, Oosterlinck W, van der Meijden APM. A single immediate postoperative instillation of chemotherapy decreases the risk of recurrence in patients with stage Ta T1 bladder cancer: a meta-analysis of published results of randomized clinical trials. J. Urol. 2004 Jun;171(6 Pt 1):2186–2190, quiz 2435.

6. Lamm DL. Carcinoma in situ. Urol. Clin. North Am. 1992 Aug;19(3):499–508.

7. Sylvester RJ, van der MEIJDEN APM, Lamm DL. Intravesical bacillus Calmette-Guerin reduces the risk of progression in patients with superficial bladder cancer: a meta-analysis of the published results of randomized clinical trials. J. Urol. 2002 Nov;168(5):1964–70.

8. Malmström P-U, Sylvester RJ, Crawford DE, Friedrich M, Krege S, Rintala E, et al. An individual patient data meta-analysis of the long-term outcome of randomised studies comparing intravesical mitomycin C versus bacillus Calmette-Guérin for non-muscle-invasive bladder cancer. Eur. Urol. 2009 Aug;56(2):247–56.

9. Shariat SF, Karakiewicz PI, Palapattu GS, Lotan Y, Rogers CG, Amiel GE, et al. Outcomes of radical cystectomy for transitional cell carcinoma of the bladder: a contemporary series from the Bladder Cancer Research Consortium. J. Urol. 2006 Dec;176(6 Pt 1):2414–22; discussion 2422.

10. European Association of Urology (EAU) - Guidelines - Online Guidelines - Guideline [Internet]. [cited 2010 Jun 16];Available from: http://www.uroweb.org/?id=218&gid=2

11. Neoadjuvant chemotherapy in invasive bladder cancer: update of a systematic review and meta-analysis of individual patient data advanced bladder cancer (ABC) meta-analysis collaboration. Eur. Urol. 2005 Aug;48(2):202–5; discussion 205–6.

12. International Collaboration of Trialists on behalf of the Medical Research Council Advanced Bladder Cancer Working Party (now the National Cancer Research Institute Bladder Cancer Clinical Studies Group) the EO for R and T of CG-UTCG. International Phase III Trial Assessing Neoadjuvant Cisplatin, Methotrexate, and Vinblastine Chemotherapy for Muscle-Invasive Bladder Cancer: Long-Term Results of the BA06 30894 Trial. JCO. 2011 Jun 1;29(16):2171–7.

13. James ND, Hussain SA, Hall E, Jenkins P, Tremlett J, Rawlings C, et al. Radiotherapy with or without chemotherapy in muscle-invasive bladder cancer. N. Engl. J. Med. 2012 Apr 19;366(16):1477–88.

14. Hoskin PJ, Rojas AM, Bentzen SM, Saunders MI. Radiotherapy with concurrent carbogen and nicotinamide in bladder carcinoma. J. Clin. Oncol. 2010 Nov 20;28(33):4912–8.

15. Adjuvant chemotherapy in invasive bladder cancer: a systematic review and meta-analysis of individual patient data Advanced Bladder Cancer (ABC) Meta-analysis Collaboration. Eur. Urol. 2005 Aug;48(2):189–99; discussion 199–201.

16. Shipley WU, Kaufman DS, Zehr E, Heney NM, Lane SC, Thakral HK, et al. Selective bladder preservation by combined modality protocol treatment: long-term outcomes of 190 patients with invasive bladder cancer. Urology. 2002 Jul;60(1):62–7; discussion 67–8.

17. Cappellen D, De Oliveira C, Ricol D, de Medina S, Bourdin J, Sastre-Garau X, et al. Frequent activating mutations of FGFR3 in human bladder and cervix carcinomas. Nat. Genet. 1999 Sep;23(1):18–20.

18. Tomlinson DC, Baldo O, Harnden P, Knowles MA. FGFR3 protein expression and its relationship to mutation status and prognostic variables in bladder cancer. J. Pathol. 2007 Sep;213(1):91–8.

19. Boulalas I, Zaravinos A, Karyotis I, Delakas D, Spandidos DA. Activation of RAS family genes in urothelial carcinoma. J. Urol. 2009 May;181(5):2312–9.

20. Jebar AH, Hurst CD, Tomlinson DC, Johnston C, Taylor CF, Knowles MA. FGFR3 and Ras gene mutations are mutually exclusive genetic events in urothelial cell carcinoma. Oncogene. 2005 Aug 4;24(33):5218–25.

21. Qing J, Du X, Chen Y, Chan P, Li H, Wu P, et al. Antibody-based targeting of FGFR3 in bladder carcinoma and t(4;14)-positive multiple myeloma in mice. J. Clin. Invest. 2009 May;119(5):1216–29.

22. Neal DE, Sharples L, Smith K, Fennelly J, Hall RR, Harris AL. The epidermal growth factor receptor and the prognosis of bladder cancer. Cancer. 1990 Apr 1;65(7):1619–25.

23. Mellon K, Wright C, Kelly P, Horne CH, Neal DE. Long-term outcome related to epidermal growth factor receptor status in bladder cancer. J. Urol. 1995 Mar;153(3 Pt 2):919–25.

24. Edwards DR, Murphy G, Reynolds JJ, Whitham SE, Docherty AJ, Angel P, et al. Transforming growth factor beta modulates the expression of collagenase and metalloproteinase inhibitor. EMBO J. 1987 Jul;6(7):1899–904.

25. Philips GK, Halabi S, Sanford BL, Bajorin D, Small EJ. A phase II trial of cisplatin (C), gemcitabine (G) and gefitinib for advanced urothelial tract carcinoma: results of Cancer and Leukemia Group B (CALGB) 90102. Ann. Oncol. 2009 Jun;20(6):1074–9.

26. Wülfing C, Machiels J-PH, Richel DJ, Grimm M-O, Treiber U, De Groot MR, et al. A single-arm, multicenter, open-label phase 2 study of lapatinib as the second-line treatment of patients with locally advanced or metastatic transitional cell carcinoma. Cancer. 2009 Jul 1;115(13):2881–90.

27. Winquist E, Moore MJ, Chi KN, Ernst DS, Hirte H, North S, et al. A multinomial Phase II study of lonafarnib (SCH 66336) in patients with refractory urothelial cancer. Urol. Oncol. 2005 Jun;23(3):143–9.

28. Rosenberg JE, von der Maase H, Seigne JD, Mardiak J, Vaughn DJ, Moore M, et al. A phase II trial of R115777, an oral farnesyl transferase inhibitor, in patients with advanced urothelial tract transitional cell carcinoma. Cancer. 2005 May 15;103(10):2035–41.

29. Davies BR, Logie A, McKay JS, Martin P, Steele S, Jenkins R, et al. AZD6244 (ARRY-142886), a potent inhibitor of mitogen-activated protein kinase/extracellular signal-regulated kinase kinase 1/2 kinases: mechanism of action in vivo, pharmacokinetic/pharmacodynamic relationship, and potential for combination in preclinical models. Mol. Cancer Ther. 2007 Aug;6(8):2209–19.

30. Platt FM, Hurst CD, Taylor CF, Gregory WM, Harnden P, Knowles MA. Spectrum of phosphatidylinositol 3-kinase pathway gene alterations in bladder cancer. Clin. Cancer Res. 2009 Oct 1;15(19):6008–17.

31. Sahai E, Marshall CJ. Differing modes of tumour cell invasion have distinct requirements for Rho/ROCK signalling and extracellular proteolysis. Nat. Cell Biol. 2003 Aug;5(8):711–9.

32. Vazquez A, Bond EE, Levine AJ, Bond GL. The genetics of the p53 pathway, apoptosis and cancer therapy. Nat Rev Drug Discov. 2008 Dec;7(12):979–87.

33. Angel P, Karin M. The role of Jun, Fos and the AP-1 complex in cell-proliferation and transformation. Biochim. Biophys. Acta. 1991 Dec 10;1072(2-3):129–57.

34. Tulchinsky E. Fos family members: regulation, structure and role in oncogenic transformation. Histol. Histopathol. 2000 Jul;15(3):921–8.

35. Mumberg D, Lucibello FC, Schuermann M, Müller R. Alternative splicing of fosB transcripts results in differentially expressed mRNAs encoding functionally antagonistic proteins. Genes Dev. 1991 Jul;5(7):1212–23.

36. Nakabeppu Y, Nathans D. A naturally occurring truncated form of FosB that inhibits Fos/Jun transcriptional activity. Cell. 1991 Feb 22;64(4):751–9.

37. Yen J, Wisdom RM, Tratner I, Verma IM. An alternative spliced form of FosB is a negative regulator of transcriptional activation and transformation by Fos proteins. Proc. Natl. Acad. Sci. U.S.A. 1991 Jun 15;88(12):5077–81.

38. Nakabeppu Y, Ryder K, Nathans D. DNA binding activities of three murine Jun proteins: stimulation by Fos. Cell. 1988 Dec 2;55(5):907–15.

39. Chinenov Y, Kerppola TK. Close encounters of many kinds: Fos-Jun interactions that mediate transcription regulatory specificity. Oncogene. 2001 Apr 30;20(19):2438–52.

40. Angel P, Imagawa M, Chiu R, Stein B, Imbra RJ, Rahmsdorf HJ, et al. Phorbol ester-inducible genes contain a common cis element recognized by a TPA-modulated trans-acting factor. Cell. 1987 Jun 19;49(6):729–39.

41. Lee W, Mitchell P, Tjian R. Purified transcription factor AP-1 interacts with TPA-inducible enhancer elements. Cell. 1987 Jun 19;49(6):741–52.

42. Halazonetis TD, Georgopoulos K, Greenberg ME, Leder P. c-Jun dimerizes with itself and with c-Fos, forming complexes of different DNA binding affinities. Cell. 1988 Dec 2;55(5):917–24.

43. Cohen DR, Ferreira PC, Gentz R, Franza BR, Curran T. The product of a fos-related gene, fra-1, binds cooperatively to the AP-1 site with Jun: transcription factor AP-1 is comprised of multiple protein complexes. Genes Dev. 1989 Feb;3(2):173–84.

44. Ryseck RP, Bravo R. c-JUN, JUN B, and JUN D differ in their binding affinities to AP-1 and CRE consensus sequences: effect of FOS proteins.

Oncogene. 1991 Apr;6(4):533–42.

45. Vogt PK. Fortuitous convergences: the beginnings of JUN. Nat. Rev. Cancer. 2002 Jun;2(6):465–9.

46. Wang ZQ, Grigoriadis AE, Möhle-Steinlein U, Wagner EF. A novel target cell for c-fos-induced oncogenesis: development of chondrogenic tumours in embryonic stem cell chimeras. EMBO J. 1991 Sep;10(9):2437–50.

47. Grigoriadis AE, Schellander K, Wang ZQ, Wagner EF. Osteoblasts are target cells for transformation in c-fos transgenic mice. J. Cell Biol. 1993 Aug;122(3):685–701.

48. Eferl R, Ricci R, Kenner L, Zenz R, David J-P, Rath M, et al. Liver tumor development. c-Jun antagonizes the proapoptotic activity of p53. Cell. 2003 Jan 24;112(2):181–92.

49. Jochum W, David JP, Elliott C, Wutz A, Plenk H, Matsuo K, et al. Increased bone formation and osteosclerosis in mice overexpressing the transcription factor Fra-1. Nat. Med. 2000 Sep;6(9):980–4.

50. Nakayama T, Higuchi T, Oiso N, Kawada A, Yoshie O. Expression and function of FRA2/JUND in cutaneous T-cell lymphomas. Anticancer Res. 2012 Apr;32(4):1367–73.

51. Nakayama T, Hieshima K, Arao T, Jin Z, Nagakubo D, Shirakawa A-K, et al. Aberrant expression of Fra-2 promotes CCR4 expression and cell proliferation in adult T-cell leukemia. Oncogene. 2008 May 22;27(23):3221–32.

52. Milde-Langosch K, Röder H, Andritzky B, Aslan B, Hemminger G, Brinkmann A, et al. The role of the AP-1 transcription factors c-Fos, FosB, Fra-1 and Fra-2 in the invasion process of mammary carcinomas. Breast Cancer Res. Treat. 2004 Jul;86(2):139–52.

53. Schröder C, Schumacher U, Müller V, Wirtz RM, Streichert T, Richter U, et al. The transcription factor Fra-2 promotes mammary tumour progression by changing the adhesive properties of breast cancer cells. Eur. J. Cancer. 2010 Jun;46(9):1650–60.

54. Vandel L, Pfarr CM, Huguier S, Loiseau L, Sergeant A, Castellazzi M. Increased transforming activity of JunB and JunD by introduction of an heterologous homodimerization domain. Oncogene. 1995 Feb 2;10(3):495–507.

55. Chiu R, Angel P, Karin M. Jun-B differs in its biological properties from, and is a negative regulator of, c-Jun. Cell. 1989 Dec 22;59(6):979–86.

56. Passegué E, Jochum W, Schorpp-Kistner M, Möhle-Steinlein U, Wagner EF. Chronic myeloid leukemia with increased granulocyte progenitors in mice lacking junB expression in the myeloid lineage. Cell. 2001 Jan 12;104(1):21–32.

57. Shaulian E, Karin M. AP-1 as a regulator of cell life and death. Nat. Cell Biol. 2002 May;4(5):E131–6.

58. Treisman R. Regulation of transcription by MAP kinase cascades. Curr. Opin. Cell Biol. 1996 Apr;8(2):205–15.

59. Chang L, Karin M. Mammalian MAP kinase signalling cascades. Nature. 2001 Mar 1;410(6824):37–40.

60. Vial E, Marshall CJ. Elevated ERK-MAP kinase activity protects the FOS family member FRA-1 against proteasomal degradation in colon carcinoma cells. J. Cell. Sci. 2003 Dec 15;116(Pt 24):4957–63.

61. Gruda MC, Kovary K, Metz R, Bravo R. Regulation of Fra-1 and Fra-2 phosphorylation differs during the cell cycle of fibroblasts and phosphorylation in vitro by MAP kinase affects DNA binding activity. Oncogene. 1994 Sep;9(9):2537–47.

62. Wisdom R, Verma IM. Proto-oncogene FosB: the amino terminus encodes a regulatory function required for transformation. Mol. Cell. Biol. 1993 May;13(5):2635–43.

63. Cohen DR, Curran T. fra-1: a serum-inducible, cellular immediate-early gene that encodes a fos-related antigen. Mol. Cell. Biol. 1988 May;8(5):2063–9.

64. Sinke RJ, Tanigami A, Nakamura Y, Geurts van Kessel A. Reverse mapping of the gene encoding the human fos-related antigen-1 (fra-1) within chromosome band 11q13. Genomics. 1993 Oct;18(1):165.

65. Schreiber M, Poirier C, Franchi A, Kurzbauer R, Guenet JL, Carle GF, et al. Structure and chromosomal assignment of the mouse fra-1 gene, and its exclusion as a candidate gene for oc (osteosclerosis). Oncogene. 1997 Sep 4;15(10):1171–8.

66. Acquaviva C, Salvat C, Brockly F, Bossis G, Ferrara P, Piechaczyk M, et al. Cellular and viral Fos proteins are degraded by different proteolytic systems. Oncogene. 2001 Feb 22;20(8):942–50.

67. Kovary K, Bravo R. The jun and fos protein families are both required for cell cycle progression in fibroblasts. Mol. Cell. Biol. 1991 Sep;11(9):4466–72.

68. Bergers G, Graninger P, Braselmann S, Wrighton C, Busslinger M. Transcriptional activation of the fra-1 gene by AP-1 is mediated by regulatory sequences in the first intron. Mol. Cell. Biol. 1995 Jul;15(7):3748–58.

69. Tsuchiya H, Fujii M, Niki T, Tokuhara M, Matsui M, Seiki M. Human T-cell leukemia virus type 1 Tax activates transcription of the human fra-1 gene through multiple cis elements responsive to transmembrane signals. J. Virol. 1993 Dec;67(12):7001–7.

70. Tsurumi C, Ishida N, Tamura T, Kakizuka A, Nishida E, Okumura E, et al. Degradation of c-Fos by the 26S proteasome is accelerated by c-Jun and multiple protein kinases. Mol. Cell. Biol. 1995 Oct;15(10):5682–7.

71. Ferrara P, Andermarcher E, Bossis G, Acquaviva C, Brockly F, Jariel-Encontre I, et al. The structural determinants responsible for c-Fos protein proteasomal degradation differ according to the conditions of expression. Oncogene. 2003 Mar 13;22(10):1461–74.

72. Okazaki K, Sagata N. The Mos/MAP kinase pathway stabilizes c-Fos by phosphorylation and augments its transforming activity in NIH 3T3 cells. EMBO J. 1995 Oct 16;14(20):5048–59.

73. Chen RH, Juo PC, Curran T, Blenis J. Phosphorylation of c-Fos at the C-terminus enhances its transforming activity. Oncogene. 1996 Apr 4;12(7):1493–502.

74. Hurd TW, Culbert AA, Webster KJ, Tavaré JM. Dual role for mitogen-activated protein kinase (Erk) in insulin-dependent regulation of Fra-1 (fos-related antigen-1) transcription and phosphorylation. Biochem. J. 2002 Dec 1;368(Pt 2):573–80.

75. Casalino L, De Cesare D, Verde P. Accumulation of Fra-1 in ras-transformed cells depends on both transcriptional autoregulation and MEK-dependent posttranslational stabilization. Mol Cell Biol. 2003 Jun;23(12):4401–15.

76. Suzuki T, Okuno H, Yoshida T, Endo T, Nishina H, Iba H. Difference in transcriptional regulatory function between c-Fos and Fra-2. Nucleic Acids Res. 1991 Oct 25;19(20):5537–42.

77. Young MR, Nair R, Bucheimer N, Tulsian P, Brown N, Chapp C, et al. Transactivation of Fra-1 and consequent activation of AP-1 occur extracellular signal-regulated kinase dependently. Mol. Cell. Biol. 2002 Jan;22(2):587–98.

78. Frost JA, Geppert TD, Cobb MH, Feramisco JR. A requirement for extracellular signal-regulated kinase (ERK) function in the activation of AP-1 by Ha-Ras, phorbol 12-myristate 13-acetate, and serum. Proc. Natl. Acad. Sci. U.S.A. 1994 Apr 26;91(9):3844–8.

79. Jochum W, Passegué E, Wagner EF. AP-1 in mouse development and tumorigenesis. Oncogene. 2001 Apr 30;20(19):2401–12.

80. Schreiber M, Wang ZQ, Jochum W, Fetka I, Elliott C, Wagner EF. Placental vascularisation requires the AP-1 component fra1. Development. 2000 Nov;127(22):4937–48.

81. Grigoriadis AE, Wang ZQ, Cecchini MG, Hofstetter W, Felix R, Fleisch HA, et al. c-Fos: a key regulator of osteoclast-macrophage lineage determination and bone remodeling. Science. 1994 Oct 21;266(5184):443–8.

82. Johnson RS, Spiegelman BM, Papaioannou V. Pleiotropic effects of a null mutation in the c-fos proto-oncogene. Cell. 1992 Nov 13;71(4):577–86.

83. Fleischmann A, Hafezi F, Elliott C, Remé CE, Rüther U, Wagner EF. Fra-1 replaces c-Fos-dependent functions in mice. Genes Dev. 2000 Nov 1;14(21):2695–700.

84. Matsuo K, Owens JM, Tonko M, Elliott C, Chambers TJ, Wagner EF. Fosl1 is a transcriptional target of c-Fos during osteoclast differentiation. Nat. Genet. 2000 Feb;24(2):184–7.

85. Wagner EF. Bone development and inflammatory disease is regulated by AP-1 (Fos/Jun). Ann. Rheum. Dis. 2010 Jan;69 Suppl 1:i86–8.

86. Eferl R, Wagner EF. AP-1: a double-edged sword in tumorigenesis. Nat. Rev. Cancer. 2003 Nov;3(11):859–68.

87. Soto U, Denk C, Finzer P, Hutter KJ, zur Hausen H, Rösl F. Genetic complementation to non-tumorigenicity in cervical-carcinoma cells correlates with alterations in AP-1 composition. Int. J. Cancer. 2000 Jun 15;86(6):811–7.

88. Yoshioka K, Deng T, Cavigelli M, Karin M. Antitumor promotion by phenolic antioxidants: inhibition of AP-1 activity through induction of Fra expression. Proc. Natl. Acad. Sci. U.S.A. 1995 May 23;92(11):4972–6.

89. Rösl F, Das BC, Lengert M, Geletneky K, zur Hausen H. Antioxidant-induced changes of the AP-1 transcription complex are paralleled by a selective suppression of human papillomavirus transcription. J. Virol. 1997 Jan;71(1):362–70.

90. Jesudasan RA, Rahman RA, Chandrashekharappa S, Evans GA, Srivatsan ES. Deletion and translocation of chromosome 11q13 sequences in cervical carcinoma cell lines. Am. J. Hum. Genet. 1995 Mar;56(3):705–15.

91. Mishra A, Bharti AC, Saluja D, Das BC. Transactivation and expression patterns of Jun and Fos/AP-1 super-family proteins in human oral cancer. Int. J. Cancer. 2010 Feb 15;126(4):819–29.

92. Ma K, Chang D, Gong M, Ding F, Luo A, Tian F, et al. Expression and significance of FRA-1 in non-small-cell lung cancer. Cancer Invest. 2009 Mar;27(3):353–9.

93. Bamberger AM, Methner C, Lisboa BW, Städtler C, Schulte HM, Löning T, et al. Expression pattern of the AP-1 family in breast cancer: association of fosB expression with a well-differentiated, receptor-positive tumor phenotype. Int. J. Cancer. 1999 Oct 22;84(5):533–8.

94. Chiappetta G, Tallini G, De Biasio MC, Pentimalli F, de Nigris F, Losito S, et al. FRA-1 expression in hyperplastic and neoplastic thyroid diseases. Clin. Cancer Res. 2000 Nov;6(11):4300–6.

95. Wang HL, Wang J, Xiao S-Y, Haydon R, Stoiber D, He T-C, et al. Elevated protein expression of cyclin D1 and Fra-1 but decreased expression of c-Myc in human colorectal adenocarcinomas overexpressing beta-catenin. Int. J. Cancer. 2002 Oct 1;101(4):301–10.

96. Hu YC, Lam KY, Law S, Wong J, Srivastava G. Identification of differentially expressed genes in esophageal squamous cell carcinoma (ESCC) by cDNA expression array: overexpression of Fra-1, Neogenin, Id-1, and CDC25B genes in ESCC. Clin. Cancer Res. 2001 Aug;7(8):2213–21.

97. Bamberger AM, Milde-Langosch K, Rössing E, Goemann C, Löning T. Expression pattern of the AP-1 family in endometrial cancer: correlations with cell cycle regulators. J. Cancer Res. Clin. Oncol. 2001 Sep;127(9):545–50.

98. Sandhu H, Dehnen W, Roller M, Abel J, Unfried K. mRNA expression patterns in different stages of asbestos-induced carcinogenesis in rats. Carcinogenesis. 2000 May;21(5):1023–9.

99. Ramos-Nino ME, Blumen SR, Pass H, Mossman BT. Fra-1 governs cell migration via modulation of CD44 expression in human mesotheliomas. Mol. Cancer. 2007;6:81.

100. Debinski W, Slagle-Webb B, Achen MG, Stacker SA, Tulchinsky E, Gillespie GY, et al. VEGF-D is an X-linked/AP-1 regulated putative onco-angiogen in human glioblastoma multiforme. Mol. Med. 2001 Sep;7(9):598–608.

101. Fung LF, Lo AK, Yuen PW, Liu Y, Wang XH, Tsao SW. Differential gene expression in nasopharyngeal carcinoma cells. Life Sci. 2000 Jul 14;67(8):923–36.

102. Zajchowski DA, Bartholdi MF, Gong Y, Webster L, Liu HL, Munishkin A, et al. Identification of gene expression profiles that predict the aggressive behavior of breast cancer cells. Cancer Res. 2001 Jul 1;61(13):5168–78.

103. Vallone D, Battista S, Pierantoni GM, Fedele M, Casalino L, Santoro M, et al. Neoplastic transformation of rat thyroid cells requires the junB and fra-1 gene induction which is dependent on the HMGI-C gene product. EMBO J. 1997 Sep 1;16(17):5310–21.

104. Roy D, Calaf G, Hei TK. Profiling of differentially expressed genes induced by high linear energy transfer radiation in breast epithelial cells. Mol. Carcinog. 2001 Aug;31(4):192–203.

105. Ramos-Nino ME, Timblin CR, Mossman BT. Mesothelial cell transformation requires increased AP-1 binding activity and ERK-dependent Fra-1 expression. Cancer Res. 2002 Nov 1;62(21):6065–9.

106. Ramos-Nino ME, Scapoli L, Martinelli M, Land S, Mossman BT. Microarray analysis and RNA silencing link fra-1 to cd44 and c-met expression in mesothelioma. Cancer Res. 2003 Jul 1;63(13):3539–45.

107. Lee HY, Chaudhary J, Walsh GL, Hong WK, Kurie JM. Suppression of c-Fos gene transcription with malignant transformation of human bronchial epithelial cells. Oncogene. 1998 Jun 11;16(23):3039–46.

108. Zhang L, Zhou W, Velculescu VE, Kern SE, Hruban RH, Hamilton SR, et al. Gene expression profiles in normal and cancer cells. Science. 1997 May 23;276(5316):1268–72.

109. Lucibello FC, Lowag C, Neuberg M, Müller R. trans-repression of the mouse c-fos promoter: a novel mechanism of Fos-mediated trans-regulation. Cell. 1989 Dec 22;59(6):999–1007.

110. Kessler R, Zacharova-Albinger A, Laursen NB, Kalousek M, Klemenz R. Attenuated expression of the serum responsive T1 gene in ras transformed fibroblasts due to the inhibition of c-fos gene activity. Oncogene. 1999 Mar 4;18(9):1733–44.

111. Mechta F, Lallemand D, Pfarr CM, Yaniv M. Transformation by ras modifies AP1 composition and activity. Oncogene. 1997 Feb 20;14(7):837–47.

112. Cook SJ, Aziz N, McMahon M. The repertoire of fos and jun proteins expressed during the G1 phase of the cell cycle is determined by the duration of mitogen-activated protein kinase activation. Mol. Cell. Biol. 1999 Jan;19(1):330–41.

113. Treinies I, Paterson HF, Hooper S, Wilson R, Marshall CJ. Activated MEK stimulates expression of AP-1 components independently of phosphatidylinositol 3-kinase (PI3-kinase) but requires a PI3-kinase signal To stimulate DNA synthesis. Mol. Cell. Biol. 1999 Jan;19(1):321–9.

114. Murphy LO, Smith S, Chen R-H, Fingar DC, Blenis J. Molecular interpretation of ERK signal duration by immediate early gene products. Nat. Cell Biol. 2002 Aug;4(8):556–64.

115. Frödin M, Gammeltoft S. Role and regulation of 90 kDa ribosomal S6 kinase (RSK) in signal transduction. Mol. Cell. Endocrinol. 1999 May 25;151(1-2):65–77.

116. Murphy LO, MacKeigan JP, Blenis J. A network of immediate early gene products propagates subtle differences in mitogen-activated protein kinase signal amplitude and duration. Mol. Cell. Biol. 2004 Jan;24(1):144–53.

117. Kikuchi A, Kishida S, Yamamoto H. Regulation of Wnt signaling by protein-protein interaction and post-translational modifications. Exp. Mol. Med. 2006 Feb 28;38(1):1–10.

118. Osaki M, Oshimura M, Ito H. PI3K-Akt pathway: its functions and alterations in human cancer. Apoptosis. 2004 Nov;9(6):667–76.

119. Tiwari G, Sakaue H, Pollack JR, Roth RA. Gene expression profiling in prostate cancer cells with Akt activation reveals Fra-1 as an Akt-inducible gene. Mol. Cancer Res. 2003 Apr;1(6):475–84.

120. Zhang Q, Adiseshaiah P, Kalvakolanu DV, Reddy SP. A Phosphatidylinositol 3-kinase-regulated Akt-independent signaling promotes cigarette smoke-induced FRA-1 expression. J. Biol. Chem. 2006 Apr 14;281(15):10174–81.

121. Kalluri R, Weinberg RA. The basics of epithelial-mesenchymal transition. J. Clin. Invest. 2009 Jun;119(6):1420–8.

122. Micalizzi DS, Farabaugh SM, Ford HL. Epithelial-mesenchymal transition in cancer: parallels between normal development and tumor progression. J Mammary Gland Biol Neoplasia. 2010 Jun;15(2):117–34.

123. Davies M, Robinson M, Smith E, Huntley S, Prime S, Paterson I. Induction of an epithelial to mesenchymal transition in human immortal and malignant keratinocytes by TGF-beta1 involves MAPK, Smad and AP-1 signalling pathways. J. Cell. Biochem. 2005 Aug 1;95(5):918–31.

124. Doehn U, Hauge C, Frank SR, Jensen CJ, Duda K, Nielsen JV, et al. RSK is a principal effector of the RAS-ERK pathway for eliciting a coordinate promotile/invasive gene program and phenotype in epithelial cells. Mol. Cell. 2009 Aug 28;35(4):511–22.

125. Shin S, Dimitri CA, Yoon S-O, Dowdle W, Blenis J. ERK2 but not ERK1 induces epithelial-to-mesenchymal transformation via DEF motif-dependent signaling events. Mol. Cell. 2010 Apr 9;38(1):114–27.

126. Lemieux E, Bergeron S, Durand V, Asselin C, Saucier C, Rivard N. Constitutively active MEK1 is sufficient to induce epithelial-to-mesenchymal transition in intestinal epithelial cells and to promote tumor invasion and metastasis. Int. J. Cancer. 2009 Oct 1;125(7):1575–86.

127. Kustikova O, Kramerov D, Grigorian M, Berezin V, Bock E, Lukanidin E, et al. Fra-1 induces morphological transformation and increases in vitro invasiveness and motility of epithelioid adenocarcinoma cells. Mol. Cell. Biol. 1998 Dec;18(12):7095–105.

128. Tkach V, Tulchinsky E, Lukanidin E, Vinson C, Bock E, Berezin V. Role of the Fos family members, c-Fos, Fra-1 and Fra-2, in the regulation of cell motility. Oncogene. 2003 Aug 7;22(32):5045–54.

129. Vial E, Sahai E, Marshall CJ. ERK-MAPK signaling coordinately regulates activity of Rac1 and RhoA for tumor cell motility. Cancer Cell. 2003 Jul;4(1):67–79.

130. Reisfeld RA, Niethammer AG, Luo Y, Xiang R. DNA vaccines suppress tumor growth and metastases by the induction of anti-angiogenesis. Immunol. Rev. 2004 Jun;199:181–90.

131. Luo Y, Zhou H, Mizutani M, Mizutani N, Liu C, Xiang R, et al. A DNA vaccine targeting Fos-related antigen 1 enhanced by IL-18 induces long-lived T-cell memory against tumor recurrence. Cancer Res. 2005 Apr 15;65(8):3419–27.

132. Luo Y, Zhou H, Mizutani M, Mizutani N, Reisfeld RA, Xiang R. Transcription factor Fos-related antigen 1 is an effective target for a breast cancer vaccine. Proc Natl Acad Sci U S A. 2003 Jul 22;100(15):8850–5.

133. Težak Ž, Kondratovich MV, Mansfield E. US FDA and personalized medicine: in vitro diagnostic regulatory perspective. Personalized Medicine. 2010 Sep;7(5):517–30.

134. Mukai H. Treatment strategy for HER2-positive breast cancer. Int J Clin Oncol [Internet]. 2010 Jul 15 [cited 2010 Jul 21];Available from: http://www.ncbi.nlm.nih.gov/pubmed/20632056

135. NICE. Breast cancer (early & locally advanced) [Internet]. [cited 2010 Jul 21];Available from: http://guidance.nice.org.uk/CG80

136. Andersen H, Mahmood S, Tkach V, Cohn M, Kustikova O, Grigorian M, et al. The ability of Fos family members to produce phenotypic changes in epithelioid cells is not directly linked to their transactivation potentials. Oncogene. 2002 Jul 18;21(31):4843–8.

137. Shariat SF, Monoski MA, Andrews B, Wheeler TM, Lerner SP, Slawin KM. Association of plasma urokinase-type plasminogen activator and its receptor with clinical outcome in patients undergoing radical cystectomy for transitional cell carcinoma of the bladder. Urology. 2003 May;61(5):1053–8.

138. Inoue T, Stuart J, Leno R, Maki CG. Nuclear import and export signals in control of the p53-related protein p73. J Biol Chem. 2002 Apr 26;277(17):15053–60.

139. Fiordalisi JJ, Johnson RL, Ulkü AS, Der CJ, Cox AD. Mammalian expression vectors for Ras family proteins: generation and use of expression constructs to analyze Ras family function. Methods Enzymol. 2001;332:3–36.

140. Acquaviva C, Brockly F, Ferrara P, Bossis G, Salvat C, Jariel-Encontre I, et al. Identification of a C-terminal tripeptide motif involved in the control of rapid proteasomal degradation of c-Fos proto-oncoprotein during the G(0)-to-S phase transition. Oncogene. 2001 Nov 8;20(51):7563–72.

141. Coronella-Wood J, Terrand J, Sun H, Chen QM. c-Fos phosphorylation induced by H2O2 prevents proteasomal degradation of c-Fos in cardiomyocytes. J Biol Chem. 2004 Aug 6;279(32):33567–74.

142. Andreucci JJ, Grant D, Cox DM, Tomc LK, Prywes R, Goldhamer DJ, et al. Composition and function of AP-1 transcription complexes during muscle cell differentiation. J Biol Chem. 2002 May 10;277(19):16426–32.

143. Basbous J, Chalbos D, Hipskind R, Jariel-Encontre I, Piechaczyk M. Ubiquitin-Independent Proteasomal Degradation of Fra-1 Is Antagonized by Erk1/2 Pathway-Mediated Phosphorylation of a Unique C-Terminal Destabilizer. Mol Cell Biol. 2007 Jun;27(11):3936–50.

144. Favata MF, Horiuchi KY, Manos EJ, Daulerio AJ, Stradley DA, Feeser WS, et al. Identification of a novel inhibitor of mitogen-activated protein kinase kinase. J. Biol. Chem. 1998 Jul 17;273(29):18623–32.

145. Fenteany G, Standaert RF, Lane WS, Choi S, Corey EJ, Schreiber SL. Inhibition of proteasome activities and subunit-specific amino-terminal threonine modification by lactacystin. Science. 1995 May 5;268(5211):726–31.

146. Chiappetta G, Ferraro A, Botti G, Monaco M, Pasquinelli R, Vuttariello E, et al. FRA-1 protein overexpression is a feature of hyperplastic and neoplastic breast disorders. BMC Cancer. 2007;7:17.

147. Song Y, Song S, Zhang D, Zhang Y, Chen L, Qian L, et al. An association of a simultaneous nuclear and cytoplasmic localization of Fra-1 with breast malignancy. BMC Cancer. 2006;6:298.

148. Singh NK, Quyen DV, Kundumani-Sridharan V, Brooks PC, Rao GN. AP-1 (Fra-1/c-Jun)-mediated induction of expression of matrix metalloproteinase-2 is required for 15S-hydroxyeicosatetraenoic acid-induced angiogenesis. J. Biol. Chem. 2010 May 28;285(22):16830–43.

149. Chen RH, Abate C, Blenis J. Phosphorylation of the c-Fos transrepression domain by mitogen-activated protein kinase and 90-kDa ribosomal S6 kinase. Proc Natl Acad Sci U S A. 1993 Dec 1;90(23):10952–6.

150. Pakay JL, Diesch J, Gilan O, Yip Y-Y, Sayan E, Kolch W, et al. A 19S proteasomal subunit cooperates with an ERK MAPK-regulated degron to regulate accumulation of Fra-1 in tumour cells. Oncogene [Internet]. 2011 online [cited 2011 Sep 1];Available from: http://dx.doi.org/10.1038/onc.2011.375

151. Bossis G, Ferrara P, Acquaviva C, Jariel-Encontre I, Piechaczyk M. c-Fos proto-oncoprotein is degraded by the proteasome independently of its own ubiquitinylation in vivo. Mol. Cell. Biol. 2003 Oct;23(20):7425–36.

152. Farràs R, Bossis G, Andermarcher E, Jariel-Encontre I, Piechaczyk M. Mechanisms of delivery of ubiquitylated proteins to the proteasome: new target for anti-cancer therapy? Crit. Rev. Oncol. Hematol. 2005 Apr;54(1):31–51.

153. Sasaki T, Kojima H, Kishimoto R, Ikeda A, Kunimoto H, Nakajima K. Spatiotemporal regulation of c-Fos by ERK5 and the E3 ubiquitin ligase UBR1, and its biological role. Mol. Cell. 2006 Oct 6;24(1):63–75.

154. Kahana C, Asher G, Shaul Y. Mechanisms of protein degradation: an odyssey with ODC. Cell Cycle. 2005 Nov;4(11):1461–4.

155. Sheaff RJ, Singer JD, Swanger J, Smitherman M, Roberts JM, Clurman BE. Proteasomal turnover of p21Cip1 does not require p21Cip1 ubiquitination. Mol. Cell. 2000 Feb;5(2):403–10.

156. Ito Y, Inoue D, Kido S, Matsumoto T. c-Fos degradation by the ubiquitin-proteasome proteolytic pathway in osteoclast progenitors. Bone. 2005 Dec;37(6):842–9.

157. Hoffmann E, Thiefes A, Buhrow D, Dittrich-Breiholz O, Schneider H, Resch K, et al. MEK1-dependent delayed expression of Fos-related antigen-1 counteracts c-Fos and p65 NF-kappaB-mediated interleukin-8 transcription in response to cytokines or growth factors. J. Biol. Chem. 2005 Mar 11;280(10):9706–18.